Advances in Colloid and Interface Science 329 (2024) 103187

Contents lists available at ScienceDirect

Advances in Colloid and Interface Science

journal homepage: www.elsevier.com/locate/cis

Exploring proteins at soft interfaces and in thin liquid films – From classical methods to advanced applications of reflectometry

Georgi G. Gochev [a,b,*], Richard A. Campbell [c], Emanuel Schneck [d], Jan Zawala [a], Piotr Warszynski [a]

[a] Jerzy Haber Institute of Catalysis and Surface Chemistry, Polish Academy of Sciences, 30239 Krakow, Poland
[b] Institute of Physical Chemistry, Bulgarian Academy of Sciences, 1113 Sofia, Bulgaria
[c] Division of Pharmacy and Optometry, University of Manchester, M13 9PT Manchester, UK
[d] Physics Department, Technical University Darmstadt, 64289 Darmstadt, Germany

ARTICLE INFO

Keywords:
Protein
Interface
Thin liquid film
Ellipsometry
X-ray reflectometry
Neutron reflectometry

ABSTRACT

The history of the topic of proteins at soft interfaces dates back to the 19th century, and until the present day, it has continuously attracted great scientific interest. A multitude of experimental methods and theoretical approaches have been developed to serve the research progress in this large domain of colloid and interface science, including the area of soft colloids such as foams and emulsions. From classical methods like surface tension adsorption isotherms, surface pressure-area measurements for spread layers, and surface rheology probing the dynamics of adsorption, nowadays, advanced surface-sensitive techniques based on spectroscopy, microscopy, and the reflection of light, X-rays and neutrons at liquid/fluid interfaces offers important complementary sources of information. Apart from the fundamental characteristics of protein adsorption layers, *i.e.*, surface tension and surface excess, the nanoscale structure of such layers and the interfacial protein conformations and morphologies are of pivotal importance for extending the depth of understanding on the topic. In this review article, we provide an extensive overview of the application of three methods, namely, ellipsometry, X-ray reflectometry and neutron reflectometry, for adsorption and structural studies on proteins at water/air and water/oil interfaces. The main attention is placed on the development of experimental approaches and on a discussion of the relevant achievements in terms of notable experimental results. We have attempted to cover the whole history of protein studies with these techniques, and thus, we believe the review should serve as a valuable reference to fuel ideas for a wide spectrum of researchers in different scientific fields where proteins at soft interface may be of relevance.

1. Introduction to proteins at soft interfaces

Natural philosophers and scientists have been identifying and dealing with problems of colloid and interface science since the 17th century. In early times of the history of this scientific field, issues related mainly to capillary phenomena, interfaces and soap bubbles/films (*thin liquid films*, TLFs), and colloidal stability in general, have been tackled [1–5]. The domain of protein-based soft colloids (foams and emulsions) has been developing for over a century. It started with early observations in the 19th century [1,3,6] on the ability of proteins to accumulate at soft (liquid/fluid) interfaces. Then, investigations of physicochemical properties of protein interfacial layers on water appeared in the early 20th century [4,7–9] and nowadays, the literature on the topic is already quite rich, and our understanding of the role of proteins in the stabilization of foams and emulsions is at an advanced level [10,11]. That has been achieved by the application of a variety of different experimental and theoretical methods in studies on different time and length scales, from investigations of real foams and emulsions on the macroscopic

Abbreviations: ACMW, air contrast matched water; BAM, Brewster angle microscopy; CBF, common black film; IRRAS, infrared reflection absorption spectroscopy; G.HCl, guanidine hydrochloride; GIXOS, grazing incidence X-ray off-specular; GIXF, grazing incidence X-ray fluorescence; NBF, Newton black film; NR, neutron reflectometry; PCMW, protein contrast matched water; SDS, sodium dodecyl sulfate; SDBS, sodium dodecyl benzenesulfonate; SLD, scattering length density; TLF, thin liquid film; W/A, water/air; W/O, water/oil; XRR, X-ray reflectometry.

* Corresponding author at: Jerzy Haber Institute of Catalysis and Surface Chemistry, Polish Academy of Sciences, 30239 Krakow, Poland.
E-mail address: georgi.gochev@ikifp.edu.pl (G.G. Gochev).

https://doi.org/10.1016/j.cis.2024.103187
Received 13 March 2024; Received in revised form 12 May 2024; Accepted 12 May 2024
Available online 16 May 2024

level to investigations of TLFs and single interfaces on the meso- and nanoscale level. Concerning soft interfaces, applicable experimental methods give access to measurements of adsorption, rheological, electrical and other properties of the relevant protein layers. On the other hand, access to the structural organization of such interfacial layers at the molecular level is of pivotal importance.

In this line, the present review article is focused on the application of reflectometric methods for probing soft interfaces – as capable of resolving interfacial structures with sub-nanometer resolution – in protein studies. Hence, we define the theme of protein layers at soft interfaces studied by reflectometric techniques as the scope of the article, being a subtopic of the larger area of proteins at interfaces. This subtopic has its own history and here we attempt to overview its development from the first reports up to the present day; therefore, we afford ourselves to classify this article as a "historical perspective". Comparative works on protein adsorption on solid surfaces [12] and the much younger topic of protein aggregates at soft interfaces [13] fall out of the scope. We also restrict ourselves from considering works on mixed interfacial systems of proteins and other surface-active species (surfactants, lipids, polymers, other proteins, nanoparticles, *etc.*) or relevant non-surface-active entities. In Section 2, a brief historical overview of experimental methods used for investigations of protein layers at soft interfaces is presented. In Section 3, we present the basics of three reflectometric techniques for investigations of the adsorption dynamics and the fine structure of protein interfacial layers, namely *ellipsometry*, *X-ray reflectometry* (XRR) and *neutron reflectometry* (NR), while in Section 4, the relevant achievements are discussed. For the sake of completeness, in Section 5, we afford ourselves to extend briefly the scope of the article to TLFs.

For the sake of clarity, here we make a note on the use of the term "*film*" in the colloid and interface science literature. According to the recommendations of IUPAC: "*The term film is a generic one referring to condensed matter restricted in one dimension*" [14]. In the context of a single surface, *film* is used for a "thin" layer. For example, oxide presents up to a few tens of nm layer on the surface of silicon. The term "*thin film*" is typical in the context of the theory of reflectometric techniques, and as such, we will also use it consistently in the following sections. Concerning liquids, "*film*" is sometimes employed as a synonym of a molecular mono- or multi-layer at a soft interface, for example, as widely used in the early studies on interfacial layers in the 19th century and mostly in the first half of the 20th century [6–9], but more rarely later on; however, one finds this type of terminology, even nowadays, usually in some interdisciplinary works. According to the recommendations of IUPAC: "*The usage of the term 'film' for an adsorption layer is confusing and discouraged*" [14]. For the sake of clarity, a TLF is a liquid layer that is sufficiently thin (of the order of $\leq$100 nm) so that disjoining pressure starts to operate, *i.e.*, such a liquid layer is no longer considered to have the properties of a bulk phase. A *symmetric* TLF is a *film* between two equivalent semi-phases, and such a TLF which spontaneously arises at the contact zone between two foam bubbles or emulsion droplets – in the first case – is called *thin foam film* and, in the second case, is called *thin emulsion film* [14].

2. Experimental methods and approaches

The affinity of proteins to soft interfaces and their ability to functionalize such interfaces have been initially investigated by means of spread layers at the interface of an aqueous phase substrate with air (hereafter called water/air, W/A interface) [7–9,15]. Spread protein layers on water/oil (W/O) interfaces have also been handled and explored [16]. On the other hand, in close relation to the properties and stability of foams and emulsions, it is helpful to investigate the dynamics of the process of adsorption of proteins from the aqueous bulk phase to W/A and W/O interfaces, respectively [4,8,16,17]. Notably, specific differences between some properties of interfacial layers of a given protein, obtained by spreading or by spontaneous adsorption, have been identified [18,19]. Pioneering studies on the adsorption kinetics of proteins have been made by du Noüy (1922) [4,20], who studied the evolution of the surface tension at the W/A interface with time t for diluted aqueous solutions of blood serum.

The characterization of protein interfacial layers is possible by making use of a variety of experimental methods. Undoubtedly, the most popular approach is measurements of the *surface tension* γ (concomitantly in terms of *surface pressure* $\Pi = \gamma_0 - \gamma$, where γ_0 is the tension of the bare water surface). There are many techniques for measuring surface tension [4,8,17,21]. However, some of them are more advantageous for protein solutions; for example, the methods of *Wilhelmy Plate* and *du Noüy* might suffer from problems with an inevitably present three-phase contact [17,22]. To overcome this problem, one can use a clean paper plate instead of traditional glass or platinum plates [22]. Furthermore, operation with those techniques involves deformation of the investigated liquid interface, which may cause disturbance of the interfacial layer by 2D rheological effects. On the other hand, certain non-invasive methods, like *maximum bubble pressure* [23] and some other techniques based on drop weight and volume, do not suffer from such drawbacks, but they may have other limitations, amongst which is the 'short' experimental time window [8,17,21]. It should be emphasised that those techniques are complementary with sensitivities to different time scales. The *axisymmetric drop/bubble profile analysis* technique provides γ-measurements in the t-range from a couple of seconds to tens of hours [17,24]. This technique has been established as a versatile surface tension method that is widely used nowadays for investigating either W/A or W/O interfaces.

Along with the surface tension, another fundamental parameter, namely the *surface excess* Γ in terms of the protein number, number of moles or mass per unit area (interchangeably being also denoted as *adsorbed amount* or simply *adsorption*), is of pivotal importance for the characterization of interfacial layers. In the case of spread protein layers, the surface excess is *a priori* known. In this case, the surface pressure is measured as a function of the available area A covered by a given amount of protein, assuming no desorption from the interface to the bulk subphase, *i.e.*, the so-called surface pressure-area (Π-A) curves are obtained, which give access to the surface equation of state $\Pi(\Gamma)$. On the contrary, in adsorption experiments, the dynamic surface excess $\Gamma(t)$ measurements for different bulk concentration c of amphiphiles are essential. The need for validation of the applicability of the Gibbs adsorption equation $\Gamma \sim (\partial\Pi/\partial \ln c)$ to experimental results has been the driving force for developing methods for *in situ* measurements of Γ. Such Γ-data, combined with Π-data, give the surface equation of state $\Pi(\Gamma)$ that can be compared with appropriate adsorption theories. Seemingly, the first attempt for experimental detection of the surface excess at a stationary interface was carried out in the early 1930s employing the so-called *microtome* method, developed to resolve previous problems with techniques based on moving bubbles (the only approach for estimating Γ of surfactants at the W/A interface at those times; however, the obtained results have not fitted to the Gibbs theoretical predictions) [25]. To the best of our knowledge, the microtome method has not been used in protein studies. Later on, the *radiotracer* method was applied to protein layers at either W/A [26–29] or W/O [28] interfaces. It is noted that the method is based on inevitable radiolabeling of the protein, usually with ^{14}C (*e.g.*, by acetylation or methylation), which can cause slight changes in the surface activity of the native protein [27]. Tritium-labeled species have also been used as radiotracers to quantify the surface excess of species, including proteins at soft interfaces [30,31]. Historically, the next generation of methods capable of measuring the surface excess at soft interfaces includes reflectometric techniques such as ellipsometry [26,28,32] as well as XRR and NR [18], which will be discussed in more detail in Section 3.

Surface rheometry techniques – operating either in *shear* or *dilation* mode – are widely employed for probing adsorption and mechanical properties of protein interfacial layers [21,33–35]. Shear rheometry, pioneered by Plateau (1873) [3], has been developed in many

modifications [16,35,36]. Dilational rheometry is a comparatively younger method [37], but it has also been extensively progressed [35]. Especially useful is monitoring the dependence of the *dilational modulus* E as a function of Π. Such relations can be investigated either at a *steady state* (near-equilibrium condition) or during adsorption [33,38–40]. In the first case, the dependence $E(\Pi)$ is considered an equation of state (provided the modulus E is assumed equal to the limiting Gibbs elasticity E_0, *i.e.*, the surface layer is elastic), and such experimental data can be modeled by appropriate theoretical approaches [38,39]. In the second case, the combination of data on the dynamic dilational modulus $E(t)$ with data on the dynamic surface pressure $\Pi(t)$ yields a "dynamic" dependence $E(\Pi(t))$, which is a convenient tool for identifying evolution steps in the process of formation of protein interfacial layers [33,40]. Another important rheological feature that is typical for protein interfacial layers is the transition from linear to non-linear viscoelasticity regime with an increase of the applied strain – a phenomenon characteristic for the interfacial response examined either in shear or in dilational area deformations [34,35,40]. The nonlinearity in the observed surface stress response can be quantified, for example, by analysis of the so-called Lissajous plots *via* the general stress decomposition method [40,41].

Only a few decades ago, reports on *in situ* microscopy imaging of protein interfacial layers at soft interfaces started to appear, as performed by Brewster angle microscopy (BAM) [42–49] and fluorescence microscopy [50,51], which were able to detect in-plane heterogeneities. Note, in the latter case, fluorescent labeling of the studied protein is a prerequisite unless autofluorescence of proteins containing an increased amount of the amino acids tryptophan, tyrosine, and phenylalanine is strong enough. The sensitivity of these techniques is restricted by the microscope's resolution. Protein layers at relatively low surface pressures (surface concentrations) do not display patterns (if not contaminated by particles such as dust), which is evidence that a smooth and homogenous monolayer is formed. The eventual appearance of patterns at higher protein surface concentrations reflects heterogeneities due to 2D network formation or 3D interfacial aggregation (multilayering) [42–46]. These techniques are especially useful in detecting microscopic heterogeneities in mixed protein-protein [50] and protein-surfactant [51] interfacial systems.

The method of the *surface potential* ΔV [52] has been used for accessing direct information about the electrical properties of protein layers at W/A and W/O interfaces [7,8,27,28,53]. However, this method has become less popular in recent decades. Instead, novel approaches using spectroscopic methods based on non-linear optics can be utilized for revealing the charging state of interfacial layers – for example, monitoring the amplitudes of the stretching vibrations of OH functional groups of adsorbed molecules in the region between 3100 and 3800 cm^{-1} in spectra by vibrational sum-frequency generation (SFG) spectroscopy as applied to W/A interfaces [54].

Adaptations and development of spectroscopic methods for liquid bulk studies towards measurements at soft interfaces [55], such as infrared reflection-absorption spectroscopy (IRRAS; also known as external reflection Fourier transform infrared spectroscopy), SFG spectroscopy, circular dichroism and others, provide access to information on conformational changes and molecular ordering of protein molecules upon adsorption by analysis of absorption spectra taken from protein covered W/A [19,54,56–59] or W/O [60] interfaces. Following these studies, one may conclude that, upon adsorption of protein globules at soft interfaces, their tertiary structure may be distorted to a certain extent, whereas their secondary structure might remain only slightly affected. Computer simulation methods are capable of providing complementary information that is experimentally inaccessible or can be validated experimentally [61]. These experimental and theoretical studies all together contribute valuable information about characteristic conformational changes in adsorbing protein globules like the much-debated protein unfolding upon adsorption.

In the early studies on protein layers at soft interfaces, it was believed that protein globules unfold once they have either adsorbed from solution or been spread at a W/A interface due to interface-induced physical denaturation. Neurath & Bull (1938) [8] wrote in their comprehensive critical review: "*Investigations of spread films of proteins have furnished valuable data for the interpretation of protein structure. A notable fact arising from this film work is that intrinsic differences between native proteins largely disappear upon spreading. Thus, the thickness of protein film is approximately the same for all proteins, whereas proteins in the native, dissolved state differ greatly in their molecular dimensions.*". This popular hypothesis was based on analysis of (truly) rich and detailed information about macroscopic layer properties (mainly Π-A curves and experimental results for ΔV, Γ and surface rheology parameters), combined with knowledge on details of the molecular structure of proteins [7,8]), but it was not supported by any direct proof – for example by precise *in situ* measurements of the overall layer thickness. Since, at those times (up to the 1970s), techniques capable of resolving such information were not yet available, the thickness of protein interfacial layers could be investigated *ex-situ* by transfer from the aqueous subphase onto a solid surface and then measured by optical means [49,62] or by atomic force microscopy as carried out in later approaches [48,49]. The need for novel methods has urgently emerged as MacRitchie (1986) [15] wrote: "*In view of the inherent uncertainty in drawing conclusions from measurements on films transferred from monolayers (particularly in relation to conformation determinations), there is a need to develop further the direct methods for examining protein films in situ. These methods have the great advantage that the films can be manipulated and measurements made as a function of different variables such as surface pressure and time.*"

In the classical spreading methods [7–9], the mechanism by which the protein molecules remain 'trapped' at the interface, more than would be the case had they been adsorbed from an equivalent dilute solution, is related to their lateral interactions in the interface plane. More recently, using more sophisticated techniques unavailable in the first half of the 20th century, White & coworkers [63,64] elaborated these concepts using a *flow trough*, where exchange of the subphase beneath a protein film at the W/A interface resulted in minimal desorption [45,63,64]. The implications of the findings were profound in that, in part, they helped to explain some of the nuances experienced by those who work with protein films, such as the lack of reproducibility of experimental data. An irreversible adsorption component to the thermodynamic concept of adsorption-desorption equilibrium means that even small details of sample preparation, such as how the sample is poured into the measurement vessel (*i.e.* the relative surface areas formed during the process), can alter the measured surface excess. The authors assert that more systematic work to resolve non-equilibrium effects in protein systems in the future can help researchers better understand the reproducibility, properties, and inherent nature of these important and intriguing systems.

3. Reflectometric methods

While the optics of light is a branch of classical physics – dating back for centuries with the seminal works of Newton and other prominent scientists – the interactions of X-rays and neutrons with condensed matter are scientific domains that emerged in the 20th century, and in particular, the scattering of X-rays and neutrons by surfaces [65–67]. Amongst existing scattering techniques for probing interfacial systems [68–70], ellipsometry, XRR and NR are well suited for *in situ* investigations of planar soft interfaces [66,71]. Experiments with reflectivity of *p*-polarized light under normal incidence ($\theta = 0^o$) [72] or at θ near the Brewster angle θ_{Br} [73] (where θ is the angle of incidence as defined in Fig. 1) have also been designed for the characterization of insoluble monolayers at W/A interface and applied to spread or adsorbed protein layers as well [42–44].

A simplified scheme of specular reflection of light, X-rays or neutrons from a soft interface is presented in Fig. 1. If 'Liquid 1' is water, then we speak about aqueous solutions, which are the most investigated liquid

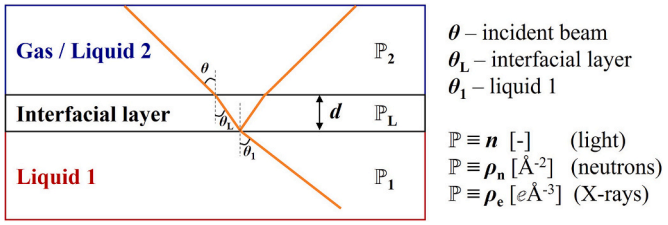

Fig. 1. Specular reflectivity from an interfacial layer. θ is angle of incidence, d is layer thickness, n is refractive index, ρ_n is neutron scattering length density (SLD) and ρ_e is electron density (e is the elementary charge).

systems. When the second semi-phase is gas (usually air), we speak about a W/A interface and when it is 'Liquid 2' (immiscible in Liquid 1, usually oil), we speak about a W/O interface.

As for other types of methods for probing soft interfaces, reflectometry techniques also suffer from certain problems when applied to a W/O interface, whereas a W/A interface is much more experimentally accessible, although it is not without its challenges, for example, under conditions away from ambient temperature. These are technical issues arising from instrumental difficulties, *e.g.*, due to reflection, refraction, attenuation and other optical or mechanical effects. Adaptations and developments of reflectivity techniques to the W/O interface are discussed in the following sections.

An important question dealt with in the literature is calibrating the reflectivity signal in ellipsometry [74–76], XRR [77,78] and NR [79,80] from a bare liquid/vapor or liquid/liquid interface before proceeding with more complex experiments involving stratified interfacial layers, which are also referred to as "slabs". This is particularly relevant because surface roughness resulting from capillary waves affects the measured data in all three techniques [77], and a reference measurement of the bare interface can help reduce systematic errors in the interpretation of models applied to obtain structural parameters from the data on protein films. It may be noted that the amplitude of capillary waves has an inverse square root dependence on the interfacial tension [78], whereas standard waves with greater amplitude and lower frequency simply result in loss of the specular reflectivity; hence, passive and active anti-vibration tables are usually used as setup platforms with all three techniques.

3.1. Ellipsometry

Ellipsometry is an optical method used to investigate surfaces as well as substrate-supported thin surface layers through the reflection of polarized light. Most modern instruments exploit a laser light source, but the coherence of the beam is not a prerequisite as many earlier instruments contained a white light source. The history of this method can be traced back to the very early 19th century, and one finds information about the roots and the early times of the topic in the review article by Hall (1969) [81], where the author writes: "*Since ellipsometry is fundamentally concerned with the analysis of reflected polarized light, it can be said that its history begins in 1808 with the detection, by Malus, of polarization by reflection.*" According to Hall [81], the application of ellipsometry to liquid surfaces has been pioneered by Jamin (1851) and Rayleigh (1892). Later on, the topic was developed in the 20th century by Hofmeister (1953) [82], den Engelsen (1973) [83], Beaglehole (1980s) [74] and others, including the investigations on W/O interfaces [74,75]. The technique was further extended to measurements at W/O interfaces in later studies, which are discussed further below. Reviews on the topic are given, for example, in [71,75,81].

If we consider the application of a monochromatic, fixed-angle ellipsometer, the reflection of polarized light at a surface can be analyzed to reveal the change in amplitude (Ψ) and phase (Δ), where both parameters are affected by the presence of an interfacial layer as well as surface roughness. These parameters, in turn, are related to the complex reflection coefficients of s- and p-polarized light, r_s and r_p, respectively, according to [84]:

$$\frac{r_p}{r_s} = tan(\Psi)e^{i\Delta} \tag{1}$$

For studies at liquid/solid interfaces, the substrate can be tuned such that both Ψ and Δ are sensitive to small changes in the properties (thickness or density) of an interfacial film. This can be achieved, for example, on a silicon wafer by thermally growing the oxide layer to a thickness of some 10s of nm. Unfortunately, one cannot perform such a trick at a fluid interface, where typically Ψ is relatively insensitive to small changes in an interfacial layer within the *thin film limit* (non-absorbing, flat, uniform, isotropic layer with $d << \lambda$, *i.e.*, d is less than a few 10s of nm), and only Δ is sensitive to changes in the thin layer properties. In this case, the ellipsometric signal from an interfacial layer is often presented in terms of $\delta\Delta = \Delta - \Delta_0$, where $\delta\Delta$ – called the phase shift – is the change of the measured ellipsometric angle Δ due to the formation of an interfacial layer compared to the value Δ_0 measured at the bare interface. This procedure also accounts for surface roughness and any errors in the instrumental calibration.

For the study of protein films at fluid interfaces, if we consider in basic terms that $\delta\Delta$ is effectively the additional optical path length of light as it refracts through the interfacial layer (before and after its reflection off the substrate), it can be understood that doubling either the film density (difference in the refractive index compared with that of air) or film thickness will result in double $\delta\Delta$. As a result, for optically transparent layers with a thickness up to the *thin film limit* of up to a few 10s of nm, ellipsometry is sensitive only to the product of density and thickness in terms of the surface excess Γ, rather than either parameter individually. Γ can be calculated according to a formalism proposed by de Feijter et al. [32]:

$$\Gamma = X{\cdot}d; X \equiv \frac{(n_L - n_1)}{\partial n_1/\partial c} \tag{2}$$

where n_L is the refractive index of the protein layer, n_1 is the refractive index of the protein solution, and $\partial n_1/\partial c$ is its increment with respect to the protein concentration; and by Cuypers et al. [85]:

$$\Gamma = 0.3 \bullet Y \bullet d; Y \equiv \frac{(n_L^2 - n_1^2)}{(n_L^2 + 2)[r(n_1^2 + 2) - V(n_1^2 - 1)]} \tag{3}$$

where r is the specific refractivity and V is the partial specific volume of the protein. However, the application of such a model relies on a numerical calculation of d and n_1 from measurements of $\delta\Psi$ and $\delta\Delta$ at the solid/liquid interface or the assumption of n_1 and a model to calculate d knowing n_1 at a fluid interface.

Campbell et al. [45] described approaches of modeling an "oil-like" layer (changing d at constant n_1) or a "particle-like" layer (changing n_1 at constant d) as extreme possibilities related to mechanisms of protein adsorption (and packing) at the W/A interface. In the former case, the model results in a linear relation, whereas in the latter case, the model results in a quadratic relation, according to

$$\delta\Delta = \frac{g(\theta)}{\lambda} \bullet \frac{(n_L^2 - n_2^2).(n_L^2 - n_1^2)}{n_L^2} \bullet d \tag{4}$$

where $g(\theta)$ is a function that depends only on bulk properties and on θ [86], and n_2 is the refractive index of the ambient phase. Substitution of d in Eq. (2) with the expression from Eq. (4) one obtains:

$$\Gamma = X{\cdot}\frac{\lambda}{g(\theta)} \frac{n_L^2}{(n_L^2 - n_2^2).(n_L^2 - n_1^2)}{\cdot}\delta\Delta \tag{5}$$

As a result of anisotropy in the interfacial layer, such a modeling approach from first principles can be challenging even for a system as simple as a monolayer of a low-molecular-weight surfactant [87]. However, the broadly isotropic nature of adsorbed protein layers means

that such an approach can be successful, as was validated, for example, by calibration of protein layers using direct measurements of Γ from NR [45]. Within the *thin film limit* for an *oil-like* layer, a linear relationship between Γ and $\delta\Delta$ exists (because of the approximate linearity at the start of a sine wave), and the deviation from linearity for a *particle-like* layer is generally modest, which motivates the notion that ellipsometry provides 'an approximate measure of the amount of interfacial material'. Depletion effects at the W/O interface in terms of a *drying layer* have also been revealed using ellipsometry [75].

Like BAM, ellipsometry also provides a measure of the lateral homogeneity of an interface in that patches (also termed domains or aggregates) on the μm-scale can result in temporal fluctuations as the domains move in and out of the illuminated area (typically on the order of 1 mm^2 [45]). Such temporal fluctuations can occur at static interfaces (fixed surface area) because of Brownian motion or local surface tension-driven flows or at dynamic interfaces (changing surface area) during, for example, compression of a film in a Langmuir trough. The above discussion focused on monochromatic fixed-angle measurements, but other approaches are acknowledged. Spectroscopic (multiple wavelength) instruments excel in providing a depth of information about thick multilayer films but have also been used on protein films at W/A interface (considered further below). In contrast, multiple angle measurements can help to reveal the refractive index profile of thin layers [76].

The application of ellipsometry at soft interfaces is not without its challenges, such as evaporation, damping vibrations and reducing thermal fluctuations at W/A interfaces. Measurements at W/O interfaces as buried interfaces, however, are even more challenging in terms of eliminating the signal from reflection at the first air/liquid interface. The application has been achieved through several experimental approaches, three of which are schematized in Fig. 2.

From a sample environment viewpoint, the simplest arrangement is letting the laser beam hit and reflect from a W/O interface created in an appropriate vessel [74,75] (Fig. 2-A). Provided the oil is the upper phase open to ambience, the incident beam firstly crosses the oil/air interface at an angle θ' (set by the instrument), then the refracted beam travels through the oil phase and hits the W/O interface at an angle θ (hence, further calculations require correction for θ [88]). Such ellipsometry experiments with protein layers are reported in Refs. [88–90].

To avoid optical effects from the oil/air interface, Benjamins et al. [91] developed an approach where the incident beam and the one reflected from the W/O interface travel through light guides (Fig. 2-B). In this arrangement, it is very important that the beam hits the optical flat windows at normal incidence (where the two polarizations become indistinguishable by construction). Therefore, care should be taken while mounting the light guides onto the arms of the ellipsometer. Such ellipsometry experiments with protein layers are reported in Refs. [92–94].

In another approach, Nylander et al. [95] constructed a special cell with a cuvette as schematized in Fig. 2-C. Here, the laser beam hits the walls of the cuvette at normal incidence. The advantage of this arrangement is that the beam path can be set by choice to travel through either of the two semi-phases (oil or aqueous), provided that the goniometer of the ellipsometer is compatible with such a geometric requirement. In this way, one can apply a co-refined procedure for matching $\delta\Delta$ (reflecting n_L and d of the interfacial layer) based on data pairs measured from both sides of the interface. A disadvantage of this experimental approach is that the angle of incidence is restricted by the

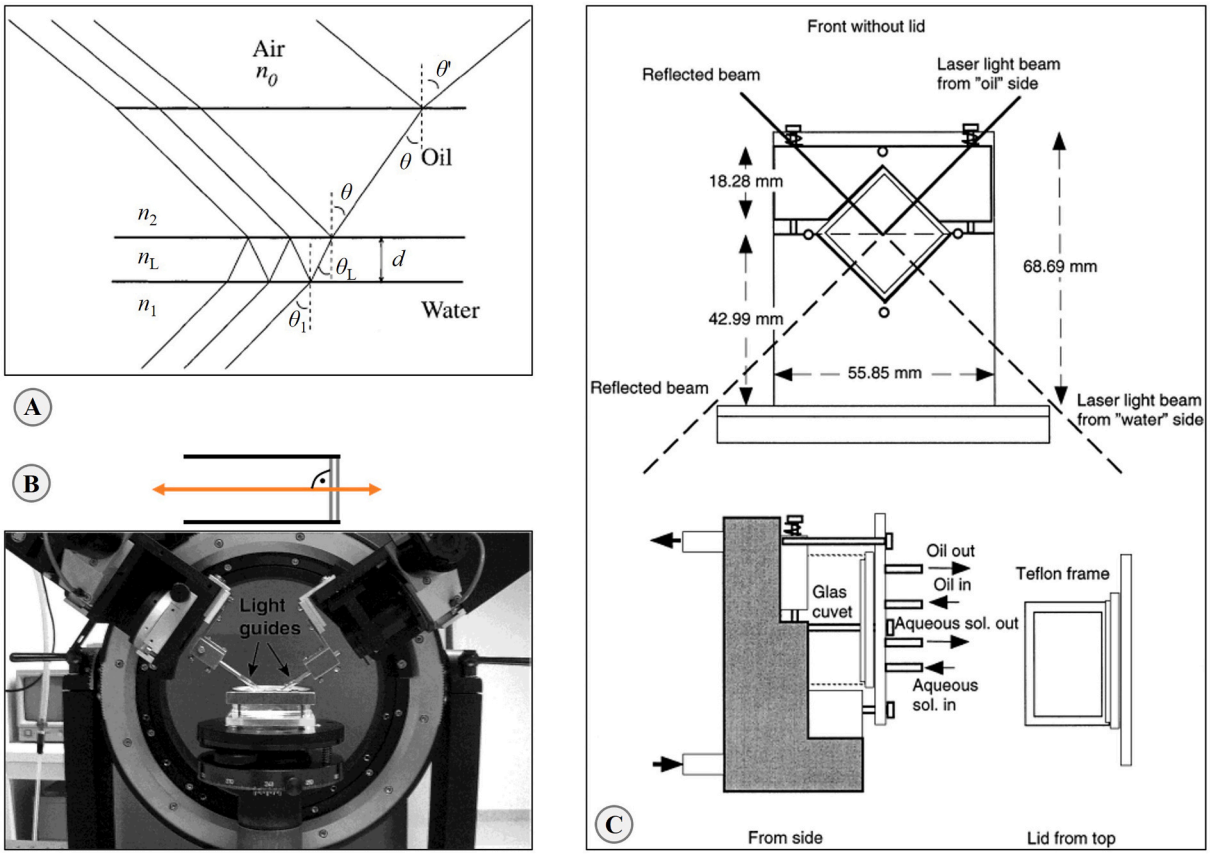

Fig. 2. Setup configurations for ellipsometry measurements at a W/O interface. A. "Simple" arrangement, where the laser beams cross the oil/air interface at a given incident angle θ'. Figure taken with permission from Bylaite et al. [90] copyright 2001 Elsevier. B. Arrangement with light guides. Figure taken with permission from Benjamins et al. [91] copyright 2002 American Chemical Society; the scheme above the photo shows the optical path through a light guide. C. Arrangement with a cuvette. Figure taken with permission from Nylander et al. [95] copyright 1999 Wiley.

geometry of the cuvette, namely $\theta = 45^{o}$ for a standard quadratic profile cuvette. This restriction was, however, overcome by Stocco and co-workers, who used a cylindrical glass cell that allowed multiangle scans to be performed [76].

It should be noted that BAM, as a related reflectometry technique using polarized light [96], has also made a significant contribution to the study of protein films at fluid interfaces [42–49]. A recent review article succinctly covers the technique's capabilities and limitations [97].

3.2. Reflectometry by X-rays and neutrons

Methods based on the reflection of X-rays (XRR) or neutrons (NR) from fluid interfaces are particularly powerful for characterizing protein adsorption layers because these methods probe structures at the relevant length scales [66]. In an XRR or NR experiment, the reflected intensity R is measured as a function of the incident wavelength λ and the grazing angle $\alpha = 90^{\circ} - \theta$ represented by the perpendicular (z) component of the scattering vector:

$$Q_z = \frac{4\pi}{\lambda} sin\alpha. \quad (6)$$

The features of the so-called reflectivity profile $R(Q_z)$ encode information on the density distribution of species normal to the interface in terms of a scattering length density (SLD) profile. For X-rays, the SLD (ρ_x) profile is proportional to the electron density profile: $\rho_x(z) = r_e \cdot \rho_e(z)$ (r_e is the classical electron radius), while for neutrons, the SLD (ρ_n) depends on the nuclear composition of the constituent atoms of the molecules (proteins and water). Reflectivity modulations at low Q_z represent SLD variations on larger length scales, while modulations at higher Q_z correspond to shorter length scales. Thus, the higher the maximum accessible Q_z-value, the greater the ability to resolve the intricate structure of thin protein layers at interfaces.

3.2.1. X-ray reflectometry

Early works with the application of XRR at soft interfaces have dealt with different cases of W/A interfaces – a bare one [77] and ones covered by insoluble organic monolayers [98] or adsorbed surfactants [99]. Further, the method was applied to bare- or surfactant-covered W/O interfaces [78]. Reviews on the topic are given, for example, in [71,78].

Because of the wide accessible Q_z-range, XRR yields sufficient depth resolution to study the structure of thin protein layers. Moreover, XRR can be carried out with laboratory sources and is, therefore, comparatively accessible. A closely related technique, *grazing incidence X-ray off-specular* (GIXOS) [100,101] is less robust with regard to absolute electron density but offers excellent temporal resolution and can, therefore, be the method of choice for studying protein adsorption kinetics [100]. An important limitation to both XRR and GIXOS is that, in contrast to NR, individual chemical components cannot be resolved. Interpretation of electron density profiles is therefore associated with ambiguities regarding the electrons belonging to adsorbed proteins and the electrons belonging to the displaced water molecules. Consequently, neither techniques are very sensitive to the protein surface excess.

When an X-ray beam is reflected from a W/A interface at small grazing angles, total reflection occurs and a standing wave is formed at the interface, which extends into the aqueous phase and decays exponentially with a decay length of typically <10 nm. Consequently, only the immediate vicinity of the interface is probed. This configuration can be exploited for element-specific studies with *grazing-incidence X-ray fluorescence* (GIXF), which exploits the evanescent tail of the standing X-ray wave [100,102]. In the illuminated interfacial region, photoelectric ionization induces the element-characteristic emission of X-ray fluorescence, which is proportional to the interfacial density of the element i of interest in terms of the number of atoms per unit area (Γ_i). Concerning proteins, relevant target elements can be S atoms as constituents of the amino acids cysteine and methionine, P atoms in phosphorylated residues, complexed metal atoms in metalloproteins or counterions accompanying the adsorption of charged proteins. When the number N_i of atoms of type i per protein molecule is known, then the element excess can be directly translated into the protein surface excess, as $\Gamma = \Gamma_i/N_i$.

3.2.2. Neutron reflectometry

NR was utilized for probing different types of surfaces in the seminal paper by Hayter et al. (1981) [79]. In this work, the authors present neutron reflectivity profiles for the following surface systems: 1) organic multilayers on a solid substrate; 2) adsorption of ions at a water/solid (electrode) interface; 3) a bare W/A interface; 4) a surfactant adsorption layer at a W/A interface; and the special case of 5) a thin foam film. A core element of this work was the exploitation of the significant difference between the neutron coherent scattering lengths b_n of deuterium D ($b_n^D = 6.67 \times 10^{-5}$ Å) and hydrogen H ($b_n^H = -3.74 \times 10^{-5}$ Å) *via* deuteration of chemicals (amphiphilic species) and/or using heavy water (D_2O) or deuterated oils. The neutron SLD $\rho_{n,W}$ of 0–100 % aqueous mixtures H_2O/D_2O can be tuned in a wide range (Table 1) by varying the ratio of the components [103]. This possibility has proven extremely useful for matching the scattering isotopic contrast of the aqueous phase to that of other phases or molecular components – for example, air contrast matched water (ACMW) is an H_2O/D_2O mixture with 8.1 % *v*/v D_2O that has the same null SLD as air. This feature of neutron scattering, in comparison to XRR, essentially allows one to highlight a particular species in a mixture to gain sensitivity to its amount and location. In comparison with optical reflectometry, a feature that enables high sensitivity of the location of species in thin films is the low neutron wavelength with around 1–30 Å being exploited on modern instruments, allowing interferometric effects to be resolved within the accessible Q_z-range.

A prerequisite concerning the versatility of the NR technique with respect to variations in the degree of isotopic substitution of the aqueous medium (isotopic contrast) is care about the changes in the SLD $\rho_{n,P}$ of a dissolved protein as a function of the H_2O/D_2O ratio [104] according to the dynamic exchange of labile H by D. Calculation of $\rho_{n,P}$ requires knowledge of both the protein volume in solution and the total scattering length b_n of the protein. Such calculations can be performed nowadays by automated web-based platforms such as, for example, the *ISIS Biomolecular Scattering Length Density Calculator* [http://psldc.isis.rl.ac.uk/Psldc/], which predicts the volume of a protein from the known solvent-excluded volumes of its constituent amino acids. The required input is simply the amino acid sequence of the polypeptide chain of a protein of interest. Protein amino acid sequences can be found, for

Table 1
Neutron scattering length densities of three common aqueous isotopic contrasts $\rho_{n,W}$ and of a protein $\rho_{n,P}$ in each contrast for several of the most frequently studied proteins.

		H_2O	ACMW	D_2O
		$\rho_{n,W}$ [10^{-6} Å^{-2}]		
		–0.56	0	6.39
Protein in water *#	UniProtKB entry	$\rho_{n,P}$ [10^{-6} Å^{-2}] #		
βCS	P02666	2.09	2.18	3.21
BLG	P02754	1.74	1.88	3.02
BSA	P02769	1.85	1.96	3.19
HSA	P02768	2.01	2.10	3.12
LYS	P61626	2.06	2.17	3.44
HFB	P79073	2.20	2.31	3.64
MYG	P02192	1.86	1.94	2.90
OVA	P01012	2.10	2.21	3.45

* The abbreviations of proteins are defined in Table 3.
# The calculations with the *Biomolecular Scattering Length Density Calculator* were performed with the assumption that 100 % of labile H-atoms exchange with the H/D-atoms according to their abundance in a given H_2O/D_2O mixture.

instance, in the UniProt Knowledgebase (UniProtKB) [https://www.uniprot.org/]. The variations of $\rho_{n,P}$ in H_2O, ACMW and D_2O for several frequently studied proteins are given in Table 1. Note that the solvent-excluded volume obtained in this way also serves to calculate the electron density ρ_e and thus the X-ray SLD ρ_x.

Early works with the application of NR on soft interfaces have dealt with the cases of a bare W/A interface and with a W/A interface covered by an insoluble organic monolayer or by an adsorption layer of a surfactant or a polymer [103]. NR has been further applied for probing W/O interfaces [80,105,106]. Reviews on the topic are given, for example, in [71,103,107,108].

NR instruments can either be monochromatic or time-of-flight type and can sit on pulsed or reactor-based neutron sources. The former category of instruments is where a continuous beam of neutrons that has a relatively narrow distribution of λ is measured sequentially at different θ. The latter category is where neutron pulses are created by the spinning discs called choppers, which are constructed of a material that absorbs neutrons but has narrow openings. The pulse generated contains neutrons with a range of λ, and measurements take place at one or only a small number of θ [109]. The latter category is much more common with the new and leading instruments worldwide adopting the approach. Advantages include the acquisition of data in a broad range of Q_z, simultaneously allowing for the resolution of kinetics or other time-dependent dynamic effects [108]. An advantage of a reactor-based source is that the pulse characteristics for time-of-flight can be defined by the choppers rather than the source, and resolution can be loosened for measurements of thin films that do not require high resolution [103], while the advantage of a pulsed source is that all the flux is in the pulses without the drawback of the choppers absorbing a large proportion of neutrons. Although the following point is seemingly obvious, it should be added that a pre-requisite for using a neutron reflectometer for measurements at fluid interfaces is the horizontal sample geometry, which rules out the use of numerous reflectometers with a vertical sample geometry.

A common approach with NR is to record data in multiple isotopic contrasts of the interfacial species and subphase(s) and fit an optical matrix model to a finite number of stratified layers that define the thickness d, volume fraction Φ, roughness and composition. In this approach, individual layers can correspond to distinct interfacial species, or there can be more layers than the types of species with smoothly changing Φ to circumvent artefacts in the analysis from the high topographical roughness, which is particularly relevant for protein films. The contrast variation approach generally relies on the assumption that the system behaves in a chemically identical way in different isotopic contrasts, which is reasonable when driving forces are dominated by the hydrophobic effect (for example, the coverage of an adsorbed surfactant monolayer below its critical micelle concentration), but it can be limited when other driving forces such as hydrogen bonding are prevalent, as the strengths of the hydrogen bonds OH···O and OD···O are different [110,111]. Proteins exhibit strong hydrogen bonding at interfaces, which limits the approach; other factors, such as gravity affecting the density of adsorbed layers in standard and deuterated solvents, might also be problematic.

Solvent deuteration may affect protein stability/flexibility [110,112], which in turn may influence the denaturation and aggregation kinetics in bulk [113], as well as the adsorption dynamics at interfaces [114,115]. Concerning the latter issue, only very recently, a simple experiment for measurements of the adsorption kinetics and dilational rheology of protein layers at liquid/fluid interfaces was proposed as a convenient test for designing the time windows in experimental protocols for NR measurements when various aqueous isotopic contrasts are used [40]. The study with a model protein revealed virtually no effect of substituting H_2O by ACMW and a weak albeit distinct isotopic effect when D_2O was used. However, the observed effect faded away after sufficient time of adsorption layer aging. This simple approach can be employed as a routine test to determine the minimum time required for attenuation of eventual isotopic effects in protein adsorption studies at soft interfaces for any given H_2O/D_2O mixture. As a result of these isotope-specific effects, the solvent is noted in the reporting of specific experimental results from NR in Section 4.

A more recent variant of NR is the low-Q_z analysis method [108]. It was introduced in conjunction with the development of the FIGARO reflectometer at the Institut Laue-Langevin (Grenoble, France), which has high flux at low Q_z, because of its low undeflected angle of incidence, its extension to relatively high wavelengths, and its situation on a reactor source where broad neutron pulses at low resolution in Q_z can be created. The concept of using low-Q_z measurements to measure $\Gamma(t)$ of a monolayer of adsorbing amphiphiles is not new [116], but key developments were: (1) resolving Γ of protein monolayers without the need for sample deuteration on the minute time scale [45,117]; and (2) using parallel measurements of a binary mixture with one component that can be deuterated and both in ACMW to resolve the interfacial composition on the minute time scale [118,119]. Further recent advances in data reduction, such as the use of a divergent beam, can lead to an increase in resolution and, therefore, sample throughput [120], alluding to a potential further increase in the sensitivity and time resolution of the low-Q_z analysis method in the future study of protein mixtures.

NR experiments with W/O interfaces were initially carried out in the early 1990s with the "simple" arrangement shown in Fig. 2-A, but in this case, the oil phase poured over the aqueous phase is present as a very thin layer, relying on the oil phase having a lower density than the aqueous phase [105,106]. This arrangement was used in several NR studies on protein adsorption [121,122]. However, experiments with this configuration rely on a low meniscus beneath the three-phase contact point wall/oil/air, as this meniscus may hamper the detection of the critical edge in the reflectivity curves at the onset of specular reflectivity at relatively low grazing angles. To overcome this problem, the "spin-freeze-thaw" technique was pioneered by Zarbakhsh & coworkers in the late 1990s [123], where a crystal of silicon or sapphire is spin-coated with a very thin layer of hexadecane (with an SLD matched to the crystal) before freezing it; then the frozen coated crystal is mounted in contact with the water solution under investigation in the NR cell (Fig. 3-A), where it is left to reach ambient temperature, at which a fluid W/O interface is formed between the thawed oil and solution. The use of a sapphire crystal was found beneficial due to the better isotopic contrast difference with water [124]. This technique became the 'gold standard' method for studying W/O interfaces using NR for more than a decade and was used in several protein adsorption studies in [124–127]. More recently, with the advent of more powerful neutron instrumentation, including the FIGARO reflectometer, where the neutron beam could be directed up at a horizontal interface (allowing transmission through the denser phase), interest resumed on bulk W/O interfaces. The cell geometries proposed by Schlossman et al. [128] (Fig. 3-B1) and Scoppola et al. [129] (Fig. 3-B2) are optimized for interfaces between two bulk liquid reservoirs and the meniscus under question is minimized at the expense of the compromise that the X-ray or neutron incident and reflected beams cross the cell walls. Lastly, one additional approach was developed, again exploiting the 'reflection down' configuration of the FIGARO reflectometer, where Protat et al. [130] placed a sapphire crystal in contact with an aqueous solution before pouring bulk oil on top and then reducing the thickness of the aqueous phase to several tens of micrometers. However, we are unaware of any protein adsorption studies that have been carried out to date using these latest cell designs.

4. Key results and achievements

The following discussion on the work carried out on protein interfacial layers by ellipsometry, XRR and NR focuses on the experimental details and obtained data, whereas analysis of the results is not given in detail. Since protein adsorption at W/A interfaces is more extensively

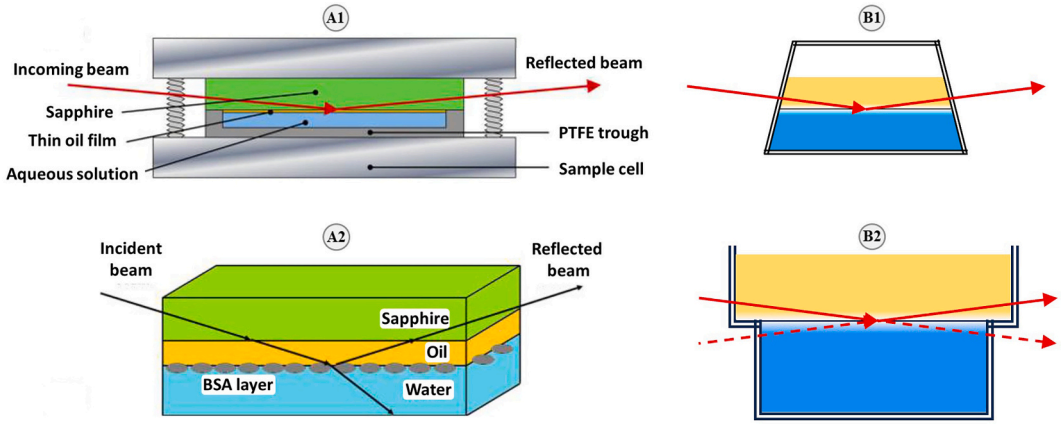

Fig. 3. A. An experimental cell (A1) for NR measurements at a W/O interface by the "spin-freeze–thaw" technique and a scheme (A2) of such an experiment with a BSA adsorption layer. Figure adapted with permission from Campana et al. [124] copyright 2015 American Chemical Society. B. Schemes of experimental cell geometries for XRR and NR measurements (for details see in the text and in [128,129].

studied than at W/O interfaces by the reflectometry techniques featured in the present review article, in Section 4.1, we discuss the achievements for the former case, while in Section 4.2, we discuss the achievements for the latter case; where possible, we provide a comparative discussion on both types of fluid interfaces. Only data obtained at room temperature are considered and information about temperature-dependent effects is omitted. As a summary, Table 2 presents an overview of relevant literature studies for several proteins. The abbreviations of various proteins used in Tables 1 and 2 and throughout the text are defined in Table 3.

4.1. Water/air interface

4.1.1. Adsorption dynamics

To the best of our knowledge, ellipsometry studies on protein layers at soft interfaces started to appear in the middle/late 1970s [26,28,32]. Our literature survey revealed that the most frequently studied proteins at W/A interfaces by ellipsometry are β-casein (βCS) [19,26,28,32,88,131–136] (also κCS [26,32,137] and αCS [135]), β-lactoglobulin (BLG) [19,32,117,138–147], bovine (human) serum albumin BSA (or HSA) [28,32,45,89,131,148–150], LYS [28,54,151–154] and ovalbumin OVA [153–161]. A number of other proteins [47–49,161–165], including enzymes [133,161,166], as well as extracted protein blends [94,167–171] and binary protein/protein mixtures [153] have been investigated by ellipsometry, as summarized in Table 2.

Ellipsometry as a convenient tool for estimating the surface excess Γ can be utilized for measurements under either dynamic conditions $\Gamma(t)$ or at a steady state $\Gamma_s(c)$ of an adsorption layer (here Γ_s is the surface excess at steady state reached after a sufficiently long time of adsorption, where a $\Gamma(t)$ measurement curve levels off). Following the dynamic surface excess $\Gamma(t)$, especially in the initial stage of adsorption, where the adsorption rate $\partial\Gamma/\partial t$ is high, requires relatively quick data acquisition by the ellipsometer. That is achievable when the measurement of the ellipsometric angle Δ is carried out at a fixed angle of incidence θ and wavelength λ (possible not only with monochromatic but also with spectroscopic ellipsometers), *i.e.*, $\Delta_{\theta,\lambda}(t)$ measurement. When the adsorption layer enters the steady state, where the $\Delta_{\theta,\lambda}(t)$ curve levels off, one may apply more complicated experimental protocols including scans at various θ and/or λ.

For example, Fig. 4 shows $\Delta_\lambda(\theta)$ and $\Psi_\lambda(\theta)$ data from 'angular scans' performed on an aging SFP adsorption layer at the W/A interface, which demonstrate two important points in ellipsometry measurements related to the Brewster angle θ_{Br}. (1) The first point is the shift of the typical minimum in the $\Psi_\lambda(\theta)$ dependence, whose position is associated with θ_{Br}. Note that within the *thin film limit*, θ_{Br} for an adsorption layer is very close to the value of $\theta^0_{Br} \approx 53.1^o$ for the bare W/A interface of an aqueous medium with $n_1 \approx 1.33$. The departure of θ_{Br} from this value is due to the formation of a thick interfacial layer. For instance, in the considered case of an aging SFP adsorption layer, the layer thickness after 1 h of adsorption was estimated as $d \approx 15$ nm and $\theta_{Br} \approx \theta^0_{Br}$, whereas after 60 h of adsorption, θ_{Br} increased by about 2^o due to the growth of a much thicker layer ($d \approx 130$ nm). In the latter case, it is not appropriate to treat the measurement data within the *thin film limit*, and the authors used a stratified layer model [94]. (2) The second point concerns the $\Delta_\lambda(\theta)$ dependence. It should be noted that the value Δ_0 for the bare W/A interface is a multiple of 2π ($\Delta_0 \approx 0^o$, 180^o or 360^o within the experimental errors) depending on θ (provided $\theta \neq \theta_{Br}$). This fact determines the typical sigmoidal shape of a $\Delta_\lambda(\theta)$ dependence provided it crosses θ_{Br} (Fig. 4). Obviously, the sensitivity of measurements of $\delta\Delta$ is much higher at the approach of θ_{Br} and this is the reason that in $\Delta_{\theta,\lambda}(t)$ measurements, θ is frequently fixed at values not far away (below or above) from θ_{Br}, but also not too close (due to minimum of the reflection intensity at θ_{Br}, which may cause larger errors of different origins). However, $\Delta_{\theta,\lambda}(t)$ measurements at θ in the vicinity of θ_{Br} have been carried out: $\theta = \theta^0_{Br} \pm 1^o$ [32,135,137,154–157,162,167,168], or even closer to θ^0_{Br} [134,166]. For larger differences between θ and θ^0_{Br}, the most popular cases are $\theta = 50^o$ [19,88,136,140–144,151,158–160] and $\theta = 55^o$ [94,131,132,170,171]. Nevertheless, one also finds studies where other incident angles have been used, for instance: $\theta = 54^o$ [163], $\theta = 48^o$ [169], $\theta = 49^o$ or 56.5^o [117] and the extreme case of $\theta = 70^o$ [164,165] (the latter being more commonly applied in adsorption studies at the solution interface of silicon wafers).

After the early works by Graham, Phillips, Benjamins & coworkers [26,28,32,155], ellipsometry investigations of protein layers at W/A interfaces were reactivated at the very beginning of this century. Studies on the dynamic surface excess $\Gamma(t)$ for various proteins at W/A interfaces *via* $\delta\Delta_{\theta,\lambda}(t)$ measurements were reported by Wierenga & coworkers [142–144,158–160], Miller & coworkers [136,138,151], Stocco & coworkers [94,170,171], Renault & coworkers [135,137,162,167] and other research teams [19,131,132,139,152,163–166]. It is worth mentioning the efforts by Martin et al. [19], who estimated $\Gamma(t)$ for GLY by following the intensity of amide-I and amide-II bands by IRRAS, where the results agree well with comparative data obtained by ellipsometry.

Poirier et al. [94,170,171] employed ellipsometry to investigate the adsorption dynamics of WHP and SFP layers at W/A interfaces. Fig. 5-A presents experimental $\Gamma(t)$ data for SFP and a theoretical prediction by an analytical model of diffusion-controlled adsorption kinetics with saturation [94]. Gochev et al. [117] measured the adsorption kinetics of BLG at different pH by ellipsometry and NR. The $\delta\Delta_{\theta,\lambda}(t)$ data were

Table 2
Studies on protein interfacial layers by ellipsometry, X-ray and neutron reflectometry.*.*

Protein	Method	Ref.	
		W/A	W/O
βCS	Ellipsometry	[19,26,28,32,88,131–136]	[88,93]
	XRR	[18,63,133]	–
	NR	[18,121,133,188,189,191,199]	[121]
κCS	Ellipsometry	[26,32,137]	–
	XRR	[63]	–
αCS	Ellipsometry	[135]	–
BLG	Ellipsometry	[19,32,117,138–147]	[89,93]
	XRR	[64,175,176]	–
	NR	[115–117,176,189,191,201–205]	[205]
BSA	Ellipsometry	[28,32,89,131,148–150]	[28,89]
	XRR	[179]	–
	NR	[122,187,194,195,207]	[124–127]
HSA	Ellipsometry	[45]	–
	XRR	[180]	–
	NR	[45,180]	–
LYS	Ellipsometry	[28,54,151–154]	[28]
	XRR	[58,177,181–186]	–
	NR	[46,154,177,192,193,200,201]	[122]
HFB	Ellipsometry	[163]	–
	XRR	[178]	–
	NR	[178,190,191]	–
MYG	Ellipsometry	[47]	–
	XRR	[175]	–
	NR	[175]	–
OVA	Ellipsometry	[153–161]	–
	NR	[154]	–
OVT	Ellipsometry	[162]	
LFR	NR	[196]	–
GLY	Ellipsometry	[19]	–
FBG	Ellipsometry	[164,165]	
COL	Ellipsometry	[48,49]	–
SPD	Ellipsometry	[167]	
AFP, CHC, HGL, LBM	Ellipsometry	[161]	–
COE-3	NR	[197,198]	[125,126]
Enzymes			
LPS	Ellipsometry	[166]	[92]
	NR	[206]	–
INV	Ellipsometry	[133]	
	NR	[133]	
GOS, ADS, URS	XRR	[174]	–
CTS, HTG, INS, RNS	Ellipsometry	[161]	–
Protein blends			
CHP	Ellipsometry	[168]	–
SPI	Ellipsometry	[169]	
WHP	Ellipsometry	[170,171]	–
SFP	Ellipsometry	[94,171]	[94]
WPB	Ellipsometry	–	[95,211]

* Some studies focused on mixtures of a protein and other species, where usually only a reference measurement of the pure protein system has been reported, are omitted.

processed *via* Eqs. (4,5) making use of the values for the layer thickness d estimated from NR measurements. The obtained $\Gamma(t)$ results for pH 7 and pH 5 → pI (where pI is the isoelectric point) from ellipsometry are presented in Fig. 5-B, along with relevant NR data (on the minute time scale) obtained by employing the low-Q_z analysis method. The agreement between ellipsometry and NR results is good.

The combination of ellipsometry and tensiometry measurements gives access to the experimental equation of state $\Pi(\Gamma)$ by combining data for the adsorption isotherm $\Gamma_s(c)$ and the surface pressure isotherm $\Pi_s(c)$ [26], where Π_s is the steady state surface pressure reached after a sufficiently long time of adsorption, and where a $\Pi(t)$ measurement curve levels off. When such a dependence is obtained from adsorption kinetics data $\Pi(t)$ and $\Gamma(t)$, for example, when measured simultaneously

Table 3
Abbreviations of proteins (including enzymes) and protein blends used in this article.

Proteins (including enzymes)	
ADS	alcohol dehydrogenase
AFP	antifreeze protein
BLG	β-lactoglobulin
BSA	bovine serum albumin
CHC	cytochrome *c*
COL	collagen
βCS	β-casein
κCS	κ-casein
αCS	α_{s1}-casein
CTS	catalase
FBG	fibrinogen
GLY	(soy) glycinin
GOS	glucose oxidase
HGL	hemoglobin
HFB	hydrophobin
HSA	human serum albumin
HTG	chymotrypsinogen
INS	insulin
INV	invertase
LBM	α-lactalbumin
LFR	lactoferrin
LPS	lipase
LYS	lysozyme
COE-3	a monoclonal antibody
MYG	myoglobin
OVA	ovalbumin
OVT	ovotransferrin
RNS	ribonuclease
SPD	spidroin
URS	urease
Protein blends	
CHP	champagne proteins
SFP	sunflower proteins extract
SPI	soy proteins isolate
WHP	wheat proteins extract
WPB	whey protein blends

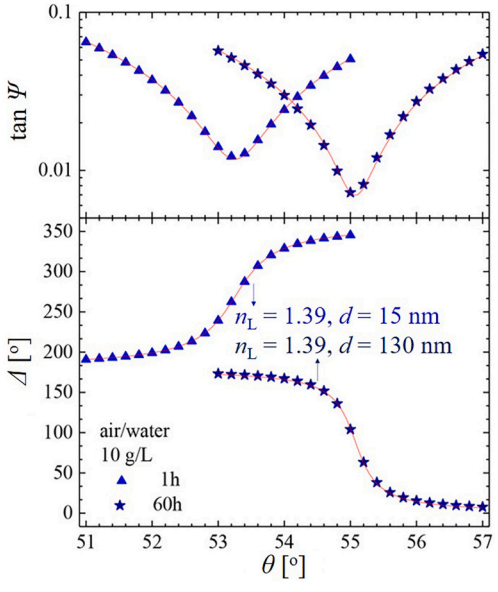

Fig. 4. Ellipsometry dependences $\Delta_\lambda(\theta)$ and $\Psi_\lambda(\theta)$ obtained from 'angular scans' performed on an aging SFP adsorption layer at the W/A interface (λ = 533 nm,); the symbols are experimental data and the solid lines are model fits by a one-layer model with the indicated values for n_L and d (for details see the original publication). Figure adapted with permission from Poirier et al. [94] copyright 2021 American Chemical Society.

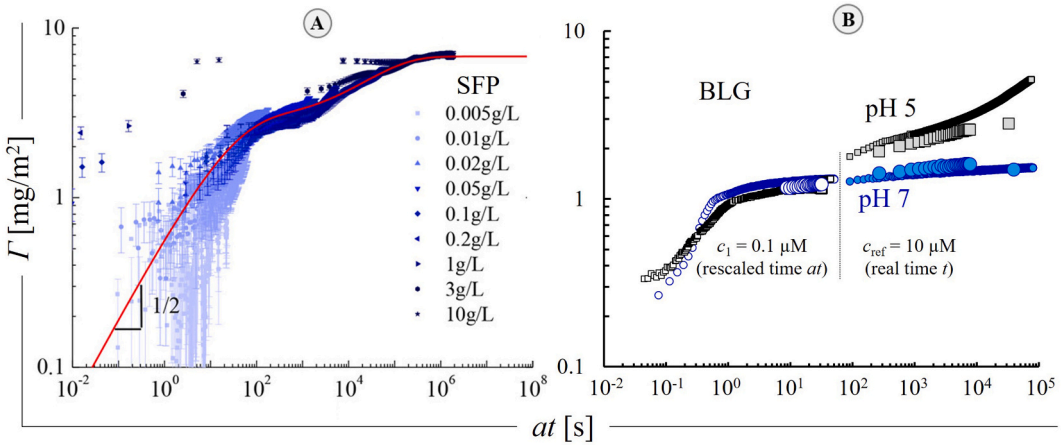

Fig. 5. Dynamic surface excess $\Gamma(t)$ for protein adsorption layers at the W/A interface; note, the time scale is presented in terms of rescaled times at for different protein concentrations c, where a is a scaling factor. A. SFP (pH 10, 0.1 mM NaOH): symbols are ellipsometry experimental data ($\lambda = 533$ nm, $\theta = 55^o$) for various c ($a = 1$ for the reference concentration of $c_{ref} = 0.1$ g/l), the solid line is a model fit (for further details about the estimation of a and the used model see the original publication [94]). Figure adapted with permission from Poirier et al. [94] copyright 2021 American Chemical Society. B. BLG (in 10 mM buffer) at $c_1 = 0.1$ μM ($a = 1.6$) and $c_{ref} = 10$ μM, and at pH 5 (□) and pH 7 (○), smaller symbols are ellipsometry data ($\lambda = 633$ nm, $\theta = 56.5^o$) and the corresponding larger symbols are NR data (on ACMW subphase). Data taken with permission from Gochev et al. [117] copyright 2019 American Chemical Society. The scaling factor used here is defined as $a = (c_1/c_{ref})^b = 6.31 \times 10^{-4}$, calculated with $b = 1.6$ as estimated from the dependence $t_{ind} \propto c^b$ (t_{ind} is induction time) using the $t_{ind}(c)$-data in Ref. [172].

in a Langmuir trough, then "dynamic" $\Pi(\Gamma(t))$ curves are obtained [155]. Fig. 6 shows a few such examples for OVA [155], SPD [167], and for SFP and WHP [171]. Such type of adsorption results was also reported for βCS [134,135], αCS [135], κCS [137], BLG [140,142] and again for OVA [158–160].

Careful inspection of the many studies summarized in Table 2 shows that measurements of the steady state surface excess Γ_s for different proteins (at different protein concentrations and solvent conditions) were performed by means of all three methods considered. One finds 'full' adsorption isotherms $\Gamma_s(c)$, *i.e.*, in a wide c-range, as measured with ellipsometry, *e.g.*, for βCS [28,135,136], κCS [26], αCS [135], LYS [151] and HSA [45], and with XRR or NR, *e.g.*, for βCS [18], HSA [45], COE-3 [197,198], HFB [190] and some others.

Fig. 7 presents a collection of literature data $\Gamma_s(c)$ for βCS at near-neutral pH > pI (from ellipsometry, XRR and NR) as reproduced from the original publications listed in Table 4. Grigoriev et al. [136] and Beaufils et al. [135] compared their experimental data sets $\Gamma_s(c)_{pH\ 7}$ from ellipsometry with a theoretical model (continuous lines in Fig. 7) accounting for the formation of a secondary protein molecular layer onto the primary monolayer. It is clear from Fig. 7 that the $\Gamma_s(c)_{pH\ 7}$ data significantly scatter. Inspection of the information in Table 4 leads to the conclusion that the ionic strengths (I) of the solutions used in the different studies cannot be the major reason for such discrepancies, which are rather large at the higher βCS concentrations, for example, through a comparison of the data by Aschi et al. [199] ($I \geq 200$ mM), by Graham-Phillips [28] ($I = 100$ mM) and by Grigoriev et al. [136] ($I \approx 10$ mM). The origin of the observed discrepancies cannot be attributed to the experimental methods applied either. The data by Puff et al. [133] revealed insignificant differences between the results from ellipsometry and NR (D_2O-rich water), while Harzallah et al. [18] reported systematically higher Γ_s-values measured with XRR than those measured with NR (on D_2O subphase). The authors discussed some reasons for this discrepancy, such as technical aspects of the models for the treatment of the measurement data (a uniform slab for NR and a power-law profile for XRR) as well as physicochemical effects originating from the isotopic solvent contrast (D_2O *vs.* H_2O). Currently, we cannot propose a reasonable explanation for the broad experimental scatter in these collected results.

To the best of our knowledge, the first XRR studies on protein layers at soft interfaces appeared in the late 1990s [18,173,174]. Those studies

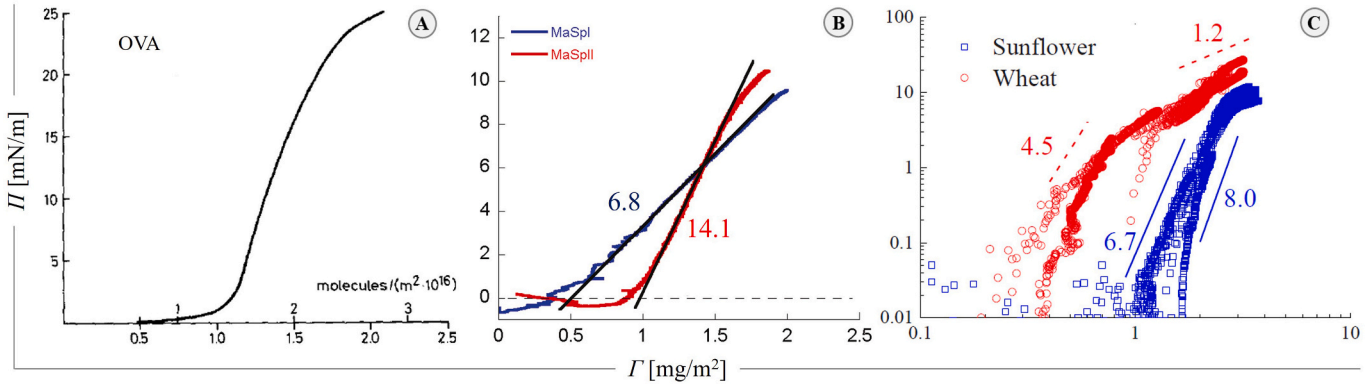

Fig. 6. Experimental "dynamic" equations of state Π(Γ(t)) for protein adsorption layers at W/A interfaces obtained from simultaneous measurements of $\Pi(t)$ (Wilhelmy plate) and $\Gamma(t)$ (ellipsometry) in a Langmuir trough. A. OVA (pH 6.7); ellipsometry ($\lambda = 632.8$ nm, $\theta = 52.04^o$). Figure adapted with permission from de Feijter and Benjamins [155] copyright 1982 Elsevier. B. Spidroin (SPD) variants MaSpI (pH 7) and MaSpII (pH 11); ellipsometry ($\lambda = 632.8$ nm, $\theta = 52.12^o$); continuous straight lines are linear regressions. Figure adapted with permission from Renault et al. [167] copyright 2009 American Chemical Society. C. (note the log scale) Sunflower protein extract SFP (pH 10) and wheat protein extract WHP (pH 3); ellipsometry ($\lambda = 533$ nm, $\theta = 55^o$); continuous and dashed straight lines are power law fits. Figure adapted with permission from Poirier et al. [171] copyright 2022 Elsevier.

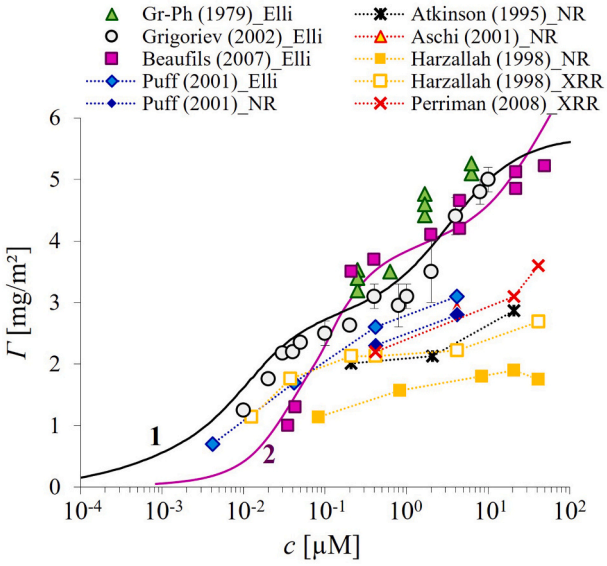

Fig. 7. Adsorption isotherms $\Gamma_s(c)_{I,\mathrm{pH}\ 7}$ for βCS measured by different methods at pH 7 > pI and at room temperatures. Symbols are experimental data as reproduced from the original figures in the relevant publications listed in Table 4; ('Gr-Ph' stands for Graham-Phillips, 'Elli' stands for ellipsometry). Dotted lines are guides to the eye and continuous lines are model fits to the respective experimental data: (1) Grigoriev et al. (2002) [136] and (2) Beaufils et al. (2007) [135]. Discussion is provided in the text.

Table 4
Experimental conditions for the measurements with ellipsometry and NR summarized in Fig. 7. '(*NA*)' stands for not available information, '—' stands for lack of experiment and '(*NC*)' stands for not considered here.

Work	Ref.	Electrolytes	Ellipsometry	NR (solvent contrast)
Graham-Phillips (1979)	[28]	$I = 100$ mM	$\lambda = 546.1$ nm, θ (*NA*)	–
Grigoriev et al. (2002)	[136]	$c_{buff} = 10$ mM	$\lambda = 532.0$ nm, $\theta = 50^o$	–
Beaufils et al. (2007)	[135]	$c_{buff} = 20$ mM	$\lambda = 632.8$ nm, $\theta^0_{Br} \pm 1^o$	–
Puff et al. (2001)	[133]	$c_{buff} \approx 10$ mM	$\lambda = 632.8$ nm, $\theta = 53.6^o$	D_2O/H_2O ($\rho_n = 5.34 \times 10^{-6}$ Å^{-2})
Atkinson et al. (1995)	[189]	$c_{buff} = 20$ mM	–	ACMW
Aschi et al. (2001)	[199]	$c_{buff} \approx 100$ mM + NaCl 100 mM	–	D_2O/H_2O (ρ_n (*NA*))
Harzallah et al. (1998)*	[18]	$c_{buff} \approx 10$ mM	–	D_2O
Perriman et al. (2008)#	[63]	$c_{buff} = 50$ mM	–	(*NC*)

* pH 7.1 (no information about correction for pD).
\# pH 6.85, XRR experiments.

Table 5
Values for the thicknesses d_1 and d_2 for the four globular proteins in Fig. 12 as resolved by NR and the solution formulations studied.

Protein	Ref.	Substrate (D_2O)	d_1 [Å]	d_2 [Å]
BSA	[194]	$c = 1.00$ g/l, pH 5, $c_{buff} = 20$ mM	42 ± 3	30 ± 5
LYS	[192]	$c = 4.00$ g/l, pH 7, $c_{buff} = 20$ mM	47 ± 3	30 ± 3
MYO	[175]	$c = 0.50$ g/l, pure D_2O	16 ± 1	30 ± 3
BLG	[117]	$c = 0.18$ g/l, pH 5, $c_{buff} = 10$ mM	15 ± 2	55

and later ones [58,63,64,133,175–186] were carried out for W/A interfaces. Protein layers at W/A interfaces were also probed by GIXOS and GIXF [100,101]. We are aware of only a handful of studies where GIXF was utilized for adsorbed proteins [100,101]. Neither XRR (GIXOS) nor GIXF appear to have been involved in studies of W/O interfaces.

As mentioned above, the estimation of the surface excess with XRR (or GIXOS) is associated with ambiguities due to the interpretation of the total electron density profiles (protein + H_2O). Nevertheless, values of Γ are reported in many of the XRR studies listed in Table 2. The high X-ray flux at synchrotron facilities is a prerequisite for fast acquisition of reflectivity data, and time-resolved measurements of the dynamic surface excess $\Gamma(t)$ are possible at a time resolution of a couple of minutes. That was demonstrated for LYS by Yano et al. by means of XRR [181–185] or of a combined XRR/GIXOS procedure [186], as well as by Singh et al. using GIXOS [100]. In the latter study, the adsorption kinetics of LYS is presented in terms of the time dependences of the surface coverage. Furthermore, the results of the GIXF measurements targeting the 10 S atoms of LYS obtained in the same study were largely consistent with the GIXOS results, which demonstrated the capabilities of GIXF for probing protein adsorption dynamics.

To the best of our knowledge, the first NR studies on protein layers at soft interfaces appeared in the early 1990s with the works of Eaglesham et al. [187] and Dickinson et al. [116,121,188] for W/A interfaces with one of the studies by Dickinson et al. also providing the first NR study on protein layers at W/O interfaces [121]. Until the present day, bodies of NR studies for W/A and W/O interfaces appeared by Dickinson & coworkers [116,121,188,189], Thomas, Penfold & coworkers [190,191], Lu & coworkers [124–126,192–198], Douillard & coworkers [18,133,199], White, Holt & coworkers [175,176,180,200,201], Fischer & coworkers [202–205], Campbell & coworkers [45,46,117,180] as well as by other scientific teams [115,122,127,154,206,207].

NR experiments with ACMW provide an unambiguous determination of the surface excess Γ, because the bare ACMW/Air interface does not reflect neutrons ($\rho_n^{ACMW} = \rho_n^{Air} = 0$) and any registered reflectivity signal originates solely from the interfacial layer having SLD $\rho_n \neq 0$. ACMW is, therefore, ideal for protein adsorption kinetic studies with NR. Application of the low-Q_z analysis approach [108] has led to improvement in the temporal resolution of $\Gamma(t)$ measurements from on the order of 1 h in earlier studies, *e.g.*, by Horne et al. on BLG [116], through to the minute time scale as reported in recent studies by Campbell & coworkers on HSA [45] and BLG [117] (see Fig. 5-B).

It is well known that changes in the dynamic surface pressure $\Pi(t)$ for protein solutions (usually in H_2O) may last for many hours depending either on the protein concentration or on the solvent conditions (pH and I) [21,27,170,208]. The same holds for the dynamic surface excess $\Gamma(t)$ as revealed mainly from ellipsometry measurements (usually on H_2O subphase) [19,88,117,131,132,135–137,154,156,162,163,167], but also by means of NR (on ACMW subphase) [115–117,188,189,198]. Already in the early NR studies, it was shown that the increase in the time scale of $\Gamma(t)$ may be of the order of several hours, for example, 4–6 h for BLG at pH 6 > pI and $c = 1$ g/l (55 μM) [188,189]. A similar situation was found in ellipsometry and NR measurements for a lower BLG concentration of $c \approx 0.18$ g/l (10 μM) at pH 7 (Fig. 5-B) [117]. However, at a higher BLG concentration of $c = 10$ g/l (550 μM) and pH 7, the build-up of a saturated BLG monolayer seems to be established within 1 h as measured by XRR (on H_2O subphase) [176]. About 1 h was also found to be sufficient time for obtaining constant NR profiles for 'high' protein concentrations (*ca.* 1 g/l) of BSA (or HSA) [194] and LYS [192], whereas for 'low' protein concentrations, 8–10 h were required. A continuous increase of the dynamic surface excess is especially pronounced under conditions where a secondary protein layer is formed, for instance, as in the generally accepted case of protein adsorption from a solution at near-isoelectric solvent conditions (in the vicinity of pI), *e.g.*, at pH 5 for 0.1 g/l (4.2 μM) βCS [88] or for 0.18 g/l (10 μM) BLG (Fig. 5-B) [117],

but not only since the formation of a secondary layer was also clearly detected by ellipsometry in the case of 0.24 g/l βCS at pH 7 [136].

Combined studies of proteins at W/A interfaces employing ellipsometry together with NR [18,45,117,133,154] have been performed by a few research teams. Douillard & coworkers [18,133] performed comparative measurements of Γ_s for βCS with ellipsometry, XRR and NR, which were considered in the above discussion in Fig. 7. In this relation, Perriman et al. encountered a similar situation with BLG [176] and with LYS [177] (both at $c = 10$ g/l and near-neutral pH), namely, $\Gamma_s^{NR/XRR} > \Gamma_s^{NR}$, where $\Gamma_s^{NR/XRR}$ is a value obtained from a co-refinement analysis of data from XRR and NR.

An essential aspect in the studies on proteins at soft interfaces is the influence of the solvent conditions, namely, pH and the ionic strength I. The strong influence of these factors originates from charge-induced effects on the protein-protein electrostatic interactions either in bulk or at the interface. Effective reduction of the protein net charge at the approach of pH towards pI or/and its electrostatic screening at high I, cause weakening of the protein-protein electrostatic repulsion, which enhances adsorption, *e.g.* [54,117,122,143,161,172,189]. At a given c and pH ≠ pI, an increase of I leads to an increase of the surface excess $\Gamma_s(I)_{c,pH}$. For example, ellipsometry measurements showed that an increase of I from 10 to 200 mM results in about 25% growth of the Γ_s-value for BLG at pH 7 > pI and $c = 0.1$ g/l (5.5 μM) [143]. Moreover, ion-specific effects, *e.g.*, associated with the type and valence of metal ions [63,146,147,156,189], salting-out effects [186,193,194,207] and others, can play a role. Various types and concentrations of electrolytes (including different types of buffers) have been used in different studies. This fact hampers comparisons of independent results. Most works that are not dedicated to investigations of electrolyte effects have been carried out usually at a fixed I-value, which varies in different studies: from the extreme case of proteins in pure water (negligible I), where I may eventually reach *ca.* 1–2 mM (depending on pH and c) due to the use of HCl/NaOH for pH-adjustment, *e.g.* [54,145,150,165,166,169,191,201], to salt (including buffers) concentrations on the order of hundreds of mM, *e.g.* [28,165,179,199]. However, the use of buffers is a typical practice when working with proteins and the most frequently used buffer concentrations in adsorption studies are $c_{buff} = 10$–50 mM, which may be counted as moderate ionic strengths (where the Debye length is significantly, but not drastically, diminished).

Renault & coworkers used ellipsometry to investigate the influence of pH on the steady-state adsorption of OVA and S-OVA (a thermostable derivative, which spontaneously forms from native OVA during egg-white storage) [156,157]. The obtained data were reported in terms of $\delta\Delta_{\theta,\lambda}$(pH) dependences (Fig. 8-A) and show that the adsorption of S-OVA is enhanced at pH ≤ pI (pI ≈ 4.5) as compared to the case for pH > pI, but the effect is much stronger at a 'high' c, whereas for a 'low' c the $\delta\Delta_{\theta,\lambda}$(pH) data appear to be linear. Surprisingly, the results for native OVA at even 'higher' c reveal almost pH-independent adsorption behavior. No significant impact of pH on Γ_s and d at a steady state was also observed in NR studies on adsorption layers from HFB [190] and the monoclonal antibody COE-3 [198].

An attempt to underline general trends in the influence of pH on Γ_s for BLG was made by Gochev et al. [117]. The authors summarized relevant adsorption data from the literature in the parameter space map $\{\Gamma_s, pH, c, I\}$ and the results are presented in Fig. 8-B in terms of $\Gamma_s(pH)_{c,I}$ plots. A maximum in Γ_s can be clearly outlined in the pH region around pI ≈ 5.1, but such a trend appears to be dependent on the protein concentration c, and the maximum disappears at comparatively low c (*ca.* 0.1 μM (1.8×10^{-3} g/l)). The observed c-dependent influence of pH on the adsorption behavior of BLG is also reflected by a crossover of the surface pressure isotherms $\Pi(c)_{I,pH}$ at pH 5 and pH 7 [39]. The same complex c-pH effect in the $\Gamma_s(pH)_{c,I}$ dependences for BSA [194,195] and LYS [193] adsorption layers was reported earlier in the NR works by Lu & coworkers. Furthermore, these authors found that for a given c, these dependencies are quite sensitive to large changes in the ionic strength (20 mM *vs.* 1 M) for both studied proteins. Enhanced adsorption in the pH region near pI was also detected in NR experiments with MYO [175].

Braunschweig & coworkers [54,145,147,150] and Guckeisen et al. [161] used a combination of ellipsometry and SFG spectroscopy to investigate the effect of pH on the adsorption and electrical properties of a range of proteins (see Table 2). They used a fixed value of $n_L = 1.40$ as a reasonable common approximation to evaluate the layer thickness from the ellipsometry measurements. In these studies, the authors were not interested in the absolute value of d, but in its systematic change with pH. The observed maximum in the d(pH) dependence for either of the studied proteins well correlates with the solution pH at which a charge reversal at the interface occurs, as detected with SFG spectroscopy. The comparison of the ellipsometry and SFG results with zeta-

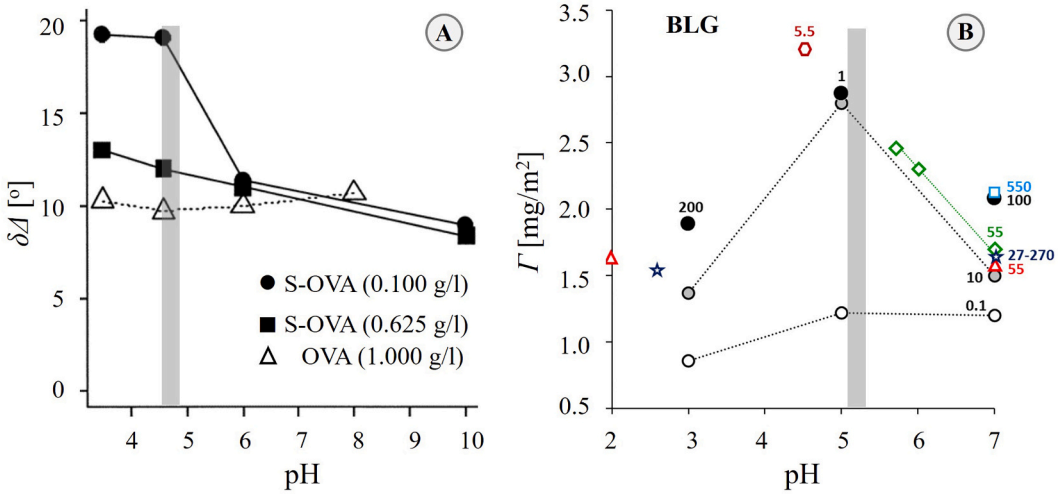

Fig. 8. Influence of pH on the adsorption of globular proteins at W/A interfaces. A. OVA and S-OVA. Steady-state ellipsometric angle $\delta\Delta$ *vs.* pH, ellipsometry measurements at $\lambda = 632.8$ nm and $\theta = \theta_{Br}^0 \pm 1°$; solutions in various buffers at $I \approx 60$ mM. Figure adapted with permission from Renault et al. [157] copyright 2002 American Chemical Society. Grey-shaded ribbons encompass the vicinities of pI. B. BLG. Steady-state surface excess Γ_s *vs.* pH obtained from NR measurements (on ACMW subphase). Circles are data at a buffer concentration of $c_{buff} = 10$ mM from Ref. [117]; other symbols are complementary literature data: red triangles (salt-free) [201], dark-blue stars (salt-free) [191], green diamonds ($c_{buff} = 20$ mM) [189], light-blue square ($c_{buff} = 50$ mM) [176], dark-red hexagon ($I = 2$ mM) [115]; labels indicate BLG concentrations in [μM]. Figure adapted with permission from Gochev et al. [117] copyright 2019 American Chemical Society. (For interpretation of the references to color in this figure legend, the reader is referred to the web version of this article.)

potential measurements led to the important conclusion that the pI of a protein in bulk solution does not significantly change upon adsorption at the W/A interface.

Another line in the studies on proteins at fluid interfaces is the effect of chemical denaturants on the adsorption characteristics and interfacial structural organization of globular proteins. Lin et al. [64] performed NR experiments in a flow trough, where a solution of the chemical denaturant guanidine hydrochloride (G.HCl) was introduced in the aqueous subphase (pH 7) beneath a pre-adsorbed BLG layer in order to monitor changes in the BLG layer due to surface reactions. In fact, only a subtle response was observed, which allowed the authors to conclude that a largely intact oriented, monomolecular BLG film had been formed at the outset of the experiment and that eventual surface reactions due to the action of the denaturant are rather weak – a situation in contrast to the one considered in other works, where protein/denaturant reactions took place in the bulk. Noskov & coworkers used ellipsometry and surface dilational rheometry to investigate changes in the adsorption and surface rheological behavior of several globular proteins at pH 7 (BLG [139], LYS [152] and MYG [47]) due to protein denaturation in solutions containing various concentrations (c_{den}) of a denaturant (G. HCl or urea). Denatured protein globules exhibit higher surface excess (and at the same time, lower dilational elasticity) than the respective native globules. However, the results by Perriman et al. [176,177] from XRR and NR experiments showed only a weak effect of these denaturants on the surface excess of BLG and LYS studied at near-neutral pH (here Γ even slightly decreases with increase of c_{den}), but complicated dependences of the layer thickness $d(c_{den})$ – either (monotonic or stepwise) increase in d for BLG [176] or the existence of a minimum in the $d(c_{den})$ data for LYS [177]. In the latter case, the authors assumed that the observed behavior of LYS is due to changes in the orientation of the protein molecules at the interface. Regardless of the interpretations of the surface excess results considered above by various research groups [47,139,152,176,177], it is evident that complementary information about either the layer thickness or the minimum number of layers required to describe the protein structure at fluid interfaces would be beneficial to gain a more detailed understanding of the interfacial behavior of proteins. Researchers most commonly model the SLD profiles with stratified layers of constant SLDs but gradual transitions between them. Each layer has adjustable parameters for its thickness, its plateau SLD, and the width of the transition to the next layer. In order to minimize the number of free parameters, the number of layers is then kept as small as possible (*e.g.*, one or two, and in some cases, three), but large enough to be able to provide the best physically reasonable fit to the experimental reflectivity data. Once such a fit is achieved, the obtained SLD profile model can be considered an accurate representation of the true laterally and temporally averaged SLD profile. Further interpretations of such profiles can then be based, for instance, on assumptions of the shapes of (deformed) protein globules as well as of protein dimers (or higher oligomers) and on the water content of each layer. We emphasize, however, that layer-based models are not the only way to model experimental reflectivity curves. Other mathematical descriptions based on molecular shapes and orientational distributions can be used as well, for instance, power law or exponential type of protein volume fraction distributions $\Phi(z)$, as will be discussed further below. Importantly, they will consistently have to yield SLD profiles that reproduce the experimental data. These aspects will be discussed in the following section.

4.1.2. Structure of protein layers

Patino & coworkers [42–44] utilized BAM to measure what they called the relative reflectivity R_r of a p-polarized laser beam ($\lambda = 690$ nm) from either spread or adsorbed protein layers. It is worth mentioning that in the case of adsorption layers from soy globulins, the authors could follow the adsorption kinetics in terms of $R(t)$ curves [44]. The experiments with spread layers of βCS [42] or soy globulins [43] showed very good complementation with corresponding pressure-area Π-A curves (further supported by BAM images), reflecting structural transitions in the studied protein monolayers through a distinct reflectivity increase in the obtained R_r-Π curves (Fig. 9), where R_r reaches a maximum at the monolayer collapse. The R_r-measurements have provided an estimation of the relative layer thickness but did not give direct access to the absolute layer thickness. A more refined optical reflectivity approach for the estimation of d at soft interfaces is ellipsometry, and an even greater depth of information can be provided by XRR and NR, which will be discussed further below.

As mentioned above, within the *thin film limit* (d lower than some 10s of nm), ellipsometry is sensitive only to the product of density and thickness of an interfacial layer in terms of the surface excess $\Gamma(n_L,d)$, rather than either parameter individually. However, existing optical models and mathematical procedures based on the theory of ellipsometry [209,210] do allow decoupling of n_L and d based on paired measurement data sets for $(\delta\Delta)_{\theta,\lambda}$ and $(\delta\Psi)_{\theta,\lambda}$, and this approach has been used in the early ellipsometry studies on proteins [26,28,32], and in many other works after that. In a recent publication, Muth et al. [166], working at $\lambda = 632.8$ nm and $\theta = 52.86^o$ (very close to θ^0_{Br}, which allows for increased sensitivity to $\delta\Psi$), and applying optimized measurement algorithms, analyzed both experimental dependences $\delta\Delta_{\theta,\lambda}(t)$ and $\delta\Psi_{\theta,\lambda}(t)$ for adsorption layers of LPS, and determined n_L and d with fairly high precision, which allowed for achieving sub-monolayer resolution and thus concluding about the orientations of the LPS (ellipsoidal) globules at the interface as a function of c and pH [166].

Multi-wavelength ellipsometry was used in several studies on protein adsorption [48,148,149,164]. Franses & coworkers investigated steady-state adsorption layers from BSA [148,149] and FBG [164] working at wavelengths λ of 405 nm, 546 nm and 633 nm and at comparatively high incident angles θ of 60° or 70°. They used two approaches: 1) analyzing the paired $\delta\Delta_{\theta,\lambda}$-$\delta\Psi_{\theta,\lambda}$ measurement data or 2) analyzing only the $\delta\Delta_{\theta,\lambda}$ measurement data by fixed d to a certain value in the range (4–14 nm for BSA and 15–50 nm for FBG) based on the size and the possible orientation of the protein molecules at the interface. The authors concluded that method 1 (when applicable) delivers more reliable results for n_L and d. A good consistency was found amongst the results obtained under different experimental conditions (θ,λ) and then analyzed by the two methods.

In fact, although the modeling of ellipsometry measurement data can be well constrained within physically reasonable limits for n_L and d, it usually appears that coupled n_L and d values are resolved with relatively high uncertainty, yet their product leads to relatively low uncertainty in the calculation of $\Gamma(n_L,d)$ (*e.g.*, Eqs. 2–5). Hence, in some works on

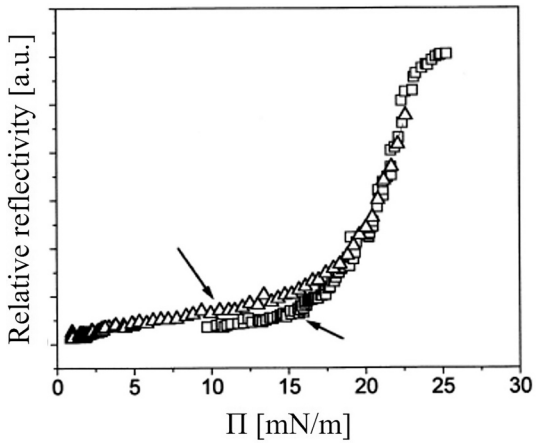

Fig. 9. BAM reflectivity *vs.* surface pressure Π in compression of spread βCS layers; aqueous subphase: $I = 50$ mM, (□) pH 5 and (Δ) pH 7. The arrows indicate structural transitions detected in corresponding pressure-area Π-*A* curves. Figure taken with permission from Patino et al. [42] copyright 1999 Elsevier.

protein layers at soft interfaces, either Γ or simply measured values of $\delta\Delta$ are reported (see previous section). Another approach is measurement data treatment by assuming the value of n_L or d to calculate the other, usually n_L in order to obtain values for d, for instance, $n_L = 1.375$ [92], $n_L = 1.40$ [54,145–147,150,161], $n_L = 1.46$ [163], $n_L = 1.49$ [169], $n_L = 1.58$ [117]. In these cases, refractive indices have been used of ≈1.40 for a layer comprising protein and water (on the assumption of the layer volume fraction) or of ≈1.58 for a 'dry' layer comprising only protein (with excluded water content), consistent with experimentally accessible data for protein densities of ≈1.3–1.4 g/cm^3 and refractive index increments of ≈0.18 cm^3/g. In the latter case, the thicknesses obtained must be understood as *equivalent thicknesses*, and they can be used to calculate Γ directly without knowing of the actual layer volume fraction [117].

To a first approximation, $\delta\Psi$ can be neglected, and then $\delta\Delta$ measurements are the only experimental source. Such information is sufficient for evaluating Γ (see Section 3.1), and this approach was used in several protein studies considered in the previous section, but it is insufficient for decoupling the product (n_L,d). Russev et al. [88] resolved this issue by applying a minimization procedure to analyse paired measurement $\delta\Delta$ data sets obtained from two types of experiments with a βCS solution in contact with either air or with xylene (an oil). Furthermore, the authors treated the measurement data with one-slab and two-slab structure models in order to resolve the double-layer structure of the βCS layers. For the studied βCS layers (c = 0.1 g/l (4.2 μM), pH 5), this was carried out by assuming values of the thicknesses of the peptide-rich part of the monolayer oriented towards the air(oil), namely with a thickness of 1.8 nm, and then evaluating the remainder of the layer oriented towards the solution (with a thickness of 5.4 nm) together with the corresponding refractive indexes of 1.450 and 1.366, respectively. Grigoriev et al. [136] interpreted their ellipsometry data by the formation of a double-layer structure of adsorbed βCS molecules (pH 7, c_{buff} = 10 mM). The measured $\delta\Delta_{\theta,\lambda}$-$\delta\Psi_{\theta,\lambda}$ data were analyzed *via* a simplified approach, which considers the βCS layer as relatively thick and inhomogeneous in density; then the evaluated layer parameters are only averaged quantities $n_{L,av}$ and d_{av}, however, still yielding reliable values for Γ. The obtained protein concentration dependence of the layer thickness $d_{av}(c)_{I,pH\ 7}$ revealed the onset of a secondary layer formation at about 2 μM (0.5 g/l), which correlates well with the corresponding adsorption isotherm $\Gamma(c)_{I,pH\ 7}$ shown in Fig. 7. More detailed information about the thickness and density of multilayered protein structures at soft interfaces has been gained by experiments with XRR and NR, and these will be considered further below.

Historically, NR has been utilized to resolve the structure of protein adsorption layers at soft interfaces earlier than XRR. Eaglesham et al. [187] performed measurements on the CRISP reflectometer at the ISIS Neutron and Muon Source (Oxfordshire, UK) and demonstrated how the capabilities of NR could be employed in protein studies by applying an elegant experimental approach to investigate the structuring of BSA at the W/A interface. Firstly, the authors used a spread protein layer on pure water (compressed to Π = 15 mN/m); hence, any issues with adsorption kinetics or electrolyte effects were excluded. Secondly, four different aqueous isotopic contrasts were used. Good quality fits to the reflectometry data were obtained with one-slab or two-slab models for the layer structure, and Fig. 10-A shows the values of the layer thickness obtained. The application of a two-slab model led to consistent results for all the used aqueous isotopic contrasts, yielding averaged values of $d_A \approx 1.1$ nm and corresponding volume fractions of $\Phi_A \approx 0.93$ for the upper slab oriented towards the air and $d_W \approx 2$ nm and corresponding volume fraction of $\Phi_W \approx 0.05$–0.1 for the bottom slab oriented towards the solution. The authors attempted to interpret these results by assuming a monolayer of protein molecules that have undergone strong distortion of their tertiary structure at the interface with a peptide-rich upper slab (d_A,Φ_A) and a peptide-poor bottom slab (d_W,Φ_W) consisting of hydrophilic chains dangling in the substrate medium. However, the authors did not exclude the possibility that the bottom slab comprises additional solubilized protein molecules, but they concluded that the state-of-the-art NR technique at those times did not provide direct information for discriminating between these two scenarios. Hence, a conceptual problem was identified, namely, whether the determined two-slab structure describes a heterogeneous monolayer or the accumulation of a secondary discrete molecular layer.

In the following NR works, Dickinson & coworkers investigated adsorption layers of βCS [121,188,189] and BLG [116,189], also involving a two-slab structure with peptide-rich (high Φ_A) and a peptide-poor (low Φ_W) regions, as schematized in Fig. 10-B for βCS. In the case of βCS (c = 0.05 g/l (2 μM), pH 7), relevant sets of reflectivity data obtained in ACMW and in D_2O were treated *via* a two-slab model, delivering partially consistent results: $d_A \approx 2$ nm (ACMW and D_2O), and $d_W \approx$ 5 nm (ACMW) and $d_W \approx 7.2$ nm (D_2O) [121]. In the latter study, the reflectivity data were obtained in a Q_z-range up to about 0.11 Å^{-1}, whereas in a study published soon afterwards by Atkinson et al. [189] performed with solutions of similar composition, but only in ACMW, a Q_z-range of only up to about 0.04 Å^{-1} was achieved, yielding $d_A \approx 1$ nm and $d_W \approx 4.4$ nm. The structure of βCS adsorption layers on ACMW was found to be dependent on pH (Fig. 10-B), as a decrease from pH 7 to 5.5 caused almost double an increase of d_A (constancy of Φ_A) and an increase of d_W of about 36 % (≈20 % increase of Φ_A) [189]. In the case of

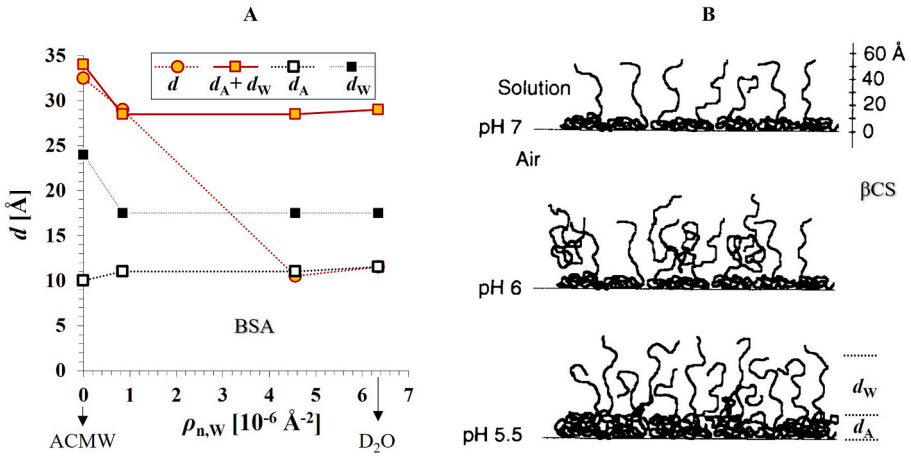

Fig. 10. A. The NR results by Eaglesham et al. [187] for BSA spread layers at the W/A interface; layer thickness as a function of the water SLD ($\rho_{n,W}$) for H_2O/D_2O mixtures, evaluated *via* a one-slab (d) or a two-slab (d_A, d_W) models (see Fig. 11). Plots were constructed from the data listed in the original publication. B. Schematic representation of the two-slab structure of βCS adsorbed on ACMW (c = 0.05 g/l (2 μM), c_{buff} = 20 mM) as a function of pH > pI. Figure adapted with permission from Atkinson et al. [189] copyright 1995 The Royal Society of Chemistry.

aged BLG layers ($c = 0.1$ g/l (5.5 μM), $c_{buff} = 20$ mM, pH 7), the two-slab model yielded $d_A \approx 1$ nm and $d_W \approx 2.1$ nm. Decreasing pH from 7 to 5.74 led to a slight increase in the overall layer thickness (from ≈3 nm to ≈4 nm), but interestingly, the BLG layer at pH 5.74 could be fitted well by a one-slab model [189]. The authors expressed that further work would be needed to resolve the more complex pH-dependent behavior found for the globular protein BLG compared to the disordered βCS. The effects of pH on the structure of protein adsorption layers will be discussed further below.

Later on, in the late 1990s, more NR works [18,192–195,206] and the first XRR works [18,173,174] on protein adsorption at A/W interfaces appeared, and >30 such works have been published in the 21st century (see Table 2). For the case of NR, the modernization of existing reflectometers and the launching of new ones have allowed for achieving higher flux over extended Q_z-ranges and, hence, higher resolution to the intricate structural details of thin protein films.

In the following, we discuss findings for individual proteins. To ease the presentation, we show in Fig. 11 a scheme of a multi-slab structural model with denotations of the slabs corresponding to different distinguishable parts of an overall interfacial layer as built up by protein molecules at the W/A interface. The presented concept for such an interfacial structure is based on the state-of-the-art approaches for XRR and NR data analysis. In the discussion on literature results, the denotations for layer thicknesses (and respective volume fractions) proposed in Fig. 11 will be used.

- *βCS*

Harzallah et al. [18] studied the structure of βCS layers (pH 7 > pI, $c_{buff} \approx 10$ mM) by XRR and NR. They concluded that XRR and NR results are consistent, although the XRR data contained more detailed structural information due to the wider accessible Q_z-range. To treat the X-ray reflectivity data, the authors adopted a power law model for the volume fraction distribution $\Phi(z)$ in a *train-loop-tail* structure. At 'low' βCS bulk concentrations, the proximal region with thickness $d_A \approx 1$ nm and volume fraction $\Phi_A \approx 0.6$ is formed by trains and loops. At βCS bulk concentrations $c > 0.005$ g/l (0.2 μM), the distal region is formed by loops and long tails with a total thickness of $d_W \approx$ 4–5 nm, where the Φ_W distribution changes from a power law type to an exponential type in the z direction normal to the interface and towards the solution bulk. This structure is consistent with the scheme presented in Fig. 10-B and is virtually unchanged up to $c = 0.1$ g/l (4.2 μM). This fact is consistent with the corresponding adsorption isotherm $\Gamma(c)$, which is relatively 'flat' in the considered c-range. That is in certain contradiction with other relevant data, as discussed in the previous section (see Fig. 7). Later studies with βCS at near-neutral pH reported the same type of layer

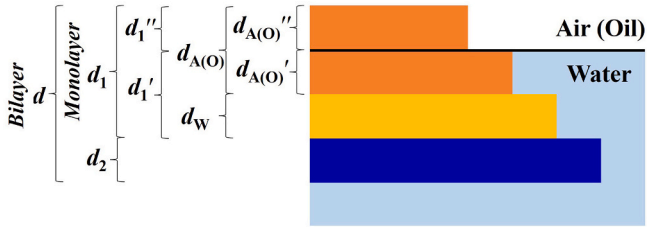

Fig. 11. Schematic of a multi-slab model of the structure of a protein layer at the W/A interface (not to scale; the length of a bar does not have a physical meaning). Legend: d - overall layer thickness; d_1 - overall thickness of a monomolecular layer; d_2 – thickness of a secondary molecular layer; d_W - thickness of peptide-poor part of monolayer oriented towards the water solution; $d_{A(O)}$ - thickness of peptide-rich part of monolayer oriented towards the air (oil); superscripts (′) and (″) correspond to the two parts of the monolayer – the one immersed in water and the one protruding into the air(oil), respectively. The proposed denotation may be analogously used for slab protein volume fractions Φ; note that usually $\Phi_{A(O)} > \Phi_W \sim \Phi_2$.

structure with the following parameters, XRR: $d_A \approx$ 1.5–2 and $d_W \approx$ 2–3 nm [63]; NR: $d_A \approx 5.3$ and $d_W \approx 8.6$ nm (in D_2O-rich water) [199], $d_A \approx$ 3 and $d_W \approx 4$ nm (in D_2O-rich water) [133], and $d_A \approx 4.5$ and $d_W \approx 4.2$ nm (in ACMW) [191]. The values are, however, subject to minor changes with the addition of κCS or Ca^{2+} [63]. Using XRR, Holt & White [173] concluded that the interfacial structure of commercial milk is dominated by βCS. The obtained data were described again within the two-slab model with $d_A \approx 2$ nm and $d_W \approx 3$ nm, which were both attributed to βCS. This structure was not qualitatively different for skimmed or aged milk.

Returning to Fig. 7, we recall the evident discrepancies in the values of the surface excess of βCS at the higher concentrations. The XRR and NR results, discussed immediately above, form a lower branch in this part of the adsorption isotherm compared to a higher branch of values obtained by ellipsometry. Furthermore, the considered XRR and NR studies do not confirm the presence of a secondary molecular layer bound to the primary monolayer, as postulated from ellipsometry data in Refs. [135, 136].

- *BLG*

After the above-considered early works by Dickinson & coworkers [116,189], BLG was further investigated with XRR [64,176] and NR [115,117,175,176,191,201–205]. It should be noted that apart from some notable differences in the reported layer thicknesses, there is a conceptual difference in the interpretation of the layer structure. An overview of most of the NR studies on BLG adsorption layers at the W/A interface was given by Gochev et al. (2019) [117]. Notably, IRRAS experiments revealed that BLG adsorbs at the W/A interface with little changes in its secondary structure [57].

Firstly, we consider the case of studies performed at near-neutral pH. Applying a co-refinement approach for evaluating the reflectivity data from XRR and NR (ACMW), Perriman et al. [176], like in the NR study by Atkinson et al. [189], concluded a two-slab structure of the investigated BLG monolayer with $d_A \approx d_W \approx 1.8$ nm. In an XRR study, Lin et al. [64] reported a three-slab structure with slab thicknesses of ≈1.6 nm, ≈2–3 nm and ≈2.3 nm in the direction from air to water. The total thickness ($d \approx$ 6–7 nm) compares well to the long axis of the BLG dimer [117], but the authors did not comment on this fact. There is an obvious difference in the layer structure between these results and those by Perriman et al. [176], although both series of experiments were performed with solutions of the same composition ($c = 10$ g/l (550 μM), $c_{buff} = 50$ mM).

In contrast to these reports, neutron reflectivity data acquired by other research teams and performed at various c and I involved the application of a one-slab structure to model BLG monolayers, where the protein globules (monomers) are deformed (flattened) at the interfaces in comparison to their almost spherical shape in solution. The obtained results are: $d \approx 1.8$ nm (ACMW, pH 6, $c_{buff} = 20$ mM) [116], $d \approx 3$ nm (ACMW, pH 2 or 7, salt-free) [201], and $d \approx$ 2–2.5 nm (ACMW, pH 2.6 or 7, salt-free) [191].

Fischer & coworkers [202–204] employed a three-slab model to fit their NR data for BLG adsorption monolayers on buffered D_2O subphase at comparatively low protein concentrations (0.01–0.18 g/l (0.55–10 μM)) and at different pH in the acidic range (excluding near-pI conditions). The authors reported overall monolayer thicknesses of $d \approx$ 1.4–2 nm, but did not comment on details about outcomes from the usage of a three-slab model.

Ganzevles et al. [115] and Gochev et al. [117] studied BLG layers under near-pI conditions with NR, applying a co-refinement analysis of data for ACMW and D_2O. In the first case at pH 4.5 < pI ($c = 0.1$ g/l (5.5 μM), $I = 2$ mM), the authors reported the highest surface excess amongst the literature data collected in Fig. 8-B, which corresponds to a one-slab layer structure with $d \approx 4$ nm. In the latter case at pH 5 → pI ($c = 0.18$ g/l (10 μM), $c_{buff} = 10$ mM), the authors reported a two-slab structure where the first slab (in contact with air) is a monolayer with thickness $d_1 \approx 1.7$

nm and the second slab (exposed to the solution) is a secondary molecular layer with thickness $d_2 \approx 5.5$ nm composed of disordered BLG dimers [117] (Fig. 12). The thicknesses ($d = 1.6 \pm 0.2$ nm) of BLG monolayers at two studied values of c (0.1 and 10 μM) for any of the studied pH values (3, 5 and 7) were found to be virtually indistinguishable, in excellent agreement with the results by Fischer & co-workers [202–204]. Hence, a conceptual difference in the interpretation of the BLG layer structure is demonstrated, namely the formation of a molecularly discrete structure of the overall interfacial layer (called *bilayer* in the following), characterized by the thickness-density parameters (d_1,Φ_1) and (d_2,Φ_2), which in the presentation in this article should be discriminated from the ones (d_A,Φ_A) and (d_W,Φ_W) that characterize a monomolecular interfacial layer with heterogeneous density distribution.

This scenario of the complex c-pH effect on the structure of protein layers has been found in earlier NR works on BSA and LYS by Lu et al. [193,194], which are considered further below. The main conclusion is that the formation of a protein *bilayer* interfacial structure requires not only near-isoelectric solvent conditions (pH → pI) but also sufficiently high protein bulk concentrations c, which, however, might be diminished by the action of salting-out effects [193,194].

- *BSA (and HSA)*

After the early report by Eaglesham et al. [187], the structure of adsorption layers of BSA was studied in a few works with NR [122,193,194] and XRR [179]. Stenger et al. [179] studied BSA at $c = 2$ g/l (30.2 μM), pH 7, $I \approx 150$ mM salts buffering mixture (NaCl/$CaCl_2$/$NaHCO_3$)); Fourier transform treatment of the XRR data displayed two peaks at $z \approx 5$ nm and $z \approx 8.5$ nm, meaning necessity for a two-slab layer structure. In a recent NR (D_2O) study, Theodoratou et al. [122] reported insignificant changes in the resolved one-slab structure ($d \approx 2$–2.4 nm) of BSA layers ($c = 1$ g/l (15 μM), pD 7, salt-free D_2O) from the addition of 150 mM NaCl.

Lu et al. [194] investigated BSA with NR (D_2O) and found a moderate effect of pH (3, 5 and 7.2) and BSA concentration (0.005 and 1 g/l) on the BSA monolayer thickness ($d \approx 2.8$–3.8), which peaked at pH 5. As for the layer structure resolved in solutions of BLG [117], for a 'high' BSA concentration of $c = 1$ g/l (70 μM) at pH 5, a *bilayer* interfacial structure was found with $d_1 \approx 4.2$ nm and $d_2 \approx 3$ nm. In addition, an appreciable influence of the ionic strength on the surface excess and layer thickness was found, which will not be discussed here. As a summary of their research, the results for the layer thickness as influenced by the interplay of effects from c, pH and I is illustrated in Fig. 13-A in terms of $d(\mathrm{pH})_{c,I}$ dependences.

Furthering their NR investigations, the same authors applied an elegant approach to account for the degree of protrusion of the BSA layer out of the solution into the air. It was achieved by combined experiments with D_2O and a *protein-contrast-matched-water* (PCMW) subphase. Note that, unlike ACMW, for PCMW, the D_2O/H_2O ratio is a protein-specific quantity since for a given solvent isotopic contrast $\rho_{n,W}$, the values of $\rho_{n,P}$ are slightly different for different proteins (see Table 1). For BSA, PCMW with $\rho_{n,W} = \rho_{n,P} = 2.5 \times 10^{-6}$ Å^{-2} was used in [194]. The thickness of the 'dry' slab d_A'' of the protein monolayer that protrudes into the air was found to be 0.5–1 nm (with the reminder d_A' staying immersed in the substrate), *i.e.*, the fraction of the 'dry' adsorption layer was resolved as 10–30 %, which is in agreement with results for a range of proteins (2–19 %) obtained with the so-called *tritium planigraphy* technique [31].

In a subsequent study that also used NR (ACMW), Lu et al. [195] performed a comparison of the behavior of BSA and HSA [195]. No significant differences were found in the pH-dependent adsorption and layer structures for both albumin forms – these albumin molecules adsorb at the W/A interface with little breakdown of their globular framework and adopt predominantly a side-on configuration to form a monolayer. Note that only small changes in the secondary structure of BSA occur upon adsorption at the W/A interface [57].

In a more recent study on HSA, Ang et al. [180] performed a combined XRR/NR study on native HSA and a "defatted" derivative (both at $c = 0.1$–10 g/l and pH 7). Although the $\Gamma(c)$ data suggest some differences between the interfacial properties of the two forms of HSA, the structural results are rather similar, showing a two-slab monolayer structure with $d_A \approx 1.6$ nm and $d_W \approx 3.5$ nm. In another combined XRR/NR work, Campbell et al. [45] investigated spread layers of HSA, where the authors exploited the formation of kinetically-trapped films. In this case, a denatured layer of HSA was shown to be present in the network structure at low spread amounts, and additional slabs were required in the modeling as the surface coverage increased.

- *LYS*

Lu et al. [192,193] used NR to study LYS adsorption layers at different c and pH (2−12) at $c_{buff} = 20$ mM. The evaluation of the layer thickness was based on experiments with ACMW, while PCMW was used to estimate the extent of protrusion of the LYS layer out of the solution into the air (for LYS, where in this case, PCMW was a 1:1 mixture of D_2O/H_2O with $\rho_{n,W} = \rho_{n,P} = 2.9 \times 10^{-6}$ Å^{-2} [192]). At pH 7, the monolayer thickness slightly increases (3–4.7 nm) within the concentration range 0.0009–4 g/l (0.06–280 μM) and protrudes into the air at some 1 nm [192], which, although slightly higher was still in qualitative agreement with the value of ≈0.4 nm found in *tritium planigraphy* experiments [31]. Surprisingly, for this pH < pI (11), a *bilayer* interfacial structure was found with $d_1 \approx 4.7$ nm and $d_2 \approx 3$ nm (Fig. 12), but only for the highest studied LYS concentration of $c = 4$ g/l. For two lower concentrations of $c = 0.03$ and 1 g/l, the monolayer thickness varies in a complex c-pH-I manner and at pH → pI virtually the same *bilayer* structure as the one mentioned above was formed (Fig. 13-B). A general conclusion from these studies is that LYS preserves, to a great extent, its globular framework upon adsorption as a monolayer independent of the

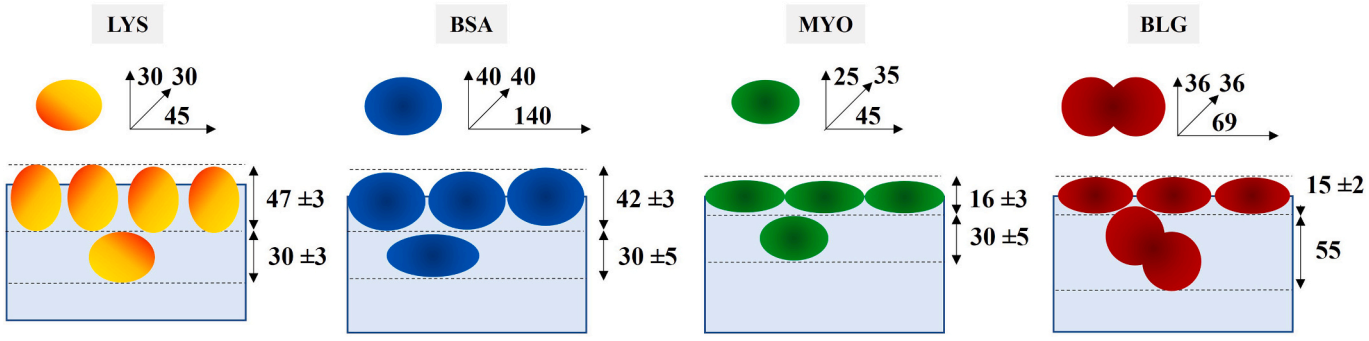

Fig. 12. Schematic representation (not to scale) of the bilayer structure (discrete molecular slabs) of adsorption layers of four globular proteins at W/A interfaces with the corresponding values for the thicknesses d_1 and d_2 [Å] as resolved by NR: LYS [192], BSA [194], MYO [175] and BLG [117]; the respective solution formulations are given in Table 5. Below the protein name labels are given the crystallographic dimensions of the species in bulk solution in [Å].

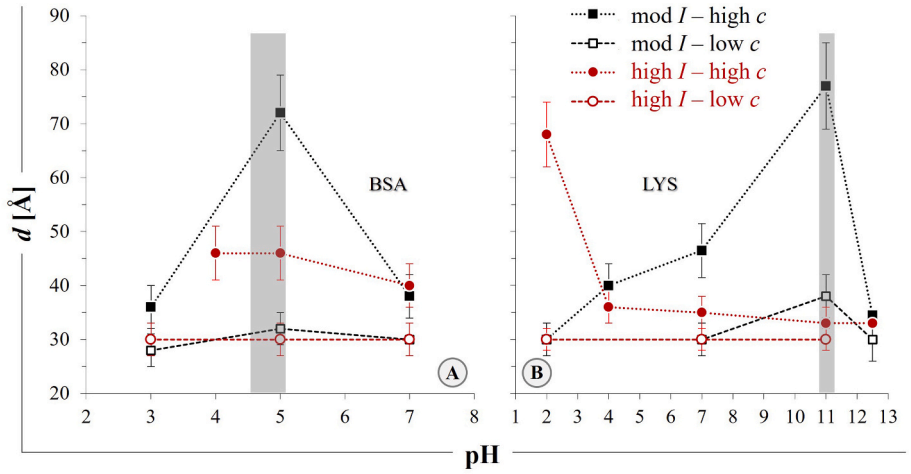

Fig. 13. NR results for $d(\mathrm{pH})_{c,I}$ dependences for BSA (A) and LYS (B) at two ionic strengths: a lower one, which is relatively moderate ionic strength, of $I = 20$ mM ("mod I") and a higher one of $I = 1$ M ("high I"), and at different protein concentrations: a lower concentration "low c" of 0.005 g/l (BSA) and 0.03 g/l (LYS), and a higher concentration "high c" of 1 g/l for both proteins. The legend is common for both figures; grey-shaded ribbons encompass the vicinities of pI. Fig. A adapted with permission from Lu et al. [194] copyright 1999 Elsevier. Fig. B adapted with permission from Lu et al. [193] copyright 1999 American Chemical Society.

pH. It is noteworthy that the presence of 1 M NaCl suppresses the formation of a secondary layer at pH → pI (Fig. 13-B) [193].

Postel et al. [58] performed a combined XRR/IRRAS study on LYS at different concentrations in the range 0.0076–0.1 g/l ($I \approx 120$ mM buffer/NaCl at near-neutral pH). They found an overall layer thickness of $d \approx 2.5$–3 nm, comparable to the two shorter axes of the LYS crystalline structure (30 × 30 × 45 Å). These results suggest that the globules are not deformed upon adsorption and may adopt a side-on configuration at the interface that is in agreement with the above-considered NR results by Lu et al. [192,193]. However, a very good fit of a two-slab model to the reflectivity data revealed the fine structure of the monolayer with $d_A \approx 1.5$ nm and $d_W \approx 1.2$ nm, suggesting that the native structure of LYS adopted in bulk is distorted upon adsorption but without significant globular deformation. This result is supported by data from IRRAS, which revealed that the secondary structure of the protein is modified in a way that most of the α-helices are replaced by β-sheets, which in turn is in agreement with the IRRAS study by Lad et al. [57] and distinguishes the behavior of LYS from that of BLG and BSA (*i.e.* minor changes in the secondary structure upon adsorption as mentioned above).

For the case of near-neutral solutions of 10 g/l LYS, the XRR/NR results by Perriman et al. [177] revealed a monolayer structure with $d_A \approx 1.9$ nm and $d_W \approx 2.8$ nm ($c_{buff} = 50$ mM), while the NR results by Holt et al. [201] revealed a one-slab monolayer structure ($d \approx 3.7$ nm) on a salt-free D_2O subphase. These overall monolayer thicknesses suggest that the adsorbed LYS globules do not deform significantly upon adsorption.

Pasquier et al. [154] used NR (D_2O) to follow changes in the structure of LYS layers with time (1 g/l (70 μM), pD 7, $c_{buff} = 20$ mM). They observed that during the increase of the dynamic surface excess $\Gamma(t)$, the two-slab structure of the LYS monolayer ($d_1 = d_A + d_W$) reorganizes, and its thickness d_1 slightly increases from 4.6 nm to 6 nm within 8–10 h. Since 6 nm is beyond the globular dimensions of LYS (Fig. 12), it is most probable that a secondary layer develops in the course of adsorption. Indeed, after 10 h of adsorption, the $\Gamma(t)$ data from different protein concentrations and buffer conditions levels off, requiring three slabs in the model with a total thickness of ~9 nm, confirming the presence of an extended interfacial topography. The results are generally in good agreement with those by Lu et al. [192] on samples recorded at pH 7 and $c = 4$ g/l, and at pH 11 and $c = 1$ g/l (Figs. 11–12). These results suggest that the globular framework of LYS (in bulk) presumably does not break up upon adsorption at the W/A interface, and the observed variations of the monolayer thickness ($d_1 = d_A + d_W$), being within the globular dimensions of LYS, describe different orientations of the ellipsoidal globules at the interface [192]. On the other hand, some studies suggest that the LYS globules do deform (flatten) upon adsorption [46,100,101,122,181,183,186].

The GIXOS experiments by Singh et al. [100,101] with LYS at the same protein concentration as in the study by Perriman et al. [177] ($c =$ 10 g/l), but in pure water, revealed the formation of an adsorption monolayer with ≈2 nm thickness, suggesting flattening of the LYS globules upon adsorption. Isothermal lateral compression of this monolayer (d-Π curve), through reduction of the surface area, causes layer thickening to about 5 nm ($\Pi \approx 36$ mN/m, a surface pressure unachievable in protein adsorption experiments) following two regimes: one due to the conformational changes and one due to layer buckling. The NR results by Theodoratou et al. [122] yielded $d \approx 2$ nm for the monolayer of adsorbed LYS ($c = 1$ g/l (15 μM), pD 7, salt-free D_2O), which was practically not affected at the addition of 150 mM NaCl.

Campbell et al. [46] used NR to follow the adsorption kinetics of native and G.HCl-denatured deuterated LYS in ACMW (150 mM buffer/NaCl, pH 7). The obtained steady-state thickness for the native LYS monolayers formed by two relatively low LYS concentrations ($c = 0.35$ and 3.5 μM (0.005 and 0.05 g/l)) were very close at $d \approx 1.5$–1.7 nm, which is less than the short axial length of the molecule, indicating interface-induced denaturation. The addition of G.HCl increased the adsorption rate and, counterintuitively, perhaps, an increase in the layer thickness, which were attributed to the incomplete collapse of LYS globules in the bulk due to interactions between remote amino acid residues.

Information about the evolution of the structure of LYS layers with time was gained by Yano et al. [181,183,186] using XRR with temporal resolution on the minute time scale. The first acquisition of a reflectivity profile was at just 1 min after injection of LYS solution into the aqueous substrate. At pH 7 and $I = 35$ mM, the monolayer had an overall thickness of $d \approx 1.5$ nm ($c = 0.01$ g/l) or $d \approx 2.7$ nm ($c = 1$ g/l) [181]. These results suggest that flattening of the LYS globules, due to interaction with the W/A interface, occurs already in the very initial stages of adsorption, even during the stage of the induction time, where the molecules are in a surface-gaseous phase [208]. For comparison, solutions of 0.01 g/l LYS at pH 7.4 and buffer/NaCl concentration of 167 mM exhibited an induction time of about 40 min. At longer times, a *bilayer* interfacial structure developed. Interestingly, these studies reveal that the presence of 2 M NaCl has indeed a certain influence on the *bilayer* interfacial structure at pH 7 [183,186], whereas it suppresses the formation of a secondary layer at pH → pI [186], in agreement with the

results by Lu et al. [193] shown in Fig. 13-B.

- *Other proteins*

The XRR study by Gidalevitz et al. [174] revealed that the enzymes GOS, ADS and URS strongly deform upon adsorption at the W/A interface and form "peptide sheets" ($d \approx 1$ nm), while the NR (D_2O) study by Lee et al. [206] revealed that LPS adsorption layers have an overall thickness of about 7 nm, which is comparable to the LPS molecular dimensions.

Recalling the NR (D_2O) study by Pasquier et al. [154], we note that the same research approach was applied also to OVA. At pH 7 and $c_{buff} =$ 20 mM, the overall layer thickness of about 8.5 nm established after 8–10 h of adsorption may be interpreted such as to describe a *bilayer* interfacial structure with $d_1 \approx 5.5$ nm and $d_2 \approx 3$ nm.

The NR (salt-free D_2O) study by Holt et al. [175] on MYO for a range of protein concentrations revealed the formation of a monolayer ($d_1 \approx$ 1.5 nm) at $c < 0.5$ g/l and *bilayer* interfacial structure ($d_2 \approx 3$ nm) at higher c (Fig. 12). The authors interpreted this monolayer thickness as a result of either deformation or unfolding of the MYO globules upon adsorption.

Lu et al. [196] used NR (ACMW and D_2O) to investigate the layer structure of LFR ($c = 0.01$–2 g/l, pH 7, $c_{buff} = 4.5$ mM). LFR has a two-domain molecular structure, where an α-helical connection bridges two symmetric lobes. The resolved two-slab structure of the monolayer is $d_A \approx 1.4$–2.6 nm, built up by adsorbed lobes that predominantly protrude into the air, and $d_W \approx 6$–7 nm, consisting of α-helical chains protruding into the water phase. These d_A thicknesses are, in any case, smaller than the approximate lobe dimensions (55 × 35 × 35 Å), suggesting deformation of the lobes upon adsorption.

Smith et al. [197] and Li et al. [198] performed complementary NR studies on the structure of adsorption layers of the monoclonal antibody COE-3 (IgG1 subtype) on different aqueous substrates: 1) D_2O; 2) ACMW; and 3) PCMW ($\rho_{n,W} = \rho_{n,P} = 2.58 \times 10^{-6}$ Å^{-2}) at pH 5.5 < pI and $c_{buff} = 25$ mM. COE-3 has a three-fragment molecular structure (Fab-Fc-Fab) with a full length of about 14 nm. The individual separated fragments Fab and Fc were also studied, but these results are not considered here. The reflectivity data with ACMW were sufficiently well fitted by a one-slab model, suggesting a monolayer with a thickness that increases only weakly ($d \approx 4.5$–5.5 nm) along the adsorption isotherm $\Gamma_s(c)_{I,pH}$ ($c =$ 0.002–0.1 g/l). Parallel experiments with PCMW revealed that the adsorption layer protrudes into the air by ≈1.5 nm. Furthermore, the results obtained from experiments with D_2O – which are expected to reflect the structural constraints obtained from the other two isotopic contrasts – showed highly consistent outcome, namely $d_1'' \approx 1$–1.5 nm and $d_1' \approx 4$ nm (for denotations, see Fig. 11). The thickness d_1'' of the 'dry' part of the BLG monolayer are in good agreement with those for BSA [194] and LYS [192], which may appear as a general feature for globular proteins adsorbed at the W/A interface.

Proteins from the HFB family are known to be highly rigid. Kisko et al. [178] studied two forms of hydrophobin (HFBI and HFBII) with XRR. One-slab and two-slab models described the reflectivity data equally well, yielding a monolayer thickness of $d \approx 2.4$–2.8 nm at moderate surface pressures of ≈20 mN/m, suggesting insignificant structural differences between the two HBF forms. The authors concluded that the studied HFB forms preserve their globular framework upon adsorption and self-assemble in a similar lateral packing (highly ordered 2D crystalline rafts) at the W/A interface, as revealed by complementary experiments with grazing-incidence X-ray diffraction. HFB adsorption layers were further studied with NR (ACMW) by Zhang et al. [190] and Tucker et al. [191], who reported very similar results for the monolayer thickness ($d \approx 3$ nm) being invariant with pH ≠ pI (pH 2.6, 3, 4, 7 and 10) and c (0.001–0.2 g/l).

4.2. Water/oil interface

As mentioned in Section 1, the topic of proteins at W/O interfaces can be tracked back to the 19th century, and then it attracted considerable attention in the 20th century and is still of interest today. Graham & Phillips [28] investigated βCS, BSA and LYS adsorption layers at W/toluene or W/decane interfaces and concluded that the general adsorption characteristics of these proteins are similar at W/A and W/O interfaces. Just a few years later, this conclusion was reinforced in the NR (ACMW and D_2O) work by Dickinson et al. [121], who reported very similar thicknesses ($d_A \approx 2$ nm and $d_W \approx 5$–7) for βCS (0.05 g/l, pH 7) at either W/A or W/hexane interfaces.

In the 1990s, a few ellipsometry works on proteins at W/O interfaces were published [89,95,211], followed by more studies in the 21st century utilizing ellipsometry [88,89,92–94,211] or NR [121–127,205]. Concerning the problem with decoupling the product (n_L,d) in ellipsometry measurements, in the already above-discussed study by Russev et al. [88], the authors performed parallel measurements at W/A ($\theta =$ 50^o) and W/xylene ($\theta = 70^o$) interfaces, which allowed for an explicit determination of n_L and d. The results obtained for βCS adsorption monolayers (0.1 g/l, pH 5) revealed that the formation of the monolayer is not significantly influenced by the type of the used hydrophobic phases, in qualitative agreement with earlier studies [28,121]. However, it should be pointed out that the protein layers were pre-formed at the W/A interface prior to the pouring of oil on top, so the presence of any kinetically trapped film may have influenced its structure to resolve at the W/O interface. The authors presented the analysis of $\delta\Delta$ from βCS layers recorded at the W/A and W/O interfaces through a minimization procedure on the assumption that the layers were structurally identical and using the known $\partial n_1/\partial c$ to resolve $d_A \approx 1.8$ nm ($n_L \approx 1.45$) and $d_W \approx$ 5.4 ($n_L \approx 1.37$) at $\Gamma_s \approx 2.5$ mg/m^2, in excellent agreement with the structural results by Dickinson et al. [121].

Nylander & coworkers employed either the "simple" W/O arrangement (θ of about 45^o) [89] or the "cuvette" W/O arrangement [95,211] (Figs. 2-A and C, respectively) to study the adsorption of different whey protein blends WPB (isolates, concentrates and fractions) [95,211] as well as isolated BLG [89] at the W/olive oil interface. In the latter study, the authors used a literature value for $d = 2$ nm for BLG in the data analysis and reported $n_L \approx 1.48$.

Although the "cuvette" experimental approach involves working at a restricted incident angle ($\theta = 45^o$), its strength is that the incident beam can be directed at the interface from either side. Hence, two complementary $\Delta_{\theta,\lambda}$ measurement data sets can be gathered, which helps to resolve the properties n_L-d of the same interface on the same sample, thus circumventing added experimental uncertainty from preparing the same system a greater number of times. In [95,211], the authors applied a procedure to match values of n_L and d to the measured $\Delta_{\theta,\lambda}$ data pairs for each sample. A range of thickness values ($d \approx 1$–6.7 nm) for the different WPB formulations were evaluated, while the refractive index was found to vary relatively weakly $n_L \approx 1.47$–1.51. These n_L values are only slightly higher than the refractive index $n_2 \approx 1.46$ of the olive oil, meaning that the measurements had poor sensitivity to n_L and d., The authors concluded that the investigated protein layers are denser than the oil phase and exhibit different thicknesses due to amphiphilic and structural specificities of different proteinaceous species in the WPB mixtures.

The *light guides* experimental water/oil arrangement (Fig. 2-B) was used in a few ellipsometry works [92–94]. Reis et al. [92] studied an LPS layer at the W/decane interface. Assuming a fixed value of $n_L \approx 1.375$, they reported a layer thickness of about 20 nm. According to the above discussion, using such a value of n_L underestimates the refractive index of the LPS layer, thus resulting in an unusually high layer thickness. However, in this study, the authors aimed to compare the interfacial properties of mixed systems from LPS and other species, and the observed relative differences in d delivered valuable information.

Day et al. [93] performed ellipsometry measurements at θ_{Br}, which

revealed higher surface activity of BLG as compared to βCS when adsorbed at the W/hexadecane interface. The authors found this result surprising since caseins are usually known as the most surface-active proteinaceous component of milk [173], however, the dynamics of adsorption processes should be considered.

Poirier et al. [94] investigated the adsorption behavior of SFP either at the W/A interface or the W/hexadecane interface. The authors employed available theoretical models to process the measured ellipsometry data $\Delta_{\theta,\lambda}$ and $\Psi_{\theta,\lambda}$ ($\theta = 55^{o}$ for W/A interface and $\theta = 45^{o}$ for W/O interface). They could account for the extent of immersion of the protein layer in the water phase. The obtained refractive index profiles $n(z)$ for both interfaces are schematized in Fig. 14. However, the data treatment revealed that the SFP layers formed at the W/A interface resided in the water phase, whereas SFP species presumably adsorbed mainly on the oil side at the W/hexadecane interface, and further growth of the protein layer proceeded with propagation into the water phase.

Now, turning to XRR and NR, as mentioned above, the authors are unaware of published studies where XRR has been applied to protein layers at W/O interfaces. The likely reason is that while applications of XRR and NR at W/O interfaces both present strong technical challenges, there is significantly less SLD contrast between the protein and solvent in XRR than in NR. Since, in both cases, researchers need to request beamtimes at large facilities, it seems they have typically preferred to tackle the technical challenges in NR rather than XRR to study protein systems to date. We note that with successful attempts to adapt the technique in probing W/O interfaces for NR, overcoming the problem of neutron beam attenuation by the bulk oil phase, through which the beam travels towards a W/O interface, has been a key challenge. The issue was first overcome by using a thin layer of oil deposited onto the water surface [105,106,121], which in Fig. 2-A is called the "simple" experimental water/oil arrangement. This approach was further used in later protein studies with NR [122,205].

In the NR study by Theodoratou et al. [122], the oil phase was mimicked with a monolayer of crosslinking-functionalized castor oil deposited onto a W/A interface, to which BSA or LYS adsorbed. Notably, the reported surface excesses are anomalously lower than values independently reported for many proteins at such relatively high concentrations. However, the behavior of the two proteins, in terms of surface excess and layer structure, were qualitatively similar. For both proteins at 1 g/l (pD 7, salt-free), the reflectivity data for the W/castor oil were adequately fitted with a two-slab model, in contrast to the W/A interface (considered above). Moreover, the addition of 155 mM NaCl not only led to an increase of the surface excess, but also to the situation where adequate fitting of the reflectivity data required a three-slab model. In summary, the reported layer thickness results suggested the formation of a secondary layer for both proteins at the studied W/O interface.

In the NR study by Bergfreund et al. [205], the W/O interface was effectively generated directly at the W/A interface, facilitating measurements in the usual configuration used for experiments at the W/A interface. The macroscopic phase of volatile oils, either n-hexane (less polar), or methyl *tert*-butyl ether (more polar), was left to evaporate on top of a D_2O-based BLG solution, such that in the final situation for measurements, the adsorbed protein layer was covered with a nanoscopic layer of oil. It was found that the conformation of adsorbed BLG globules depends on the polarity of the oil, with a thicker protein layer formed in contact with the more polar oil (Fig. 15). Notably, effects of oil polarity on BLG adsorption were also found in molecular dynamics simulation studies [61].

The spin-freeze-thaw technique (Fig. 3-A) with hexadecane was employed in several works [124–127]. Campana et al. [124] used it in combination with a sapphire crystal and three aqueous isotopic contrasts: 1) sapphire/hexadecane-matched water (in analogy to the ACMW in studies at the W/A interface); 2) PCMW with $\rho_{n,W} = \rho_{n,P} = 2.2 \times 10^{-6}$ Å^{-2} (extent of immersion); and 3) H_2O (maximum structural sensitivity) to resolve the structure of BSA at the W/O interface. They were able to distinguish between the structural configurations of BSA adsorption layers at the W/O interface in their own study with that published at the W/A interface [194], and they concluded a remarkable difference. The result from the experiments with PCMW revealed a thick portion of the monolayer (≈7.5 nm) residing in the oil phase. Making use of this value in the analysis of the data from experiments with H_2O, the authors resolved the overall thickness (≈ 14.2 nm) of the BSA layer at 'high' c, which, according to the discussion in [124] and the denotation proposed

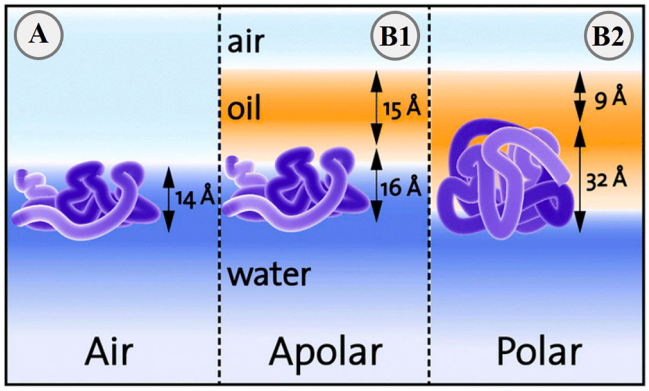

Fig. 15. Schematic illustration of the conformational and localization arrangement of BLG (NR on D_2O, pH 7, 10 mM buffer) adsorbed at different interfaces: (A) W/A and (B) W/O (B1: n-hexane, B2: methyl *tert*-butyl ether). Figure adapted with permission from Bergfreund et al. [205] copyright 2021 The Royal Society of Chemistry.

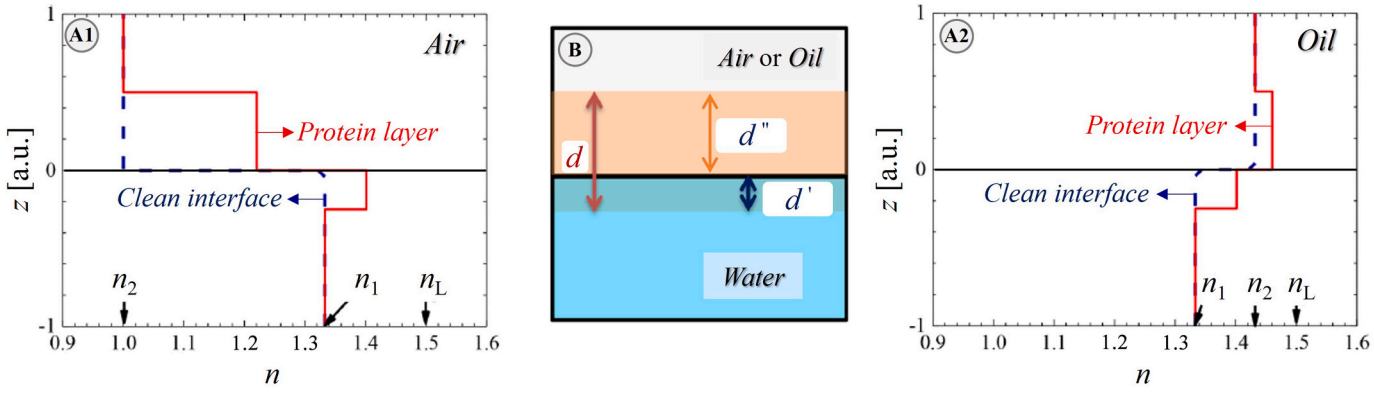

Fig. 14. A1,A2. Refractive index profiles $z(n)$ of clean W/A (A1) and W/O (A2) interfaces and for SFP adsorption layers at the respective interface. B. Schematic representation of the protein layer at an interface; d - overall layer thickness, d' - thickness of the portion of the protein layer immersed in water, d'' - thickness of the portion of the protein layer protruding into the air. Figure adapted with permission from Poirier et al. [94] copyright 2021 American Chemical Society.

in Fig. 11, may be depicted as a *bilayer* structure with $d_1'' \approx 7.5$ nm, $d_1' \approx 3.7$ nm and $d_2 \approx 3$ nm. The authors explained this extended structure by strong changes in the BSA globular framework upon adsorption, despite results from surface-sensitive spectroscopic methods, which had previously suggested only partial loss of the secondary structure of BSA upon adsorption at W/O interfaces (tetradecane or hexadecane) [60]. Kong et al. [127] employed this technique (with a silicon crystal) to study BSA and reported a *bilayer* structure with $d_1 \approx 7.2$–7.7 nm and $d_2 \approx 3.3$–3.6 nm.

The same experimental approach as in [124] was applied in the works by Ruane et al. [125,126] on the adsorption of COE-3 at the W/O interface as a continuation of the works discussed above on COE-3 at the W/A interface [197,198]. The measurements revealed that the antibody adsorbs in a predominantly flat-on orientation (one-slab model: $d \approx 5.4$–6 nm, two-slab model: $d_A \approx 4.6$ nm and $d_W \approx 1.7$ nm), with their domains remaining in native globular structure [125]. In contrast to the case for the W/A interface, no significant penetration into the oil phase was detected. In a subsequent study [126], the authors refined the NR data analysis by making use of a rigid body rotation model, providing additional insight into the configuration of the interfacial protein layers.

5. Thin liquid films

The history of TLF (or soap films as called in early studies) is quite long – it can be tracked back to the pioneering observations by Boyle, Hooke and Newton in the second half of the 17th century, through the seminal studies of Plateau and Gibbs in the 19th century, to the works of Derjaguin, Mysels, Scheludko and others in the 20th century [1,3]. The most intriguing issue has been the accurate estimation of the film thickness, and after Newton's method of color bands succession [1], various electrical and optical approaches have been invented and applied [1,212–214]. Milestones in the theoretical and experimental development of the field of TLFs are undoubtedly the introduction of the concept of the *disjoining pressure* by Derjaguin (1930s), the appearance of the celebrated DLVO theory (Derjaguin-Landau-Verwey-Overbeek, 1940s) and the invention of the *microinterferometric* method [1,213] that has led to the first experimental verification of the DLVO theory on TLFs [215]. This method is based on measurements of the disjoining pressure and the thickness (interferometrically) of a horizontal circular plane-parallel symmetric microscopic TLFs (of either foam or emulsion type).

Clunie et al. (1966) [216] performed a unique experiment with vertical foam films in a frame (~cm^2) drawn from a surfactant solution (decyltrimethylammonium decyl sulfate). A special cell arrangement was employed to allow for simultaneous experiments with X-ray diffraction at glancing incident angles and with (monochromatic) light reflectivity. The light reflectivity data have been analyzed *via* a three-slab optical model with an overall film thickness $h = 2h_L(n_L) + h_C(n_C)$, where h_L is the thickness of the slab corresponding to the adsorption layer (with refractive index n_L) centred at each surface plane of the film and h_C is the thickness of the slab corresponding to the film's core (with refractive index n_C, usually fixed to that of the bulk water solution [83,212–214]). The data for the overall film thickness h, resolved from both measurements, were in very good correlation, thus confirming the used optical model, which yielded a limiting value of $h_C \approx 2$ nm for the case of a *Newton Black Film* (NBF). The NBF [14] – also historically called "*second black film*", "*primary black film*" or "*Perrin film*" [212,213]) – is an amphiphilic bilayer, where the two surfactant layers at the W/A interfaces of the film mutually adhere, and the film's core (h_C) contains only a restricted amount of hydration water [216,217]. Larger h_C corresponds to a *Common Black Film* (CBF) [14] that contains a core of free liquid water. The thickness of CBFs (on the order of 10–30 nm) is determined by the action of DLVO surface forces [212–215].

The first works on TLFs employing ellipsometry [83,218] or NR [79,219] appeared in the 1970s and 1980s, respectively. To the best of our knowledge, these are the only such studies found in the literature. On the other hand, XRR was more intensively involved in TLF studies, and these are the works by Benattar & coworkers; their first literature reports appeared in the early 1990s [220,221]. All these studies involving ellipsometry, XRR or NR dealt with vertical foam films in a frame. To the best of our knowledge, relevant reflectometric studies on any emulsion films have not been documented in the literature.

The first ellipsometry study on TLFs was reported by den Engelsen (1973) [83]. A subsequent and more detailed study, complemented with (monochromatic) light reflectometry measurements, dealt with either CBFs or NBFs stabilized by sodium dodecyl sulfate (SDS) or sodium dodecyl benzenesulfonate (SDBS) [218]. A three-slab optical model was found superior to a one-slab model for description of the refractive index profile for CBFs, while the structure of the NBFs could be well described by a one-slab model of a film with thickness $h_{NBF} \equiv 2h_L = 3.6$ nm and a homogeneous refractive index n_{NBF} equal to that of the adsorption layers, namely $n_{NBF} \equiv n_L = 1.365$ (SDS) or 1.390 (SDBS).

In their seminal paper on NR, Hayter et al. (1981) [79] obtained neutron reflectivity data from a surfactant foam film, paving the way for further experiments of this kind. Highfield et al. [219] studied vertical foam films obtained from a mixed solution of hydrogenous decyltrimethylammonium bromide and decanoic acid in D_2O with the same methodology. Hence, the measured film thickness was, in fact, that of the film's core h_C, which was confirmed by the measured critical angle in the reflectivity profiles. The positions of the latter displayed interference *Kiessig fringes*, which encode information about the film thickness at higher Q_z. The reflectivity data were analyzed using a simple model of a single homogeneous slab with sharp boundaries, yielding values of h_C in the range 55–160 nm, meaning relatively thick films, which presumably had not reached equilibrium thickness as suggested by the observed time dependence of the measured h_C.

Benattar & coworkers (1990s) employed XRR to investigate NBFs stabilized by surfactants [220,221] as well as by proteins [222,223] (Fig. 16). In the first such XRR work, Bélorgey & Benattar [220] argued that the earlier work by Clunie et al. [216] had suffered from technical and data analysis issues, and had subsequently led to overestimation of the NBF thickness, and consequently to an incorrect interpretation of the limiting core thickness ($h_C \approx 2$ nm). For the studied SDS foam films at 0.4 M NaCl, the overall thickness of the NBF was reported as $h_{NBF} \approx 3.3$ nm with a film's core thickness of $h_C \approx 0.4$ nm [220,221]. The authors found that the reflectivity data were best fitted by a five-slab model: ($h_{L,tail}/h_{L,head}/h_C/h_{L,head}/h_{L,tail}$, which account for the hydrophobic tail ($h_{L,tail}$) and hydrophilic head ($h_{L,head}$) regions of the SDS adsorption layer as $h_{L,tail} \approx 1.1$ nm and $h_{L,head} \approx 0.4$ nm [221]. Interestingly, when 2 M LiCl was used (instead of NaCl), only the core thickness changed to $h_C \approx 1.3$ nm with insignificant modifications in the other structural parameters. In later XRR studies, Benattar & coworkers investigated NBFs stabilized by phospholipids or by various surfactants. The authors also studied the intriguing case of spontaneous insertion of protein molecules (BSA) into the interior of a surfactant NBF. However, those studies are not considered here as they fall out of the scope of this article, while in the following, we discuss the XRR works involving TLFs stabilized solely by proteins [222,223].

Perhaps Plateau (1873) was the first scientist to study protein TLFs in detail [1,3]. The author investigated the persistence of *bubble caps* (spherically curved TLFs) resting on the surface of an albumin solution and associated the observed film stability with the ability of albumin to decrease the surface tension of the solution and to produce *special superficial viscosity*. In the second half of the 20th century and up to the present day, either foam or emulsion TLFs obtained from protein solutions have been studied [1,224–230]. All these studies used microscopic horizontal TLFs, but we do not consider such studies in further detail in the present article.

In the XRR works by Benattar & coworkers discussed above, foam film experiments with pure protein solutions with BLG were also performed [222,223]. Fig. 16 presents some experimental details. A monochromatic X-ray beam with the wavelength of $\lambda = 1.5405$ Å was used as sourced from a copper tube (CuKα1 line) and the incident angle

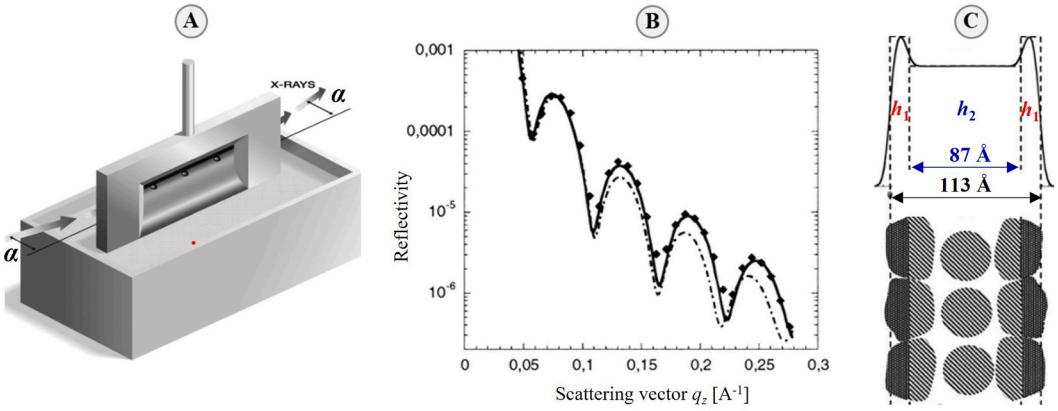

Fig. 16. X-ray reflectivity experiments with foam film stabilized by BLG. A. Experimental cell for formation of a foam film in a frame drawn from solution. B. Reflectivity profile for a foam film from solution of 0.25 g/l (≈13.7 μM) BLG in 5 mM NaCl at pH 5.3. Symbols are experimental data, and lines are fits of a one-slab (dotted line) and a three-slab (continuous line) film models. C. Film thickness profile corresponding to the three-slab film model and a schematic representation of the structure of the film (for details see the text). Figures adapted with permission from Petkova et al. [222] copyright 2003 American Chemical Society.

was varied in the range $\theta = 6$–70 mrad (with 0.1 mrad divergence), hence, a Q_z-range 0.03–0.5 Å^{-1} could be covered. Unlike the case of a single interface, here, interference of the beams reflected from its two W/A interfaces in close proximity gives rise to four distinct and strong interference *Kiessig fringes* (Fig. 16-B), and the position of these fringes allows for determination of the film thickness with high accuracy (≈1 Å in that particular case). A one-slab film model was shown not to be suitable for describing the reflectivity data because it does not allow for simultaneously reproducing the shape of the first fringe and the rest of the experimental reflectivity data at high Q_z. A significant density gradient was inferred to exist within the film, and the best fit to the data was found by assuming a three-slab model of the structure of the film. Such a three-slab model is the typical way of treating light interferometry measurements on TLFs, as mentioned above. The results for two BLG concentrations obtained in two separate studies [222,223], revealed the same value $h_L \approx 1.3$ nm, but different values for h_C, namely $h_C \approx 8.7$ nm ($c \approx 13.7$ μM) [222] and $h_C \approx 12.6$ nm ($c \approx 54.7$ μM) [223], which yield an overall film thicknesses of $h \approx 11.3$ nm and $h \approx 15.2$ nm, respectively. For comparison, (monochromatic) light interferometry measurements yielded thicknesses of the thinnest BLG black films on the order of $h \approx 5$–9 nm for solutions at pH 7 and at 100 mM NaCl [228], or $h \approx 6.0$ nm for solutions at pH 5 → pI [226]. The thickness differences for the thinnest BLG foam films in the studies with macroscopic vertical films and microscopic horizontal films may have originated from hydrodynamic issues. In studies [226,228], circular microscopic films (radius of ≈100 μm) were investigated, whereas in the XRR experiments in [222,223], comparatively much larger and vertical films were investigated. Hence, it is very probable that the films undergo somewhat different drainage behavior in these two types of experiments.

The XRR foam film experiments under consideration were performed with BLG solutions at pH 5.3 → pI [222,223], hence, the investigated foam films are expected to be of a protein-NBF type, as claimed in [226]. Interpretation of the obtained XRR data resulted in the conclusion of a structure where the higher electron density slabs at the W/A interfaces of the film correspond to a portion of the interfacial layer of adsorbed BLG globules, while the remainder of the interfacial layer (in the z direction) is characterized by a lower electron density compared to that in the interior of the film (Fig. 16-C). Notably, the estimated electron density values suggested no presence of free liquid water in the film's core, which allowed the authors to define such a protein film as an NBF.

We should note here that the true definition of a protein NBF should involve a protein bilayer film structure analogous to the definition of an NBF originally introduced for amphiphile bilayers, usually composed of low-molecular-weight surfactants [213,216–218,220,221] or lipids [217]. Indeed, a protein bilayer structure was adopted in the interpretation of interferometry measurements for microscopic foam films from BSA ($h \approx 8.6$ nm) [132], HFB ($h \approx 6.0$ nm) [229,230] and BLG ($h \approx 6.0$ nm) [226]. Interestingly, in their study on BSA foam films, Cascão Pereira et al. [132] concluded the structure of a protein bilayer film structure for the case of foam films obtained at pH 8.3 (away from pI, but in the presence of 25 mM NaCl), but for the case of films at pH 5.2 → pI a structure comprising three molecular layers was proposed ($h \approx 11.5$ nm) that is equivalent to the one in Fig. 16-C. Such a structure intuitively recalls the phenomenon of stratification in foam films from micellar surfactant solutions [231,232].

We draw this discussion to a close with two general remarks. Firstly, the XRR technique gives access to the real physical film thickness h, whereas the interferometry technique yields an *equivalent film thickness* [213]. Furthermore, the advantage of the former technique is that the reflectivity signal contains explicit information about the (electron) density profile of the film, encoded in the shape of the experimental reflectivity profile, which allows for direct discrimination in the structure of the film in terms of stratified layers (or slabs). In the latter case, the reflectivity signal, as given by the ratio of the incident and the reflected monochromatic light beams (normal to the film) and the corresponding interference phase lag, is insensitive to the density profile of the film. Then, any further details on the structure of the film are obtained indirectly by manipulating the estimated overall equivalent thickness. However, knowing the adsorption layer thickness d from reliable, independent experiments with single interfaces (XRR or NR) and assuming $h_L \equiv d$, one may translate the equivalent thickness into h *via* an optical model [213] with reasonable accuracy [132,226,229,230].

Secondly, the resolved three-layer film structure in some studies [132,222,223] is evidence for the existence of a stratified protein film. Such stratification behavior is elegantly illustrated by disjoining pressure isotherms for microscopic HFB foam films, which reveal stepwise film thinning [229], as in the case of stratified surfactant films [231,232]. The observed step size of ≈3.0 nm reflects reorientations of HFB tetramers (6 × 6 × 3 nm) sandwiched in the film's core, and the final step is the formation of an NBF ($h \approx 6.0$ nm). The formation of this bilayer structure proceeds with fast expansion of the NBF area, which evidences the action of strong adhesive forces. A similar situation was observed in the case of microscopic BLG black films, and hence, these films were also classified as NBFs ($h \approx 6.0$ nm) [226].

6. Concluding remarks

Various experimental and data analysis approaches have allowed researchers to unravel the potential of ellipsometry as a powerful tool for

the study of protein layers at liquid/fluid interfaces. The technique can be used to provide information about the adsorption dynamics and steady-state surface excess, and it can be considered more widely accessible than XRR or NR. It is, therefore, suitable for pre-screening samples prior to applications for beamtime. The good correlation found between data of the dynamic surface excess $\Gamma(t)$ measured by ellipsometry and NR (in ACMW) [45,117] and the reasonable assumption that any isotopic effects of ACMW over H_2O on the adsorption dynamics of proteins are minimal [40], allows one to employ ellipsometry for obtaining accurate measurements of Γ in order to limit the need for beamtime [45].

The broad Q_z-range accessible with XRR gives the technique high resolution in resolving intricacies of stratified layer structures, but the technique suffers from poor scattering contrast between the protein and solvent. In the case of NR, the use of dedicated aqueous isotopic contrasts allows for probing specific aspects of the adsorption dynamics and interfacial structure of protein layers. For the W/A interface, the common contrasts are: 1) ACMW – robust determination of Γ on the minute time scale through the low-Q_z analysis approach; 2) D_2O – detailed structural analysis from the acquisition of data in different isotopic contrasts over the fully accessible Q_z-range; 3) PCMW – resolution of the extent of protrusion of the protein into the air phase. For the W/O interface, the approach is analogous, but the contrast difference between water and different oils is favorable and in such cases, H_2O solutions can be used instead of D_2O ones, but only when the oil is deuterated or fluorinated as at least one medium must be transparent to neutrons. However, oil-matched water is used instead of ACMW to evaluate Γ, and PCMW is used with an analogous same aim as for the W/A interface, *i.e.* protrusion of protein into the oil phase.

Concerning the interfacial structuring of adsorbed proteins, it is essential to distinguish between the 'unfolding' and 'deformation' (flattening) of a protein globule upon adsorption. In the first case, (partial) unfolding, *i.e.*, (partial) loss of tertiary structure, causes inhomogeneous volume fraction profiles along the z direction normal to the interface, which has been modeled mainly in two ways: 1) power law and/or exponentially decaying profiles were used for the case of random coils [18,206]; for globular proteins, however, the usual case is 2) a model of two or three homogeneous slabs, with a peptide-rich upper slab (d_A,Φ_A) and a peptide-poor bottom slab (d_W,Φ_W) with the formation of a molecularly discrete secondary layer at relative high bulk protein concentrations. In the second case, deformation means that a protein globule deforms (flattens) upon adsorption but may largely retain its globular framework. The formation of a secondary discrete molecular layer (d_2) is a conceptually important issue in the science of protein-based soft colloids. It appears that it is a common scenario for many proteins, but it takes place under required solution formulation conditions, namely, protein concentration, pH and ionic strength. Other studies have shown more extended interfacial denaturation of proteins at relatively low bulk concentrations, resulting in a one-slab interfacial layer with a thickness of <2 nm, *i.e.* much less than the smaller diameter of the native globules.

Recapitulation of the currently available results obtained using complementary approaches involving ellipsometry, XRR, NR and other techniques points to a state-of-the-art level of detailed resolution of the volume fraction distribution of the protein interfacial structure normal to the interface according to the scheme shown in Fig. 11. Implementation of appropriate experimental approaches, novel sample environments and advanced data analysis (mainly from but not limited to NR) are already an excellent achievement in the scientific domain of protein layer structuring at liquid/fluid interfaces. For comparison, the relatively accessible pathways for synthesis and/or chemical modification of low-molecular-weight surfactants (and even some polymers) allow for their partial deuteration, which opens additional options for isotopic contrast combinations in future work [233].

Experimental studies of TLFs using ellipsometry, XRR and NR remain rare. The reason for this limitation is most probably the substantial technical difficulties with the experimental arrangement, combined with complications related to interferometric effects from two interfaces in close proximity. To date, these challenges have been most successfully overcome using XRR [222,223].

Recent progress in computer technology allows molecular simulation methods such as molecular dynamics (MD) or Monte Carlo simulations to become a complementary tool for analysis of the state of proteins in bulk and at solid and soft interfaces [234]. They allow for the exploration of the adsorption behavior of proteins at the molecular level, their orientation at interfaces, and changes in their conformation compared to bulk. The results of molecular simulations may be directly confronted with the ones obtained with reflectivity techniques. It allows verification of the applicability of the models used for the interpretation of experimental data (one-, two- or many-slab models) [60,235]. On the other hand, input from the experimental approaches reviewed in this article can contribute to optimizing the force field and model of water to reproduce experimental findings [236].

In most studies involving molecular simulations, single proteins and their interactions with medium or interface are considered [234]. However, the adsorption of proteins involves not only protein-surface interactions but also protein-protein interactions that may involve electrostatic, dispersive, hydrophobic, and protein-protein hydrogen bonds. Currently, the MD simulations are still unable to predict the adsorbed amount Γ. For this reason, it should be known *a priori* from an experimental measurement before the simulations can be set up in a meaningful way.

Molecular simulation studies of such systems are currently scarce due to very high computational effort. It can be expected that with the improvement of computer performance, simulation methods, and force fields, future research will focus on the investigation of the multiple-protein systems, the results of which can be used for an adequate description of the reflectivity experimental results.

CRediT authorship contribution statement

Georgi G. Gochev: Writing – review & editing, Writing – original draft, Data curation, Conceptualization. **Richard A. Campbell:** Writing – review & editing, Writing – original draft. **Emanuel Schneck:** Writing – review & editing, Writing – original draft. **Jan Zawala:** Writing – review & editing, Writing – original draft. **Piotr Warszynski:** Writing – review & editing, Writing – original draft.

Declaration of competing interest

The authors declare that they have no known competing financial interests or personal relationships that could have appeared to influence the work reported in this paper.

The author is an Editorial Board Member for *Advances in Colloid and Interface Science* and was not involved in the editorial review or the decision to publish this article.

Data availability

We have used adapted literature data; permissions from the publishers were managed and the respective copyrights are indicated accordingly.

Acknowledgments

J.Z. thanks for partial financial support from the Polish National Science Centre (NCN) grant No. 2020/38/E/ST8/00173. G.G.G. and P. W. acknowledge the statutory subsidy from the Ministry of Science and High Education of Poland for the Jerzy Haber Institute of Catalysis and Surface Chemistry Polish Academy of Sciences.

References

[1] Gochev G, Platikanov D, Miller R. Chronicles of foam films. Adv Colloid Interface Sci 2016;233:115.
[2] Millington EC. A Theories of cohesion in the seventeenth century. 1945; 5: 253-269. Ann Sci 1947;5:352–69.
[3] Plateau JAF. Statique experimentale et theoryque des liquides soumis aux seules forces moleculaires (Eng. Experimental and Theoretical Statics of Liquids Subject to Molecular Forces Only); Paris, Gauthier - Villars; London, Trübner & Co.; Gand et Leipzig: F. Clemm. 1873.
[4] Du Noüy PL. Surface Equilibria of Biological and Organic Colloids. ACS Monograph N⍰ 27. Chemical Catalog Co., Inc.; 1926.
[5] Vincent B. Early (pre-DLVO) studies of particle aggregation. Adv Colloid Interface Sci 2012;170:56.
[6] Ramsden W. Separation of solids in the surface-layers of solutions and 'suspensions'. Proc Royal Soc (London) A 1903;72:156.
[7] Hughes AH, Rideal EK. On protein Monolayers. Proc Roy Soc A 1932;137:62.
[8] Neurath H, Bull HB. The surface activity of proteins. Chem Rev 1938;23:391–435.
[9] Langmuir I, Schaefer VJ. Properties and structure of protein monolayers. Chem Rev 1939;24:181–202.
[10] Murray BS. Recent developments in food foams. Curr Opin Colloid Interface Sci 2020;50:101394.
[11] Cai Z, Wei Y, Shi A, Zhong J, Rao P, Wang Q, et al. Correlation between interfacial layer properties and physical stability of food emulsions: current trends, challenges, strategies, and further perspectives. Adv Colloid Interface Sci 2023; 3013:102863.
[12] Rabe M, Verdes D, Seeger S. Understanding protein adsorption phenomena at solid surfaces. Adv Colloid Interface Sci 2011;162:87–106.
[13] Noskov BA, Bykov AG, Gochev G, Lin SY, Loglio G, Miller R, et al. Adsorption layer formation in dispersions of protein aggregates. Adv Colloid Interface Sci 2020;276:102086.
[14] Ter Minassian-Saraga L, et al. Thin films including layers: terminology in relation to their preparation and characterization IUPAC Recommendations 1994. Thin Solid Films 1996;277:7–78.
[15] MacRitchie F. Spread monolayers of proteins. Adv Colloid Interface Sci 1986;26: 341.
[16] Cumper CWN, Alexander AE. The surface chemistry of proteins. I. Spread monolayers at oil-water interfaces. II. The viscosity, elasticity and thickness of adsorbed films. Trans Faraday Soc 1950;46:235.
[17] Proteins at Liquid Interfaces. In: Möbius D, Miller R, editors. Studies in Interface Science. 7. Elsevier; 1998.
[18] Harzallah B, Aguié-Béghin V, Douillard R, Bosio L. A structural study of β-casein adsorbed layers at the air–water interface using X-ray and neutron reflectivity. Int J Biol Macromol 1998;23:73–84.
[19] Martin AH, Meinders MBJ, Bos MA, Cohen Stuart MA, van Vliet T. Conformational aspects of proteins at the air/water interface studied by infrared reflection−absorption spectroscopy. Langmuir 2003;19:2922–8.
[20] Du Noüy PL. Spontaneous decrease of the surface tension of serum. I J Exp Med 1922;35:575–97.
[21] Zhou B, Tobin J, Drusch S, Hogan SA. Interfacial properties of milk proteins: A review. Adv Colloid Interface Sci 2020;295:102347.
[22] Coke M, Wilde PJ, Russell EJ, Clark DC. The influence of surface composition and molecular diffusion on the stability of foams formed from protein/surfactant mixtures. J Colloid Interface Sci 1990;138:489–504.
[23] Sugden S. XCVII.–The determination of surface tension from the maximum pressure in bubbles. J Chem Soc Trans 1922;121:858–66.
[24] Rotenberg Y, Boruvka L, Neumann AW. Determination of surface tension and contact angle from the shapes of axisymmetric fluid interfaces. J Colloid Interface Sci 1983;93:169–83.
[25] McBain JW, Humphreys CW. The Microtome Method of the Determination of the Absolute Amount of Adsorption. J Phys Chem 1932;36:300–11.
[26] Benjamins J, de Feijter JA, Evans MTA, Graham DE, Phillips MC. Dynamic and static properties of proteins adsorbed at the air/water interface. Faraday Discuss Chem Soc 1975;59:218–29.
[27] Graham DE, Phillips MC. Proteins at liquid interfaces. I. Kinetics of adsorption and surface denaturation. J Colloid Interface Sci 1979;70:403–14.
[28] Graham DE, Phillips MC. Proteins at liquid interfaces. II. Adsorption isotherms. J Colloid Interface Sci 1979;70:415–26.
[29] Razumovski L, Damodaran S. Surface Activity−Compressibility Relationship of Proteins at the Air−Water Interface. Langmuir 1999;15:1392–9.
[30] Chernysheva MG, Badun GA. Liquid scintillation spectrometry of tritium in studying lysozyme behavior in aqueous/organic liquid systems. The influence of the organic phase. Langmuir 2011;27:2188–94.
[31] Bogacheva EN, Gedrovich AV, Shishkov AV. Iceberg model of the structure of globular protein adsorption layers at the air–water interface. Study by the tritium planigraphy technique. Colloid J 2004;66:137–40.
[32] de Feijter JA, Benjamins J, Veer FA. Ellipsometry as a tool to study the adsorption behavior of synthetic and biopolymers at the air-water interface. Biopolym 1978; 17:1759–72.
[33] Noskov BA. Protein conformational transitions at the liquid-gas interface as studied by dilational surface rheology. Adv Colloid Interface Sci 2014;206: 222–38.
[34] Mitropoulos V, Mütze A, Fischer P. Mechanical properties of protein adsorption layers at the air/water and oil/water interface: A comparison in light of the thermodynamical stability of proteins. Adv Colloid Interface Sci 2014;206:195.
[35] Interfacial Rheology. In: Miller R, Liggieri L, editors. Progress in Colloid and Interface Science. 1. CRC Press; 2019.
[36] Klein CO, Theodoratou A, Rühs PA, Jonas U, Loppinet B, Wilhelm M, et al. Interfacial Fourier transform shear rheometry of complex fluid interfaces. Rheol Acta 2019;58:29–45.
[37] Lucassen J, van den Tempel M. Dynamic measurements of dilational properties of a liquid interface. Chem Eng Sci 1972;27:1283–91.
[38] Joos P. Approach for an equation of state for adsorbed protein surfaces. Biochim Biophys Acta-Biomembran 1975;375:1–9.
[39] Gochev G, Kovalchuk VI, Aksenenko EV, Fainerman VB, Miller R. β-Lactoglobulin Adsorption Layers at the Water/Air Surface: 5. Adsorption isotherm and equation of state revisited, impact of pH. Coll Interf 2021;5:14.
[40] Gochev G, Schneck E, Miller R. Effects of aqueous isotopic substitution on adsorption dynamics and dilational rheology of β-lactoglobulin layers at the water/air interface. J Phys Chem B 2024;128:2821–30.
[41] de Groot A, Yang J, Sagis LMC. Surface stress decomposition in large amplitude oscillatory interfacial dilatation of complex interfaces. J Colloid Interface Sci 2023;638:569–81.
[42] Rodríguez Patino JM, Carrera Sánchez C, Rodríguez Niño MR. Structural and morphological characteristics of β-casein monolayers at the air–water interface. Food Hydrocoll 1999;13:401–8.
[43] Carrera Sánchez C, Rodríguez Niño MR, Molina Ortiz SE, Cristina Añón M, Rodriguez Patino JM. Soy globulin spread films at the air–water interface. Food Hydrocoll 2004;18:335–47.
[44] Rodríguez Patino JM, Carrera Sánchez C, Molina Ortiz SE, Rodríguez Niño MR, Cristina Añón M. Adsorption of soy globulin films at the air–water interface. Ind Eng Chem Res 2004;43:1681–9.
[45] Campbell RA, Ang JC, Sebastiani F, Tummino A, White JW. Spread films of human serum albumin at the air−water interface: optimization, morphology, and durability. Langmuir 2015;31:13535–42.
[46] Campbell RA, Tummino A, Varga I, Milyaeva Oyu, Krycki MM, Lin S-Y, et al. Adsorption of denaturated lysozyme at the air-water interface: structure and morphology. Langmuir 2018;34:5020–9.
[47] Krycki MM, Lin SY, Loglio G, Michailov AV, Miller R, Noskov BA. Impact of denaturing agents on surface properties of myoglobin solutions. Colloids Surf B Biointerfaces 2021;202:111657.
[48] Bhuvanesh T, Machatschek R, Lysyakova L, Kratz K, Schulz B, Ma N, et al. Collagen type-IV Langmuir and Langmuir-Schäfer layers as model biointerfaces to direct stem cell adhesion. Biomed Mater 2019;14:024101.
[49] Zhang S, Liu Y, Machatschek R, Lendlein A. Ultrathin collagen type I films formed at the air-water interface. MRS Adv 2022;7:56–62.
[50] Sengupta T, Damodaran S. Lateral phase separation in adsorbed binary protein films at the air−water interface. J Agric Food Chem 2001;49:3087–91.
[51] Liao Z, Lampe JW, Ayyaswamy PS, Eckmann DM, Dmochowski IJ. Protein assembly at the air-water interface studied by fluorescence microscopy. Langmuir 2011;27:12775–81.
[52] Yamins HG, Zisman WA. A new method of studying the electrical properties of monomolecular films on liquids. J Chem Phys 1933;1:656–61.
[53] Thomas C, Ter Minassian-Saraga L. Characterization of monolayers of a structural protein from myelin spread at the air/water interface. Effect of pH and ionic strength. J Colloid Interface Sci 1976;56:412–25.
[54] Engelhardt K, Peukert W, Braunschweig B. Vibrational sum-frequency generation at protein modified air–water interfaces: Effects of molecular structure and surface charging. Curr Opin Colloid Interface Sci 2014;19:207–15.
[55] Tweet AG. Spectrometer for optical studies of ultra-thin films. Rev Sci Instrum 1963;34:1412–7.
[56] Flach CR, Brauner JW, Taylor JW, Baldwin RC, Mendelsohn R. External reflection FTIR of peptide monolayer films in situ at the air/water interface: experimental design, spectra-structure correlations, and effects of hydrogen-deuterium exchange. Biophys J 1994;67:402–10.
[57] Lad MD, Birembaut F, Matthew JM, Frazier RA, Green RG. The adsorbed conformation of globular proteins at the air/water interface. Phys Chem Chem Phys 2006;8:2179–86.
[58] Postel C, Abillon O, Desbat B. Structure and denaturation of adsorbed lysozyme at the air–water interface. J Colloid Interface Sci 2003;266:74–81.
[59] Hosseinpour S, Roeters SJ, Bonn M, Peukert W, Woutersen S, Weidner T. Structure and dynamics of interfacial peptides and proteins from vibrational sum-frequency generation spectroscopy. Chem Rev 2020;120:3420–65.
[60] Day L, Zhai J, Xu M, Jones NC, Hoffmann SV, Wooster TJ. Conformational changes of globular proteins adsorbed at oil-in-water emulsion interfaces examined by synchrotron radiation circular dichroism. Food Hydrocoll 2014;34: 78–87.
[61] Dalkas G, Euston SR. Molecular simulation of protein adsorption and conformation at gas-liquid, liquid–liquid and solid–liquid interfaces. Curr Opin Colloid Interface Sci 2019;41:1–10.
[62] Langmuir I, Schaefer VJ, Wrinch DM. Built-up films of proteins and their properties. Sci 1937;85:76–80.
[63] Perriman AW, McGillivray DJ, White JW. Reactions of isolated mono-molecular protein films. Soft Matter 2008;4:2192–8.
[64] Lin J-M, White JW. Denaturation resistance of β-lactoglobulin in monomolecular films at the air-water interface. J Phys Chem B 2009;113:14513–20.
[65] a Bragg WL. The specular reflection of x-rays. Nature 1912;90:410.
b Compton AH. The intensity of x-ray reflection, and the distribution of the electrons in atoms. Phys Ther Rev 1917;9:29–57.
[66] Daillant J, Gibaud A. X-ray and Neutron Reflectivity: Principles and Applications. Berlin, Heidelberg: Springer; 1999.

[67] Hayter JB, Penfold J, Williams WG. Observation of the interference of neutrons reflected from thin films. Nature 1976;262:569–70.
[68] Cristofolini L. Synchrotron X-ray techniques for the investigation of structures and dynamics in interfacial systems. Curr Opin Colloid Interface Sci 2014;19:228–41.
[69] Langevin D. Light scattering by liquid surfaces, new developments. Adv Colloid Interface Sci 2021;289:102368.
[70] Gilbert EP. Neutron techniques for food hydrocolloids. Curr Opin Colloid Interface Sci 2023;67:101730.
[71] Maestro A, Gutfreund P. In situ determination of the structure and composition of Langmuir monolayers at the air/water interface by neutron and x-ray reflectivity and ellipsometry. Adv Colloid Interface Sci 2021;293:102434.
[72] Grüniger H, Möbius D, Meyer H. Enhanced light reflection by dye monolayers at the air–water interface. J Chem Phys 1983;79:3701–10.
[73] Rodríguez Patino JM, Carrera Sánchez C, Rodríguez Niño MR. Morphological and structural characteristics of monoglyceride monolayers at the air-water interface observed by brewster angle microscopy. Langmuir 1999;15:2484–92.
[74] Beaglehole D. Structure of electrolyte/vapor and electrolyte/oil interfaces. J Phys Chem 1989;93:2004–9.
[75] Day JRP, Bain CD. Ellipsometric study of depletion at oil-water interfaces. Phys Rev E 2007;76:041601.
[76] Stocco A, Tauer K. High-resolution ellipsometric studies on fluid interfaces. Eur Phys J E 2009;30:431.
[77] Braslau A, Deutsch M, Pershan PS, Weiss AH, Als-Nielsen J, Bohr J. Surface roughness of water measured by x-ray reflectivity. Phys Rev Lett 1985;54:114–7.
[78] Schlossman ML. X-ray scattering from liquid–liquid interfaces. Physica B: Condens Matter 2005;357:98–105.
[79] Hayter JB, Highfield RR, Pullman BJ, Thomas RK, McMullen AI, Penfold J. Critical reflection of neutrons. A new technique for investigating interfacial phenomena. J Chem Soc Faraday Trans 1981;1(77):1437–48.
[80] Zarbakhsh A, Bowers J, Webster JRP. Width of the hexadecane-water interface: a discrepancy resolved. Langmuir 2005;21:11596–8.
[81] Hall AC. A century of ellipsometry. Surf Sci 1969;16:1–13.
[82] Hofmeister E. Bestimmung des Brechungsindex monomolekularer Fettsäureschichten (Eng. Determination of the refractive index of monomolecular fatty acid layers). Z Phys 1953;136:137–51.
[83] den Engelsen D. Ellipsometry of fluid interfaces and membrane-like systems. Chem Ing Tech 1973;45:1107–9.
[84] Azzam RMA, Bashara NM. Ellipsometry and Polarized Light. Amsterdam: North Holland; 1977.
[85] Cuypers PA, Corsel JW, Janssen MP, Kop JM, Hermens WT, Hemker HC. The adsorption of prothrombin to phosphatidylserine multilayers quantitated by ellipsometry. J Biol Chem 1983;258:2426–31.
[86] Motschmann H, Teppner R. Ellipsometry in Interface Science. New York: Elsevier; 2001.
[87] Tyrode E, Magnus Johnson C, Rutland MW, Day JPR, Bain CD. A study of the adsorption of ammonium perfluorononanoate at the air−liquid interface by vibrational sum-frequency spectroscopy. J Phys Chem C 2007;111:316–29.
[88] Russev SC, Arguirov TVL. Gurkov TD. β-Casein adsorption kinetics on air–water and oil–water interfaces studied by ellipsometry. Colloids Surf B Biointerfaces 2000;19:89–100.
[89] Beaglehole D, Lawson F, Harper G, Hossain M. Tryptophan, Tryptophan-Leucine, and BSA Adsorption at an Oil-Water Interface. J Colloid Interface Sci 1997;192:266–8.
[90] Bylaite E, Nylander T, Venskutonis R, Jönsson B. Emulsification of caraway essential oil in water by lecithin and beta-lactoglobulin: emulsion stability and properties of the formed oil-aqueous interface. Colloids Surf B Biointerfaces 2001;20:327–40.
[91] Benjamins J-W, Jönsson B, Thuresson K, Nylander T. New experimental setup to use ellipsometry to study liquid-liquid and liquid-solid interfaces. Langmuir 2002;18:6437–44.
[92] Reis P, Holmberg K, Miller R, Krägel J, Grigoriev DO, Leser ME, et al. Competition between lipases and monoglycerides at interfaces. Langmuir 2008;24:7400–7.
[93] Day JRP, Pudney PDA, Bain CD. Ellipsometric study of the displacement of milk proteins from the oil–water interface by the non-ionic surfactant C10E8. Phys Chem Chem Phys 2010;12:4590–9.
[94] Poirier A, Stocco A, Kapel R, In M, Ramos L, Banc A. Sunflower Proteins at Air–Water and Oil–Water Interfaces. Langmuir 2021;37:2714–27.
[95] Nylander T, Hamraoui A, Paulsson M. Interfacial properties of whey proteins at air/water and oil/water interfaces studied by dynamic drop tensiometry, ellipsometry and spreading kinetics. Int J Food Sci Technol 1999;34:573–85.
[96] Hénon S, Meunier J. Microscope at the Brewster angle: direct observation of first-order phase transitions in monolayers. Rev Sci Instrum 1991;62:936–9.
[97] Daear W, Mahadeo M, Prenner EJ. Applications of Brewster angle microscopy from biological materials to biological systems. Biochim Biophys Acta Biomembr 2017;1859:1749–66.
[98] Grundy MJ, Richardson RM, Roser SJ, Penfold J, Ward RC. X-ray and neutron reflectivity from spread monolayers. Thin Solid Films 1988;159:43–52.
[99] Zhang Z, Mitrinović DM, Williams SM, Huang Z, Schlossman ML. X-ray scattering from monolayers of F(CF2)10(CH2)2OH at the water–(hexane solution) and water–vapor interfaces. J Chem Phys 1999;110:7421–32.
[100] Singh A, Konovalov O, Novak J, Vorobiev A. The sequential growth mechanism of a protein monolayer at the air–water interface. Soft Matter 2010;6:3826–31.
[101] Singh A, Konovalov O. Measuring elastic properties of a protein monolayer at water surface by lateral compression. Soft Matter 2013;9:2845–51.
[102] Schneck E, Deme B. Structural characterization of soft interfaces by standing-wave fluorescence with X-rays and neutrons. Curr Opin Colloid Interface Sci 2015;20:244–52.
[103] Penfold J, Thomas RK. The application of the specular reflection of neutrons to the study of surfaces and interfaces. J Phys Condens Matter 1990;2:1369–412.
[104] Efimova YM, van Well AA, Hanefeld U, Wierczinski B, Bouwman WG. On the neutron scattering length density of proteins in H2O/D2O. Physica B: Condens Matter 2004;350:E877–80.
[105] Lee LT, Langevin D, Farnoux B. Neutron reflectivity of an oil-water interface. Phys Rev Lett 1991;67:2678–81.
[106] Cosgrove T, Phipps JS, Richardson RM. Neutron reflection from a liquid/liquid interface. Colloids Surf 1992;62:199–206.
[107] Penfold J, Richardson RM, Zarbakhsh A, Webster JRP, Bucknall DG, Rennie AR, et al. Recent advances in the study of chemical surfaces and interfaces by specular neutron reflection. J Chem Soc Faraday Trans 1997;93:3899–917.
[108] Campbell RA. Recent advances in resolving kinetic and dynamic processes at the air/water interface using specular neutron reflectometry. Curr Opin Colloid Interface Sci 2018;37:49–60.
[109] de Haan V-O, van Well AA. Comparison between a time-of-flight and a monochromatic neutron reflectometer at a continuous neutron source. J Neutron Res 1996;3:63–8.
[110] Cioni P, Strambini GB. Effect of heavy water on protein flexibility. Biophys J 2002;82:3246–53.
[111] Giubertoni G, Bonn M, Woutersen S. D2O as an imperfect replacement for H2O: problem or opportunity for protein research? J Phys Chem B 2023;127:8086–94.
[112] Efimova YM, Haemers S, Wierczinski B, Norde W, van Well AA. Stability of globular proteins in H2O and D2O. Biopolym 2007;85:264–73.
[113] Verheul M, Roefs SP, de Kruif KG. Aggregation of β-lactoglobulin and influence of D2O. FEBS Lett 1998;421:273–6.
[114] Grunwald C, Kuhlmann J, Wöll C. In deuterated water the unspecific adsorption of proteins is significantly slowed down: results of an SPR study using model organic surfaces. Langmuir 2005;21:9017–9.
[115] Ganzevles RA, Fokkink R, van Vliet T, Cohen Stuart MA, de Jongh HHJ. Structure of mixed β-lactoglobulin/pectin adsorbed layers at air/water interfaces; a spectroscopy study. J Colloid Interface Sci 2008;317:137–47.
[116] Horne DS, Atkinson PJ, Dickinson E, Pinfield VJ, Richardson RM. Neutron reflectivity study of competitive adsorption of β-lactoglobulin and nonionic surfactant at the air–water interface. Int Dairy J 1998;8:73–7.
[117] Gochev GG, Scoppola E, Campbell RA, Noskov BA, Miller R, Schneck E. β-Lactoglobulin adsorption layers at the water/air surface: 3. Neutron reflectometry study on the effect of pH. J Phys Chem B 2019;123:10877–89.
[118] Campbell RA, Tummino A, Noskov BA, Varga I. Polyelectrolyte/surfactant films spread from neutral aggregates. Soft Matter 2016;12:5304–12.
[119] Matyszewska D, Nazaruk E, Campbell RA. Interactions of anticancer drugs doxorubicin and idarubicin with lipid monolayers: New insight into the composition, structure and morphology. J Colloid Interface Sci 2021;581:403–16.
[120] Cubitt R, Saerbeck T, Campbell RA, Barker R, Gutfreund P. An improved algorithm for reducing reflectometry data involving divergent beams or non-flat samples. J Appl Cryst 2015;48:2006–11.
[121] Dickinson E, Horne DS, Phipps JS, Richardson RM. A neutron reflectivity study of the adsorption of β-casein at fluid interfaces. Langmuir 1993;9:242–8.
[122] Theodoratou A, Lee L-T, Oberdisse J, Aubert-Pouëssel A. Equilibrium protein adsorption on nanometric vegetable oil hybrid film/water interface using neutron reflectometry. Langmuir 2019;35:6620–9.
[123] Zarbakhsh A, Bowers J, Webster JRP. A new approach for measuring neutron reflection from a liquid/liquid interface. Meas Sci Technol 1999;10:738–43.
[124] Campana M, Hosking SL, Petkov JT, Tucker IM, Webster JRP, Zarbakhsh A, et al. Adsorption of bovine serum albumin (BSA) at the oil/water interface: a neutron reflection study. Langmuir 2015;31:5614–22.
[125] Ruane S, Li Z, Campana M, Hu X, Gong H, Webster JRP, et al. Interfacial adsorption of a monoclonal antibody and its Fab and Fc fragments at the oil/water interface. Langmuir 2019;35:13543–52.
[126] Ruane S, Li Z, Hollowell P, Hughes A, Warwicker J, Webster JRP, et al. Investigating the orientation of an interfacially adsorbed monoclonal antibody and its fragments using neutron reflection. Mol Pharm 2023;20:1643–56.
[127] Kong D, Peng L, Bosch-Fortea M, Chrysanthou A, Alexis CVJ, Matellan C, et al. Impact of the multiscale viscoelasticity of quasi-2D self-assembled protein networks on stem cell expansion at liquid interfaces. Biomaterials 2022;284:121494.
[128] Schlossman ML, Mitrinovic DM, Zhang Z, Li M, Huang Z. X-ray scattering from single liquid-liquid interfaces. Synch Rad News 1999;12:53–8.
[129] Scoppola E, Watkins E, Destri GL, Porcar L, Campbell RA, Konovalov O, et al. Structure of a liquid/liquid interface during solvent extraction combining X-ray and neutron reflectivity measurements. Phys Chem Chem Phys 2015;17:15093–7.
[130] Protat M, Bodin-Thomazo N, Malloggi F, Daillant J, Campbell RA, Fragneto G, et al. Neutron reflectivity measurements at the oil/water interface for the study of stimuli-responsive emulsions. Eur Phys J E 2018;41:85.
[131] Cascão Pereira LG, Théodoly O, Blanch HW, Radke CJ. Dilatational rheology of BSA conformers at the air/water interface. Langmuir 2003;19:2349–56.
[132] Cascão Pereira LG, Johansson C, Radke CJ, Blanch HW. Surface Forces and Drainage Kinetics of Protein-Stabilized Aqueous Films. Langmuir 2003;19:7503–13.
[133] Puff N, Marchal R, Aguié-Béghin V, Douillard R. Is grape invertase a major component of the adsorption layer formed at the air/champagne wine interface? Langmuir 2001;17:2206–12.

[134] Hambardzumyan A, Aguié-Béghin V, Daoud M, Douillard R. β-Casein and symmetrical triblock copolymer (PEO-PPO-PEO and PPO-PEO-PPO) surface properties at the air-water interface. Langmuir 2004;20:756–63.
[135] Beaufils S, Hadaoui-Hammoutène R, Vié V, Miranda G, Perez J, Terriac E, et al. Comparative behaviour of goat β and αs1-caseins at the air–water interface and in solution. Food Hydrocoll 2007;21:1330–43.
[136] Grigoriev DO, Fainerman VB, Makievski AV, Krägel J, Wüstneck R, Miller R. β-Casein bilayer adsorption at the solution/air interface: experimental evidences and theoretical description. J Colloid Interface Sci 2002;253:257–64.
[137] Vié V, Moreno J, Beaufils S, Lesniewska E, Léonil J, Renault A. Interfacial behavior of goat kappa casein: ellipsometry and atomic force microscopy study. Single Mol 2002;3:127–33.
[138] Grigoriev DO, Kolodziejczyk E, Leser ME, Michel M, Miller R. Effect of fluorescence labelling on the properties of protein adsorption layers at the air/water interface. Food Hydrocoll 2009;23:221–4.
[139] Noskov BA, Grigoriev DO, Latnikova AV, Lin SY, Loglio G, Miller R. Impact of globule unfolding on dilational viscoelasticity of β-lactoglobulin adsorption layers. J Phys Chem B 2009;113:13398–404.
[140] Gurkov TD, Russev SC, Danov KD, Ivanov IB, Campbell B. Monolayers of globular proteins on the air/water interface: applicability of the Volmer equation of state. Langmuir 2003;19:7362–9.
[141] Trofimova D, de Jongh HH. Modification of β-lactoglobulin by oligofructose: impact on protein adsorption at the air-water interface. Langmuir 2004;20:5544–52.
[142] Wierenga PA, Egmond MR, Voragen AG, de Jongh HH. The adsorption and unfolding kinetics determines the folding state of proteins at the air-water interface and thereby the equation of state. J Colloid Interface Sci 2006;299:850–7.
[143] Delahaije RJBM, Gruppen H, Giuseppin ML, Wierenga PA. Quantitative description of the parameters affecting the adsorption behaviour of globular proteins. Colloids Surf B Biointerfaces 2014;123:199–206.
[144] Lech FJ, Delahaije RJBM, Meinders MBJ, Gruppen H, Wierenga PA. Identification of critical concentrations determining foam ability and stability of β-lactoglobulin. Food Hydrocoll 2016;57:46–54.
[145] Engelhardt K, Lexis M, Gochev G, Konnerth C, Miller R, Willenbacher N, et al. pH effects on the molecular structure of β-lactoglobulin modified air-water interfaces and its impact on foam rheology. Langmuir 2013;29:11646–55.
[146] Beierlein FR, Clark T, Braunschweig B, Engelhardt K, Glas L, Peukert W. Carboxylate Ion Pairing with Alkali-Metal Ions for β-Lactoglobulin and Its Role on Aggregation and Interfacial Adsorption. J Phys Chem B 2015;119:5505–17.
[147] Braunschweig B, Schulze-Zachau F, Nagel E, Engelhardt K, Stoyanov S, Gochev G, et al. Specific effects of Ca2+ ions and molecular structure of β-lactoglobulin interfacial layers that drive macroscopic foam stability. Soft Matter 2016;12:5995–6004.
[148] Wen X, Franses EI. Adsorption of bovine serum albumin at the air/water interface and its effect on the formation of DPPC surface film. Coll Surf A 2001;190:319–32.
[149] McClellan SJ, Franses EI. Effect of concentration and denaturation on adsorption and surface tension of bovine serum albumin. Colloids Surf B Biointerfaces 2003;28:63–75.
[150] Engelhardt K, Rumpel A, Walter J, Dombrowski J, Kulozik U, Braunschweig B, et al. Protein adsorption at the electrified air-water interface: implications on foam stability. Langmuir 2012;28:7780–7.
[151] Alahverdjieva VS, Grigoriev DO, Ferri JK, Fainerman VB, Aksenenko EV, Lesser ME, et al. Adsorption behaviour of hen egg-white lysozyme at the air/water interface. Coll Surf A 2008;323:167–74.
[152] Tihonov MM, Milyaeva Oyu, Noskov BA. Dynamic surface properties of lysozyme solutions. Impact of urea and guanidine hydrochloride. Colloids Surf B Biointerfaces 2015;129:114–20.
[153] Le Floch-Fouéré C, Pezennec S, Lechevalier V, Beaufils S, Desbad B, Pézolet M, et al. Synergy between ovalbumin and lysozyme leads to non-additive interfacial and foaming properties of mixtures. Food Hydrocoll 2009;23:352–65.
[154] Pasquier C, Pezennec S, Bouchoux A, Cabane B, Lechevalier V, Le Floch-Fouéré C, et al. Protein transport upon advection at the air/water interface: when charge matters. Langmuir 2021;37:12278–89.
[155] de Feijter JA, Benjamins J. Soft-particle model of compact macromolecules at interfaces. J Colloid Interface Sci 1982;90:289–92.
[156] Pezennec S, Gauthier F, Alonso C, Graner F, Croguennec T, Brulé G, et al. The protein net electric charge determines the surface rheological properties of ovalbumin adsorbed at the air–water interface. Food Hydrocoll 2000;5:463–72.
[157] Renault A, Pezennec S, Gauthier F, Vié V, Desbat B. Surface rheological properties of native and S-ovalbumin are correlated with the development of an intermolecular β-sheet network at the air−water interface. Langmuir 2002;18:6887–95.
[158] Wierenga PA, Meinders MBJ, Egmond MR, Voragen Fons AGJ, de Jongh HHJ. Protein exposed hydrophobicity reduces the kinetic barrier for adsorption of ovalbumin to the air−water Interface. Langmuir 2003;19:8964–70.
[159] Wierenga PA, Meinders MB, Egmond MR, Voragen AG, de Jongh HH. Quantitative description of the relation between protein net charge and protein adsorption to air-water interfaces. J Phys Chem B 2005;109:16946–52.
[160] de Jongh HH, Wierenga PA. Assessing the extent of protein intermolecular interactions at air-water interfaces using spectroscopic techniques. Biopolym 2006;82:384–9.
[161] Guckeisen T, Hosseinpour S, Peukert W. Isoelectric Points of Proteins at the Air/Liquid Interface and in Solution. Langmuir 2019;35:5004–12.
[162] Le Floch-Fouéré C, Pezennec S, Pézolet M, Rioux-Dubé JF, Renault A, Beaufils S. Unexpected differences in the behavior of ovotransferrin at the air-water interface at pH 6.5 and 8.0. J Colloid Interface Sci 2011;356:614–23.
[163] Hähl H, Griffo A, Safaridehkohneh N, Heppe J, Backes S, Lienemann M, et al. Dynamic assembly of class II hydrophobins from T. reesei at the air-water interface. Langmuir 2019;35:9202–12.
[164] Hernández EM, Phang TL, Wen X, Franses EI. Adsorption and direct probing of fibrinogen and sodium myristate at the air/water interface. J Colloid Interface Sci 2002;250:271–80.
[165] Hernández EM, Franses EI. Adsorption and surface tension of fibrinogen at the air/water interface. Coll Surf A 2003;214:249–62.
[166] Muth M, Schmid RP, Schnitzlein K. Ellipsometric study of molecular orientations of Thermomyces lanuginosus lipase at the air-water interface by simultaneous determination of refractive index and thickness. Colloids Surf B Biointerfaces 2016;140:60–6.
[167] Renault A, Rioux-Dubé JF, Lefèvre T, Pezennec S, Beaufils S, Vié V, et al. Surface properties and conformation of Nephila clavipes spider recombinant silk proteins at the air-water interface. Langmuir 2009;25:8170–80.
[168] Péron N, Cagna A, Valade M, Marchal R, Maujean A, Robillard B, et al. Characterisation by drop tensiometry and by ellipsometry of the adsorption layer formed at the air/champagne wine interface. Adv Colloid Interface Sci 2000;88:19–36.
[169] Piazza L, Dürr-Auster N, Gigli J, Windhab EJ, Fischer P. Interfacial rheology of soy proteins – high methoxyl pectin films. Food Hydrocoll 2009;8:2125–31.
[170] Poirier A, Banc A, Stocco A, In M, Ramos L. Multistep building of a soft plant protein film at the air-water interface. J Colloid Interface Sci 2018;526:337–46.
[171] Poirier A, Banc A, Kapel R, In M, Stocco A, Ramos L. Impact of structural flexibility in the adsorption of wheat and sunflower proteins at an air/water interface. Coll Surf A 2022;648:129317.
[172] Ulaganathan V, Retzlaff I, Won JY, Gochev G, Gehin-Delval C, Leser ME, et al. β-Lactoglobulin adsorption layers at the water/air surface: 1. Adsorption kinetics and surface pressure isotherm: effect of pH and ionic strength. Coll Surf A 2017;519:153–60.
[173] Holt SA, White JW. The molecular structure of the surface of commercial cow's milk. Phys Chem Chem Phys 1999;1:5139–45.
[174] Gidalevitz D, Huang Z, Rice SA. Protein folding at the air–water interface studied with x-ray reflectivity. PNAS 1999;96:2608–11.
[175] Holt SA, McGillivray DJ, Poon S, White JW. Protein Deformation and Surfactancy at an Interface. J Phys Chem B 2000;104:7431–8.
[176] Perriman AW, Henderson MJ, Holt SA, White JW. Effect of the air-water interface on the stability of β-lactoglobulin. J Phys Chem B 2007;111:13527–37.
[177] Perriman AW, Henderson MJ, Evenhuis CR, McGillivray DJ, White JW. Effect of the air-water interface on the structure of lysozyme in the presence of guanidinium chloride. J Phys Chem B 2008;112:9532–9.
[178] Kisko K, Szilvay GR, Vuorimaa E, Lemmetyinen H, Linder MB, Torkkeli M, et al. Self-assembled films of hydrophobin proteins HFBI and HFBII studied in situ at the air/water interface. Langmuir 2009;25:1612–9.
[179] Stenger PC, Wu G, Miller CE, Chi EY, Frey SL, Lee KY, et al. X-ray diffraction and reflectivity validation of the depletion attraction in the competitive adsorption of lung surfactant and albumin. Biophys J 2009;5:777–86.
[180] Ang JC, Henderson MJ, Campbell RA, Lin J-M, Yaron PN, Nelson A, et al. Human serum albumin binding to silica nanoparticles-effect of protein fatty acid ligand. Phys Chem Chem Phys 2014;16:10157–68.
[181] Yano YF, Uruga T, Tanida H, Toyokawa H, Terada Y, Takagaki M, et al. Driving force behind adsorption-induced protein unfolding: A time-resolved x-ray reflectivity study on lysozyme adsorbed at an air/water interface. Langmuir 2009;25:32–5.
[182] Yano YF, Uruga T, Tanida H, Toyokawa H, Terada Y, Takagaki M, et al. Rapid X-ray reflectivity measurement using a new liquid interface reflectometer at SPring-8. Eur Phys J: Spec Topics 2009;167:101–5.
[183] Yano YF, Uruga T, Tanida H, Toyokawa H, Terada Y, Takagaki M, et al. X-ray specular and off-specular reflection from a protein adsorbed at a liquid surface. Trans Mater Res Soc Jpn 2009;34:631–8.
[184] Yano YF, Uruga T. Effect of salt ions on protein layers at the air–water interface under a crystallization condition. Chem Phys 2013;419:153–5.
[185] Yano YF, Arakawa E, Voegeli W, Matsushita T. Real-time investigation of protein unfolding at an air-water interface at the 1 s time scale. J Synchrotron Radiat 2013;20:980–3.
[186] Yano YF, Uruga T, Tanida H, Terada Y, Yamada H. Protein salting out observed at an air-water interface. J Phys Chem Lett 2011;2:995–9.
[187] Eaglesham A, Herrington TM, Penfold J. A neutron reflectivity study of a spread monolayer of bovine serum albumin. Colloids Surf 1992;65:9–16.
[188] Dickinson E, Horne DS, Richardson RM. Neutron reflectivity study of the competitive adsorption of β-casein and water—soluble surfactant at the planar air-water interface. Food Hydrocoll 1993;7:497–505.
[189] Atkinson PJ, Dickinson E, Horne DS, Richardson RM. Neutron reflectivity of adsorbed β-casein and β-lactoglobulin at the air/water interface. J Chem Soc Faraday Trans 1995;91:2847–54.
[190] Zhang XL, Penfold J, Thomas RK, Tucker IM, Petkov JT, Bent J, et al. Adsorption behavior of hydrophobin and hydrophobin/surfactant mixtures at the air-water interface. Langmuir 2011;27:11316–23.
[191] Tucker IM, Petkov JT, Penfold J, Thomas RK, Cox AR, Hedges N. Adsorption of hydrophobin-protein mixtures at the air-water interface: The impact of pH and electrolyte. Langmuir 2015;31:10008–16.

[192] Lu JR, Su TJ, Thomas RK, Penfold J, Webster J. Structural conformation of lysozyme layers at the air/water interface studied by neutron reflection. J Chem Soc Faraday Trans 1998;94:3279–87.
[193] Lu JR, Su TJ, Howlin BJ. The effect of solution pH on the structural conformation of lysozyme layers adsorbed on the surface of water. J Phys Chem B 1999;103:5903–9.
[194] Lu JR, Su TJ, Thomas RK. Structural Conformation of bovine serum albumin layers at the air–water interface studied by neutron reflection. J Colloid Interface Sci 1999;213:426–37.
[195] Lu JR, Su TJ, Penfold J. Adsorption of serum albumins at the air/water interface. Langmuir 1999;15:6975–83.
[196] Lu JR, Perumal S, Zhao X, Miano F, Enea V, Heenan RR, et al. Surface-induced unfolding of human lactoferrin. Langmuir 2005;21:3354–61.
[197] Smith C, Li Z, Holman R, Pan F, Campbell RA, Campana M, et al. Antibody adsorption on the surface of water studied by neutron reflection. MAbs 2017;9:466–75.
[198] Li Z, Li R, Smith C, Pan F, Campana M, Webster JRP, et al. Neutron reflection study of surface adsorption of Fc, Fab, and the whole mAb. ACS Appl Mater Interfaces 2017;9:23202–11.
[199] Aschi A, Gharbi A, Bitri L, Calmettes P, Daoud M, Aguié-Béghin V, et al. Structure and properties of adsorption layers of β-casein formed from guanidine hydrochloride rich solutions. Langmuir 2001;17:1896–904.
[200] Perriman AW, White JW. Kinetics of adsorption of lysozyme at the air–water interface and the role of protein charge. Physica B: Condens Matter 2006;385-386:716–8.
[201] Holt SA, Henderson MJ, White JW. Thermal denaturation of interfacial protein layers. Aust J Chem 2002;55:449–59.
[202] Scheuble N, Geue T, Windhab EJ, Fischer P. Tailored interfacial rheology for gastric stable adsorption layers. Biomacromolecules 2014;15:3139–45.
[203] Scheuble N, Lussi M, Geue T, Carrière F, Fischer P. Blocking gastric lipase adsorption and displacement processes with viscoelastic biopolymer adsorption layers. Biomacromolecules 2016;17:3328–37.
[204] Bertsch P, Thoma A, Bergfreund J, Geue T, Fischer P. Transient measurement and structure analysis of protein-polysaccharide multilayers at fluid interfaces. Soft Matter 2019;15:6362–8.
[205] Bergfreund J, Diener M, Geue T, Nussbaum N, Kummer N, Bertsch P, et al. Globular protein assembly and network formation at fluid interfaces: effect of oil. Soft Matter 2021;17:1692–700.
[206] Lee L-T, Jha BK, Malmsten M, Holmberg K. Lipase−surfactant interactions studied by neutron reflectivity and ellipsometry. J Phys Chem B 1999;103:7489–94.
[207] Yuan G, Kienzle PA, Satija SK. Salting up and salting down of bovine serum albumin layers at the air-water interface. Langmuir 2020;36:15240–6.
[208] Tripp BC, Magda JJ, Andrade JD. Adsorption of globular proteins at the air/water interface as measured via dynamic surface tension: concentration dependence, mass-transfer considerations, and adsorption kinetics. J Colloid Interface Sci 1995;173:16–27.
[209] McCrackin FL, Passaglia E, Stromberg RR, Steinberg HL. Measurement of the thickness and refractive index of very thin films and the optical properties of surfaces by ellipsometry. J Res Natl Bur Stand A Phys Chem 1963;67:363–77.
[210] Bootsma GA, Meyer F. Ellipsometry in the sub-monolayer region. Surf Sci 1969;14:52–76.
[211] Holt C, McPhail D, Nylander T, et al. Some physico-chemical properties of nine commercial or semi-commercial whey protein concentrates, isolates and fractions. Int J Food Sci Technol 1999;34:587–601.
[212] Mysels KJ, Shinoda C, Frankel S. Soap films: studies on their thinning. Pergamon; 1959.
[213] a Scheludko A. Über das Ausfließen der Lösung aus Schaumfilmen (Eng. On the drainage of liquid from foam films). Kolloid-Z 1957;155:39.b Thin liquid films. Adv Colloid Interface Sci 1967;1:391–464.
[214] Vrij A, Joosten JGH, Fijnaut HM. Light Scattering from Thin Liquid Films. In: Prigogine I, Rice SA, editors. Advances in Chemical Physics. 48. Wiley; 1981. p. 329–96.
[215] a Scheludko A, Exerowa D, Kolloid Z. Über den elektrostatischen Druck in Schaumfilmen aus wässerigen Elektrolytlösungen (Eng. On the electrostatic pressure in foam films from aqueous electrolyte solutions)165; 1959. p. 148–51.
b Über den elektrostatischen und van der Waalsschen zusätzlichen Druck in wässerigen Schaumfilmen (Eng. On the electrostatic and van der Waals pressure in aqueous foam films). 168; 1960. p. 24–8.
[216] Clunie JS, Corkill JM, Goodman JF. Structure of black foam films. Discuss Faraday Soc 1966;42:34–41.
[217] Exerowa E, Kashchieva D, Platikanov D. Stability and permeability of amphiphile bilayers. Adv Colloid Interface Sci 1992;40:201–56.
[218] den Engelsen D, Frens G. Ellipsometric investigation of black soap films. J Chem Soc Faraday Trans 1974;1(70):237–48.
[219] Highfield RR, Humes RP, Thomas RK, Cummins PG, Gregory DP, Mingins J, et al. Critical reflection of neutrons from a soap film. J Colloid Interface Sci 1984;97:367–73.
[220] Bélorgey O, Benattar JJ. Structural properties of soap black films investigated by x-ray reflectivity. Phys Rev Lett 1991;66:313–6.
[221] Benattar JJ, Schalchli A, Bélorgey O. X-ray reflectivity investigation of Newton and common black films. J Phys I France 1992;2:955–68.
[222] Petkova V, Sultanem C, Nedyalkov M, Benattar J-J, Leser ME, Schmitt C. Structure of a freestanding film of β-Lactoglobulin. Langmuir 2003;19:6942–9.
[223] Kolodziejczyk E, Petkova V, Benattar J-J, Leser ME, Michel M. Effect of fluorescent labeling of β-lactoglobulin on film and interfacial properties in relation to confocal fluorescence microscopy. Coll Surf A 2006;279:159.
[224] Mussellwhite PR, Kitchener JA. The limiting thickness of protein films. J Colloid Interface Sci 1967;24:80.
[225] Dimitrova TD, Leal-Calderon F, Gurkov TD, Campbell B. Surface forces in model oil-in-water emulsions stabilized by proteins. Adv Colloid Interface Sci 2004;108-109:73–86.
[226] Gochev G, Retzlaff I, Exerowa D, Miller R. Electrostatic stabilization of foam films from β-lactoglobulin solutions. Coll Surf A 2014;460:272–9.
[227] Janssen F, Wouters AGB, Chatzigiannakis E, Delcour JA, Vermant J. Thin film drainage dynamics of wheat and rye dough liquors and oat batter liquor. Food Hydrocoll 2021;116:106624.
[228] Delahaije RJBM, Wierenga PA, Van Nieuwenhuijzen NH, Giuseppin MLF, Gruppen H. Protein concentration and protein-exposed hydrophobicity as dominant parameters determining the flocculation of protein-stabilized oil-in-water emulsions. Langmuir 2013;29. 11567-54.
[229] Basheva ES, Kralchevsky PA, Christov NC, Danov KD, Stoyanov SD, Blijdenstein TBJ, et al. Unique properties of bubbles and foam films stabilized by HFBII hydrophobin. Langmuir 2011;27:2382–92.
[230] Basheva ES, Kralchevsky PA, Danov KD, Stoyanov SD, Blijdenstein TBJ, Pelan EG, et al. Self-Assembled Bilayers from the protein HFBII hydrophobin: nature of the adhesion energy. Langmuir 2011;27:4481–8.
[231] a Perrin J. The stratification of liquid lamellae. Ann Phys 1918;10:165.
b Wells PV. On the thickness of stratified lamellae. Ann Phys 1921;16:79.
c Bruil HG, Lyklema J. Stratification in free liquid films. Nature 1971;233:19–20.
[232] Ochoa C, Gao S, Srivastava S, Sharma V. Foam film stratification studies probe intermicellar interactions. PNAS 2021;118:e2024805118.
[233] Lu JR, Thomas RK, Penfold J. Surfactant layers at the air/water interface: structure and composition. Adv Colloid Interface Sci 2000;84:143–304.
[234] Ozboyaci M, Kokh DB, Corni S, Wade RC. Modeling and simulation of protein–surface interactions: achievements and challenges. Q Rev Biophys 2016;49:e4.
[235] Quan X, Liu J, Zhou J. Multiscale modeling and simulations of protein adsorption: progresses and perspectives. Curr Opin Colloid Interface Sci 2019;41:74–85.
[236] Hamid MK, Månsson LK, Meklesh V, Persson P, Skepö M. Molecular dynamics simulations of the adsorption of an intrinsically disordered protein: Force field and water model evaluation in comparison with experiments. Front Mol Biosci 2022;9:958175.